SYNTHESIS AND CHARACTERIZATION OF

NANO-SIC REINFORCED AL ALLOYS

BY

ATIF S. AL-ZAHRANI

A Thesis Presented to the

DEANSHIP OF GRADUATE STUDIES

KING FAHD UNIVERSITY OF PETROLEUM & MINERALS

DHAHRAN, SAUDI ARABIA

In Partial Fulfillment of the
Requirements for the Degree of

MASTER OF SCIENCE
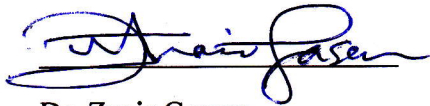
In

MECHANICAL ENGINEERING

December 2014

KING FAHD UNIVERSITY OF PETROLEUM & MINERALS

DHAHRAN- 31261, SAUDI ARABIA

DEANSHIP OF GRADUATE STUDIES

This thesis, written by Atif Saeed Al-Zahrani under the direction his thesis advisor and

approved by his thesis committee, has been presented and accepted by the Dean of

Graduate Studies, in partial fulfillment of the requirements for the degree **MASTER OF**

SCIENCE IN MECHANICAL ENGINEERING.

Dr. Nasser Al-Aqeeli
(Advisor)

Dr. Zuair Gasem
Department Chairman

Dr. Tahar Laoui
(Member)

Dr. Salam A. Zummo
Dean of Graduate Studies

Dr. Saheb Nouari
(Member)

3/2/15

Date

DEDICATION

This work is dedicated To

My father and mother, my brothers and sisters

My sincere wife and my beloved son, Ammar and the coming sons and
daughters if any.

ACKNOWLEDGMENTS

TABLE OF CONTENTS

LIST OF TABLES

LIST OF FIGURES

LIST OF ABBREVIATIONS

Al	Aluminum
Al/SiC	Aluminum/Silicon Carbide
Ar	Argon
BPR	Ball-to-Powder Ratio
CIP	Cold Isostatic Pressing
EDS	Energy Dispersive Spectroscopy
HIP	Hot Isostatic Pressing
Hv	Vickers' Hardness
hr	hour
KN	Kilo Newton
MA	Mechanical Alloying
Mins	Minutes
MM	Mechanical Milling
MMCs	Metal Matrix Composites
MPa	Mega Pascal
nm	Nanometer
PM	Powder Metallurgy
PCA	Process Control Agent
SEM	Scanning Electron Microscope

SiC	Silicon Carbide
SPS	Spark Plasma Sintering
wt.%	Weight Percent
XRD	X-Ray Diffraction

ABSTRACT

Full Name   : Atif Saeed Al-Zahrani

Thesis Title   : PM Synthesis And Characterization Of Nano-SiC Reinforced Al 2124 And Al 6061 Aluminum Alloys

Major Field   : Mechanical Engineering

Date of Degree : Nov, 2014

Metal matrix composites (MMCs) have received an appreciable attention due their unique properties over conventional materials. The advantages of MMC have positioned them as suitable materials for multiple structural- and thermal management-applications in addition to wear service benefits. The most used metals as a matrix in research and development and in industries are aluminum and its alloys. This global recognition, embraced by the wide-range application, is due to aluminum light weight, excellent corrosion resistance and low cost. Silicon carbide (SiC), on the other hand, becomes the main type used as filler for aluminum and its alloys due to its exceptional mechanical and physical-chemical characteristics. As a ceramic reinforcement, it enjoys the remarkable hardness, yield strength, low density and thermal expansion. This useful combination yields to compromised values of the toughness of the matrix and hardness, strength, wear resistance and stiffness of the hard particles.

Nevertheless, the current methodologies for fabricating Al/SiC composites face challenges, which include homogenous distribution of SiC in the Al matrix. Therefore, mechanical milling is utilized in this research to develop Al 2124 and Al 6061 nanocomposites reinforced with nano-sized SiC. It has been proven that after 5 hour of milling, a comparable homogenous distribution is attained with crystallite sizes in the range of 20 nm by using XRD and SEM. Consolidation of the developed nanocomposites was carried on using non-conventional technique; i.e. spark plasma sintering (SPS) versus a conventional hot isostatic pressing (HIP). Values of micro-hardness were improved with increasing nano-SiC content from 0,5,10 and 15 (117, 188, 241 and 256 Hv, respectively) for Al 2124 composites sintered at 500 ^{o}C using SPS. Densification, also, was found to increase with increasing sintering temperature from 400 ^{o}C to 500 ^{o}C and to decrease with nano-SiC content. However, sintering at 450 and 500 ^{o}C showed higher densification with increasing the content of nano-SiC as opposed to 400 ^{o}C. SPS, in general, gave improved densification and hardness values due to the different mechanism of heating. The maximum densification by SPS reached 98% for Al 6061/ 15% SiC and hardness value (211 Hv) sintered at 500 ^{o}C, while HIP only achieved 85% and (145 Hv) for the same alloy.

ملخص الرسالة

الاسم الكامل: عاطف سعيد الزهراني

عنوان الرسالة: تصنيع و تشخيص كربيد السيلكا كمعززات مناهية الصغر لفلزات الألمنيوم

التخصص: الهندسة الميكانيكية

تاريخ الدرجة العلمية: نوفمبر , 2014

لاقت المواد المركبة المبنية على المعادن كمصفوفات اهتماما معبرا في السنوات الأخيرة كونها تحمل خصائص تميزها عن باقي المواد الإعتيادية. المميزات الإيجابية لهذه المواد جعلت منها محل دراسة و أيضا قابلة للتطبيق في العديد من الوظائف اللي تحتاج إلى مواد قادرة على احتمال الأوزان, تحمل الحرارة العالية وهذا بالإضافة إلى التطبيقات اللتي يغلب على المادة الإحتكاكات مع مواد أخرى. من بين كل المصفوفات , يعتبر الألمنيوم بمختلف فلزاته هو الأكثر شيوعا و استخداماً في مجال البحث و التطوير أو المجال الصناعي وهذا يرجع إلى خفة وزن الألمنيوم, قابليته لتحمل عوامل التعرية و مقاومة الصدأ و أخيراً إلى سعره المقبول. وفي الجهة المقابلة, كربيد السيليكا, يعتبر هو الأكثر شيوعاً ,أيضاً, كمعزز للمصفوفات لإنه يتمتع بمزايا قل أن نجدها في بقية المواد وتشمل على : صلابته وقوته العالية, و كثاقته و معامل التمدد الحراري القليلتان. بدمج خصائص الألمنيوم و كربيد السيليكا, تنتج لنا مواد ذات خصائص متوازنة ما بين متانة الألمنيوم و صلابة و قوة كربيد السيليكا.

و مع هذا, لا زال تصنيع هذا النوع من المواد المركبة يعتبر تحدياً على مستويات مختلفة, ومن ضمن هذه التحديات التوزع المتساوي لكربيد السيليكا بين مصفوفات الألمنيوم. ولذلك فإن الهدف من هذا المشروع البحثي هو تعزيز مصفوفات الألمنيوم (Al 6061, Al 2124) بكربيد السيليكا ذات حجم متناهي الصغر عن طريق الطحن الميكانيكي. في هذا البحث استُخدمت كميات مختلفة من كربيد السيليكا و تمت عملية الطحن لمدد مختلفة لمعرفة تأثير هذه المتغيرات على توزيع كربيد السيليكا بين مصفوفات الألمنيوم و الحجم الكريستالي للمادة المركبة. بعد خمس ساعات من الطحن الميكانيكي, تم إثبات أن التوزيع بين المعززات و المصفوفات وصلت إلى مرحلة جيدة بناء على الصور المأخوذة عن طريق EDS و الحجم الكريستالي وصل إلى قرابة 20 نانوميتر عن طريق XRD. تم دمج هذه المواد عن طريق SPS وهي طريقة غير معتادة و تمت مقارنتها مع الطريقة الإعتيادية HIP. القيمة الصلابة بعد دمج المعززات مع المصفوفات تحسنت مع ارتفاع كمية نانو كربيد السيليكا المضافة من 0, 5, 10 و 15 (117.1, 188.26, 240.58 و 256.41 تباعاً) للمصفوفة AL 2124 دمجت عند حرارة 500°C بإستخدام SPS. معامل التكثيف أيضاً تحسن مع زيادة درجة حرارة الدمج من 400, 450 إلى 500°C و تناقصت مع ازدياد كمية المعززات المضافة. و على كل حال, عندما تم الدمج عند درجة حرارة 500°C , معامل التكثيف ازداد مع زيادة كمية المعززات وهذا يرجع إلى احتمال ذوبان فلزات الألمنيوم. بشكل عام, SPS أعطى معامل كثافة و صلابة أعلى مقارنة بـ HIP وهذا يرجع إلى الإختلاف الكلي بميكانيكية الدمج. أعلى قيمة لمعامل التكثيف وصلت إلى 98% بإستخدام SiC %Al 6061/15 و صلابة وصلت إلى (211 Hv) دمجت عند درجة حرارة 500°C. بينما بإستخدام HIP لنفس المركب ونفس درجة الحرارة حققت معامل تكثيف 85% و صلابة قدرها (145 Hv) تباعاً.

CHAPTER 1

INTRODUCTION

With the advent of technology, natural and conventional material becomes a hindrance in front of the wheel of development. This has led material scientists to continuously thrive to develop materials with improved properties to match the global needs.

Metal matrix composites (MMCs) are class of materials that combine the toughness of metal matrices and hardness of ceramic reinforcements to achieve enhanced properties that are not attainable by an individual component [1, 2, 3, 4, 5]. MMC, for the past years, have received an appreciable attention due its unique properties over the base metal. The advantages of MMC have positioned them as suitable materials for many structural, thermal management and wear service benefits [6, 7].

The most used metals as a matrix in research and development as well as in industries are aluminum and its alloys. This global recognition embraced by the wide-range applications is due to aluminum light weight, excellent corrosion resistance and relatively low cost [5, 6, 8, 9]. In fact, the density of most MMCs is measured to be one-third of that of steel which boost the strength to weight ratio [10]. The low density is very essential characteristic for future materials in order to be used in automotive and aerospace sectors.

Al alloy designated 2124 and 6061 are two commonly used alloys in a verity of applications. Al 2124 series is alloyed mainly with copper and combines both high strength as well as high fracture toughness [table 1]. Examples of its application are internal structures of aircraft and tanks trucks. On the other hand, Al 6061 main alloying elements are silicon and magnesium and it shows an excellent corrosion resistance combined with moderate strength. The main use of Al 6061 is in welded structures such as; marine frames, pipelines and railcars [11]. Al 2124 is stronger and harder than Al 6061. Consequently, Al 2124/SiC composite shows higher value of strength, hardness and yield strength but lower ductility and toughness compared to Al 6061/SiC composites [1].

Alloy	Si (wt. %)	Cu (wt. %)	Mn (wt. %)	Mg (wt. %)	Cr (wt. %)
Al 6061	0.6	0.28	-	1	0.2
Al 2124	-	4.4	0.6	1.5	-

Table 1: The nominal composition of Al 6061 and 2124 [58]

Nevertheless, the application of Al and its alloys is limited by their low hardness, wear resistance and stiffness for utilizations requiring high tribological and mechanical properties [12, 13]. One way to overcome these inferiors is to incorporate hard particles such as: Al_2O_3, AlN, SiC, TiC and TiB_2 within the Al matrix. Successful augmentation of the mentioned fillers into Al matrix have been reported and achieved a combination of the toughness of the matrix and hardness, strength, wear resistance and stiffness of the hard particles[14, 15, 16]. Structurally, reinforcements can be divided into whisker, fiber, short fiber or particulate ceramic [4, 17]. Particulate reinforced metal matrix (PMMC) offers numerous advantages compared to its counterparts. In addition of giving the best

combination of strength, toughness and ductility, they can be processed by secondary means (i.e. forging, extrusion and rolling etc.). Furthermore, the ease of producing particle reinforcements at comparatively low cost at a large scale is an extra advantage [1, 4, 5, 18].

1.1   Motivation and objective

Our motivation is to gain a through understanding on the role of nano-SiC content, milling time and consolidation methods on the properties of Al 2124/SiC and Al 6061/SiC nanocomposites.

The objectives of this project are to:

- Synthesize Al 2124/SiC and Al 6061/SiC nano-composites utilizing high energy ball milling.

- Characterize the microstructural and mechanical properties of the consalidated Al 2124/SiC and Al 6061/SiC nano-composites.

- Compare non-conventional consolidation technique; Spark Plasma Sintering (SPS) with conventional Hot Isostatic Pressing (HIP).

CHAPTER 2

LITERATURE REVIEW

2.1   Silicon reinforced Al-based Alloys

Silicon carbide (SiC) becomes the main type used as filler for aluminum and its alloys due to its exceptional mechanical and physical-chemical characteristics [5, 8]. As reinforcement ceramic, it enjoys the remarkable hardness, yield strength, good thermal conductivity and low density and thermal expansion [1, 5]. Fortunately, the improvement of SiC reinforced Al matrix comes with only small penalty increase over the density of the Al matrix [12].

With this valuable combination, it is believed that aluminum composites will replace iron components in automotive industries. The low density of Al matrix composite reduces the weight of automotive components and thus reduces fuel consumption and cost [20]. In fact, some of the Al composites have already reached the automotive market, for example; brake drums, pistons, cylinder blocks, connecting rods and drive shafts [15, 21]. Other properties such as; high thermal conductivity and low thermal expansion can be tailored to many automotive and aerospace, sport and instrument industries [1, 5, 6, 20, 22, 26]

The two major methods to fabricate Al-SiC composites are: powder metallurgy P/M and liquid metallurgy [5, 22]. In the liquid rout, the SiC particles are added to the molten

Aluminum and then the composite is left to solidify by cooling. Unfortunately, Al/SiC composite cannot be successfully fabricated by liquid metallurgy due to the large gap of melting points between the constituents and the poor wettability of molten Al and SiC [17, 23]. Wettability is defined of the ability of a liquid to spread over a solid surface and it represents how compatible the phases are [23]. This basic method produces composite with non-uniform particle distribution and poor adherent phases which ultimately results in poor mechanical properties [3, 24, 25].

In addition to the aforementioned drawbacks, undesirable aluminum carbide (Al_4C_3) and dissolved Silicon resulted from the dissolution of SiC in the molten Al are produced [17, 26]. Al_4C_3 and dissolved silicon can significantly deteriorate the mechanical of the composites due degradation of the useful SiC particles [17]. Furthermore, the corrosion properties are worsening due to the expansion of aluminum carbide under humid environment (e.g. water and ethanol) which break the composite material and increase the composite's sensitivity toward corrosion [27].

Lowering the temperature of the molten Al to avoid such reactions is not valid since it worsens the wettability, whereas elevating the temperature promotes the interfacial reaction further [27]. Several strategies have been investigated to overcome these obstacles such as: increasing the wettability between molten Al and solid SiC by adding Mg or Li. Another one is to coat silicon carbide particles by SiO_2 to inhibit the undesirable reaction products [28].

Powder metallurgy (PM), on the other hand, operates at a lower temperature which leads to less or even elimination of unwanted interfacial reaction [29]. In addition, the nature of

the PM approach makes it feasible to add higher volume fraction of hard particle and assure the highest possible dispersions [30, 31, and 32]. Therefore, they are nearly free of the downsides of liquid phase metallurgy [33].

Powder metallurgy is highly developed method for fabricating net-finish products. For the last seven decades, the PM technology has matured from manufacturing simple to intricate parts [5, 24, 32, 34, 35]. It is widely accepted as a green technology due to its contribution in minimizing the overall energy consumption and material wastage [36]. While liquid processes involve melting and essential mechanical finishing, PM rout consume energy for heating during sintering below melting temperature and needs little finishing occasionally. Processing through PM comprise three stages; powder blending, shaping and sintering.

The feedstock of PM –blended powder- can be divided broadly into two types: conventional powder blending, and then consolidate the mixed powder. Or, they can be produced through Mechanical alloying (MA) where the hard particles are embedded within the soft matrix.

Conventional blending often faces agglomeration problem which explains the poor performance of MMCs, especially, when nanofillers is added [37, 38]. This is attributed to the frictional forces originated from electrostatic, van der Waals, and surface adsorption between hard particles. At the nano level, these forces are found to be high which promote the agglomeration of particles. Thus, the uniform dispersion of Nano particles considered to be the prim challenging tasks in nanocomposite manufacturing. However, when the process parameters of MA are optimized, a homogenous

nanocomposite powder even at large reinforcement proportion at low temperature can be feasible [3, 8, 17, 24, 39, 40].

2.2   Mechanical Alloying

Mechanical Alloying (MA) is a useful technique to produce both equilibrium and non-equilibrium material such as: Amorphous phases, supersaturated alloys, nanostructured materials, nanoparticles, intermetallics, immiscible phases, nanocomposite and other reassured powders [41, 42, 43, 44]. In MA, high energy ball milling processes, including: attrition mills, SPEX shaker mills or planetary ball mills are utilized to develop various and novel materials [42]. It has been well-conceived MA enhances the characteristics of the mixed since it inhibits the clustering of particles, refine the powder sizes and promote the adhesion between the particles and matrix which improve the mechanical properties [5, 25, 30].

In non-equilibrium process, MA energizes a blend of powders by mechanical means, and then quenches it to reach a metastable level [Figure 1]. The advantages of non-equilibrium processing are the production of stable dispersoids, super saturated solid solution, altering the microstructure to reach to the nanometer level, and synthesis of novel crystalline and amorphous material [40, 45].
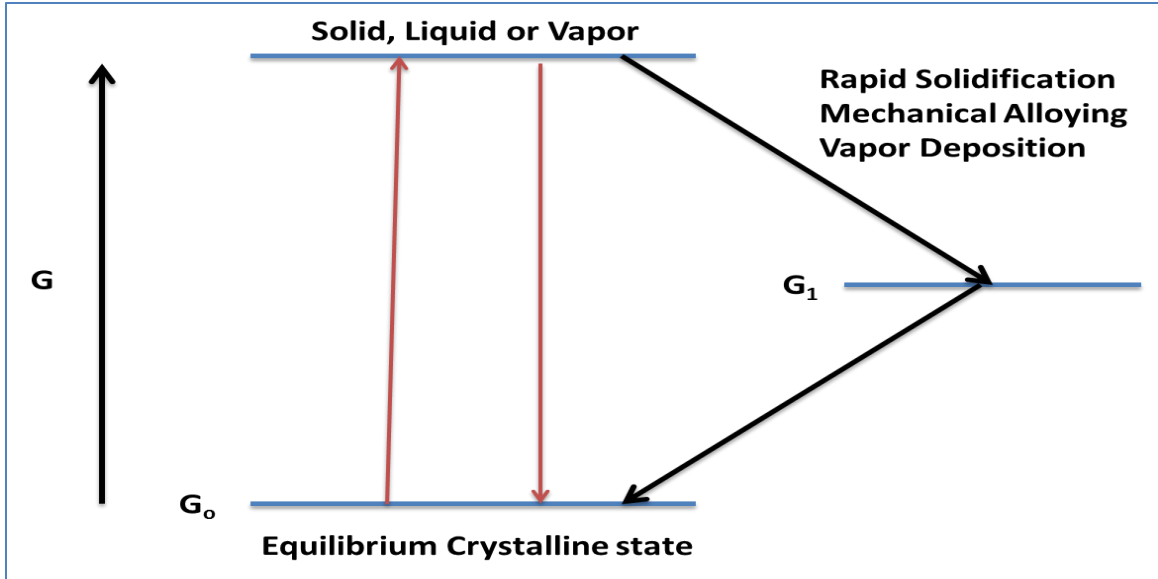
Figure 1: The variation of Gibbs free energy (G) in processing under non-equilibrium condition [40]

It utilizes high-energy ball mills with the aid of agitating media to cause plastic deformation to powder material. When two powder or more are charged in the chamber (vial), grinding balls cause particles to aggregate within the matrix to form layered composite material. The starting powder that form the composite will combine chemically either through diffusion process or chemical reaction [46].

Mechanically alloyed nanocomposites can be fabricated in situ processing where micro-size particles are fractured during the process to finally reach to the nanometer range. Though this approach seems to be more cost effective, but longer operation time and higher energy is required to achieve that, especially when the hard phase possess high energy of formation such as: SiC, WC, B_4C and c-BN. Introducing pre-fabricated nanofillers (i.e. ex situ) offers an alternative way of making mechanically alloyed nano composites with varied types of reinforcement [42, 38, 47].

2.2.1 Development of Mechanical alloying

Mechanical milling is a routinely used process in mineral and powder industries. Those industries used this process to crush rocks and blend powder, respectively. At that time, the concept of plastic deformation and cold welding of ingredients was absent.

The first attempt in mechanical alloying has been conducted by Benjamin and his colleagues at Paul D. Merica Research Laboratory of the International Nickel Company (INCO) at 1960s [48, 49]. They first milled nickel based alloys in oxidizing environment and then extend it to Al and Fr- based alloys. They obtained new powder with different characteristics from the starting powder. It is clear during milling that surfaces are oxidized and raptures due to the impact of grinding balls. The oxides then incorporate within the powder and impeded within the alloy powder. They have noticed a very well dispersed oxides within the matrix with interfaces were so perfect and become part of the original particle due to the cold welding.

Later they recognized that excessive plastic deformation and cold welding are responsible for having such structures. They term it as mechanical alloying, since the oxides and the matrix were truly alloyed. Benjamin in his work suggested that mechanical alloying should be a method to fabricate other metastable structure. However, the terminology "mechanical alloying" was not spread widely since the alloying was between an alloy and its oxide and alloying occurred between distinct elements [50].

In 1983, Koch and his colleagues at North Carolina state university published a breakthrough paper on mechanical alloying of elemental powder for the first time [51].

They mechanically alloyed Nickel and niobium powders ($Ni_{60}Nb_{40}$) for 11 and 14 hours in helium and air atmosphere, respectively. Samples were taken at every hour and subjected to XRD analysis for structural studies. They noticed that with time the peaks of XRD pattern deviate from the original Nickel and Niobium. After the milling, a true alloying was accomplished evident by the creation of amorphous Ni-Nb alloy phase. Later, it is widely accepted that mechanical alloying facilitates a true alloying and many researchers have been attracted to this field.

In the late 1980s, Schaffer and MacCormick published a new piece of work which considered as divergence from the original application of MA/MM mentioned earlier [52]. They demonstrated for the first time the applicability of mechanical alloying to be used as a vehicle for chemical reactions (i.e. mechanochemcial processing). In order to support that, they chose a reaction with large thermodynamic driving force (i.e. reduction of copper oxide in the presence of calcium). They noticed a complete reduction of copper oxide after milling for 100 minutes. Additionally, they examined the concept with ZnO and CuO-ZnO with calcium and obtained Zn and beta brass after 24h, respectively. So, not only a pure element, rather an alloy with a single process can be obtained which is an advantage over conventional milling processes.

2.2.2 Mechanisms of mechanical alloying

Indeed, the central process of MA is the ball-powder-ball and ball-powder-container collisions. At every collision, around 1000 particles weighting 0.2 mg are trapped between the colliding balls and suffer from moderate to high plastic deformation [Figure 2] [40, 46]. The mechanism of MA is dependent on the mechanical properties of

10

constitutes, their phase equilibriums and the state of brittleness of the components; i.e. ductile-ductile, ductile-brittle or brittle-brittle [43].
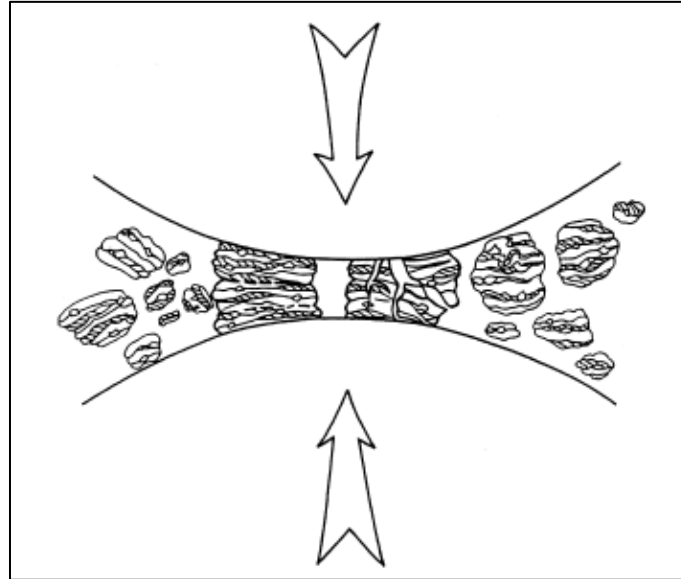
At the beginning of the milling and due to collision, Surfaces of the powders are automatically cleaned from contaminates [46, 52]. The newly cleaned surfaces are necessary for cold welding occurrence between the powder particles.   In ductile/ductile system, sever plastic deformation due to ball-powder-ball collision causes the ductile metals to flatten and then cold welded. This process will happen when both flattened particles are in contact and they will form lamellae structure. While in ductile-brittle system the brittle component is fractured and reduced in size due to excessive collision between the grinding balls. The small brittle fragments are embedded within the ductile flattened particles. Again, this step will result in forming layered composite comprising the brittle and ductile constitutes [Figure 3]. Continuous collisions tend to work harden and induce fatigue to the developed structures and fragment it into smaller particles size [40].

11
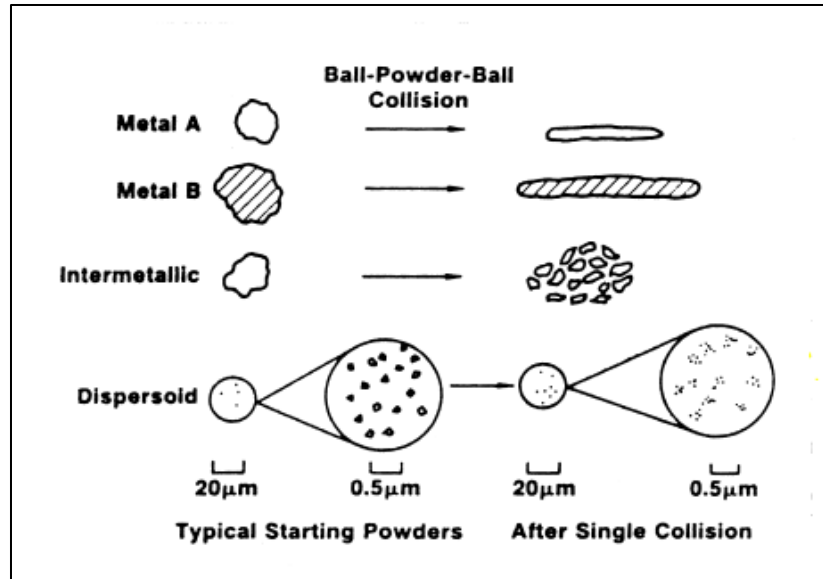
Figure 3: Deformation of different types of starting constitutes in MA [40]

Though it seems not possible to have MA between brittle powders due to the absence of ductile part which promote welding, it has been demonstrated in many articles. This is presumable when understanding that ductility of brittle material increases as their sizes remarkably decreased. So, the softer component will behave as a ductile material and the harder component will be dispersed within it [40, 53].

The layers of the composite as a result of MA will continue to add up and more layers will be deposited with no change in the particle size. As a result, interlayers distance between the layers is shortened during the process. The interplay between cold welding and the fragmentation will reach a steady state situation after a variable time of ball milling. At this stage, the composite particles possess the same amount of starting ingredients and size distribution is narrowed toward the average between both starting powders [40].

As mentioned earlier, MA involves a transfer of material through chemical bonding between the initial ingredients. The chemical bonding through diffusion process is activated by the existence and multiplication of crystalline defects, the decrease in interlayer distance and temperature rise during ball collision. However, sometimes further alloying is necessary and achieved by annealing the composite at higher temperature for a period of time [40].

2.3   Consolidation

The potential application of powder material lies on the successful consolidation of powder into a bulk material. It is of that important since most of the density and hence the strength is developed in this stage [20, 54]. Eliminating pores to densify powders require both temperature and time, depending on the pores' sizes and density. Thus, the traditional sintering at high temperature with prolong time promotes grain growth and by thus distorting nanocomposite powder structures [54].

Two approaches have been followed in order to retain the structure of the developed nano powders. One is to add a second phase to cause grain boundary binning, while the other approach is to apply pressure with fast heating rate at shorter time. With the latter method, it is possible to pass through surface diffusion which promotes grain growth to the regime where diffusion occur at the lattice or boundary which causes densification [55, 56]. Non-equilibrium consolidation processes such as: Spark Plasma Sintering (SPS), Microwave sintering (MS), Thermal spray and laser based techniques are practiced to restrict the grain growth.

2.3.1 Spark Plasma Sintering (SPS)

Spark plasma sintering (SPS) or at times referred by other names, such as field assisted sintering techniques (FAST), electric field assisted sintering (EFAS), plasma assisted sintering (PAS), and plasma pressure consolidation (PPC) is a consolidation method to fabricate bulk out of novel powder materials that is difficult or impossible to consolidate it by other means [Figure 4] [57]. Basically, SPS employs moderate pressure, electric field and plasma for rapid heating and densification with improved bulk properties [Figure 5] [58, 59]. In addition, it has the ability to densify various metal, ceramic, intermetallics, cemets, nano composite and nano carbon tube reinforced ceramics to near full density [60, 61, 62].
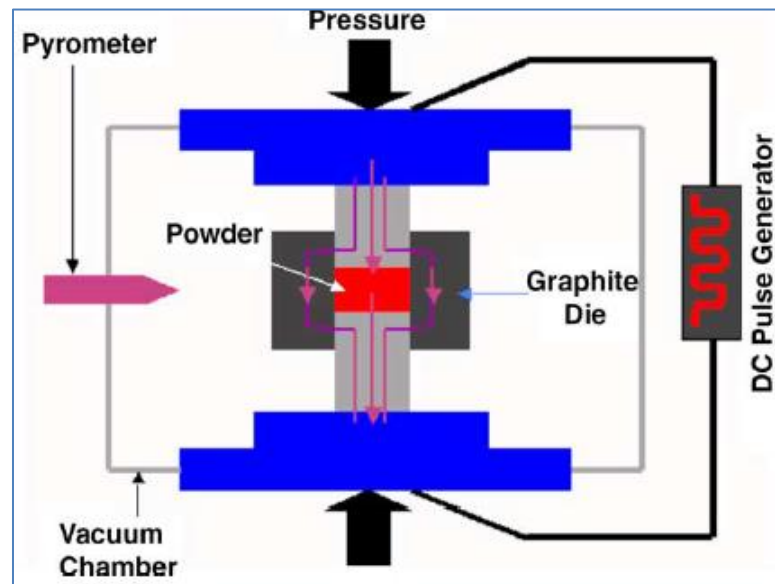
Figure 4: A schematic diagram of a typical SPS machine

An ON-OFF DC pulse voltage is applied across powders which generates momentarily plasma between the particles causing spark plasma, spark impact pressure, joule heating and electric field diffusion process [Figure 5] [62, 63]. In addition to the heat generated,

the created plasma cleans powder surfaces leading to densification enhancement of pure powder. There are several advantages of SPS [64], including:

- Reducing of temperature needed in the conventional sintering for densification due to resistance sintering of particles.

- Shortening of time required for sintering which due to the application of both electric field as well as mechanical pressure.

- Enhancing particles sinteriblity due to the cleaning process of powders' surfaces by discharge plasma generated between the powders.

Therefore, it is possible to fabricate with SPS highly purified with potential of 100% density bulk nanocomposites with improved mechanical properties [64, 65].
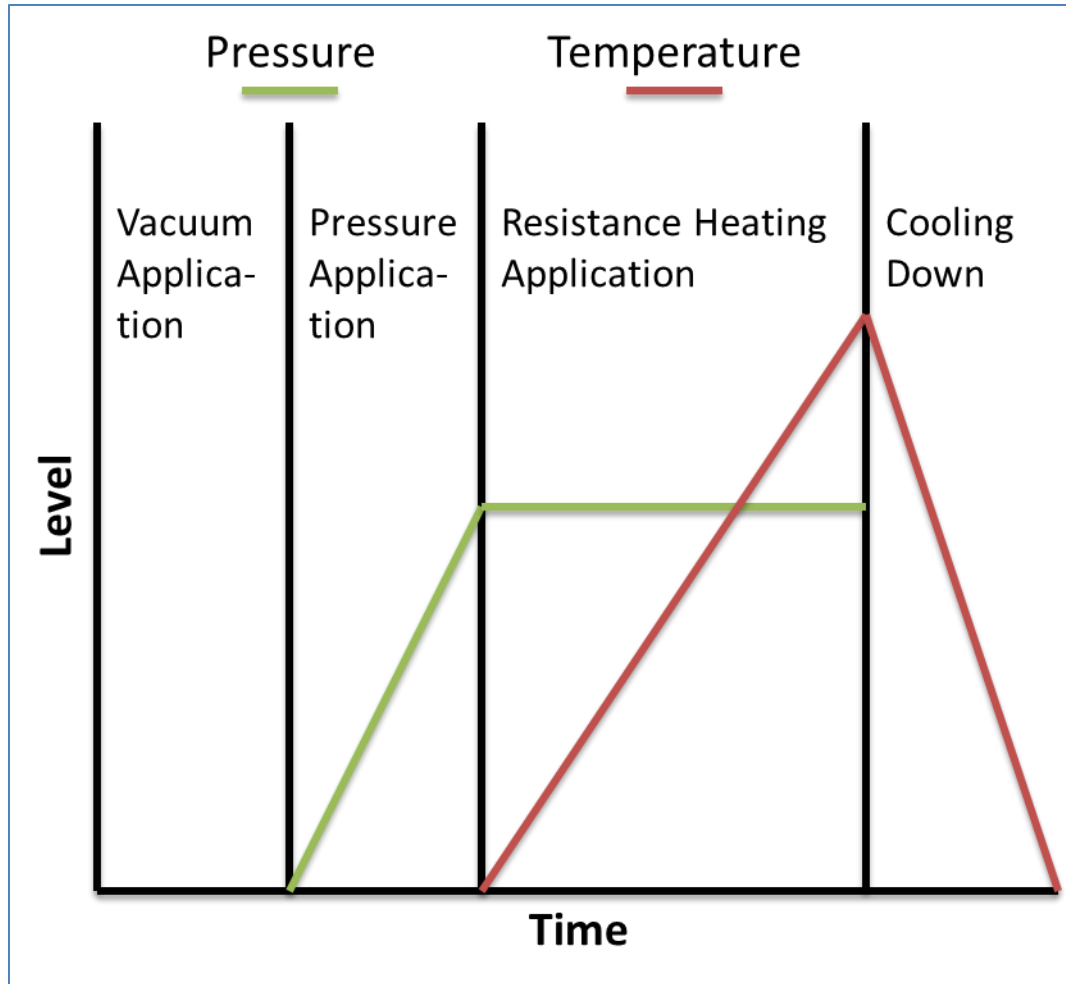
Figure 5: Different stages during sintering using SPS

2.4 Effect of Mechanical alloying and consolidation techniques on processed powders

Several researchers investigated the characteristics of powders processed by mechanical alloying versus those by conventional blending. To show the difference between powders processed through mechanical alloying. The mechanically alloyed 5 micron SiC with Al showed improved mechanical properties compared to the blending with the same composition sintered using Spark Plasma Sintering (SPS) [25]. It has been related to the improved microstructure and work hardening of the mechanically alloyed composite

powder. Moreover, experiments showed that finer microstructure, higher hardness and more uniform distribution can be attained by MA when compared with conventional powder blending [66, 67]. Parvin and his colleagues have shown than MA process has more pronoun effect on the hardness than SiC addition. This is due to the improved hardness value using MA compared to conventional blended composite and to unreinforced Al 6061 alloy [68].

Nevertheless, achieving homogenous composites with the desired features requires optimization of the interdependent factors that are related to the MA process. To exemplify, ball-to-powder ratio, milling speed/time, environment, both powder sized, mill and ball type should be adjust according to the design requirement. Another example is process control agent (PCA) which is a chemical added during MA to facilitate composite formation. Kollo and his colleagues investigated the alloying of nano-SiC with Al using stearic acid and heptane. It was found that composite particles within micron range are produced when using stearic acid, while heptane promotes cold welding and the formed powder was in millimeter range [69]. Lu reported that duration of milling factor caused a huge increase in 0.2% YS due to the uniformity of particle distribution [70]. Hardness has increased remarkably with milling time of Al 6061/SiC composites and has been attributed to the induced hardening during MA process [87].

2.5 The effect of SiC augmentation on Al-based alloys

It has been shown through experimentation that increasing the percentage of SiC addition generally enhanced the properties of the composites. When silicon carbide is added at a volume percentage of 50 or more, the thermal expansion of the composite is reduced to

the fifth of that bare aluminum. Moreover, the low thermal expansion combined with high thermal conductivity the composite makes a viable option for electronic packaging and high temperature applications [19, 27, 71].

Studies have agreed that increasing the reinforcement content weather fibers, particles, whisker or hybrid particles/whisker leads to an improvement of the tensile properties [1, 32, 72] and tribological properties [73, 74]. The addition of as low as 0.5% of SiC improved the mechanical and tribological properties of Al 6061 through powder injected molding process [74]. More interestingly, the 10% difference of SiC addition on Al 2124 resulted in 30% improvement of the tensile properties (i.e. tensile strength, yield strength and elastic modulus) of Al 2124/SiC composites [75]. However, some researchers have reported the decrease in strength with the reinforcement addition which is explained by clustering of ceramic particles [1].

Bhagat and House [76] have shown that improvement as a result of incorporating SiC particles into Al 6061 composite stood still at high temperature as well as at room temperature. At room temperature the addition of 20% SiC boost the tensile strength to 114% more than alloy, whereas at 350 $^{\mathrm{o}}$C, the composite still has 60% higher tensile strength compared to the alloy. Similarly, the elastic modulus have shown to be 111% greater than unreinforced alloy at room temperature, while it decreased to 56% improvement only at 350 $^{\mathrm{o}}$C [76].

Other mechanical properties, such as hardness, fracture toughness and ductility are also affected by volume fraction of the reinforcement. Hardness has been found to improve with the addition of SiC particulates; this is mainly due to the presence of hard phase

compared to unreinforced alloys [4, 32]. The Al 6061/SiC composites have shown lower

fracture toughness and ductility compared to the Al 6061 alloys. Indeed, the presence of

larger number of dislocations in the composites coupled with the amplified possibility of

clustering associated with increasing the volume fraction magnify the residual of stress at

the matrix and crack tip. The higher state of stress leads ultimately to faster crack

propagation and lower fracture toughness [1]. Figure 6 shows the stress-strain diagram

for hybrid Al 2124 15% (SiCw-SiCp) hybrid composite for illustrating the

aforementioned effects of SiC addition [77].
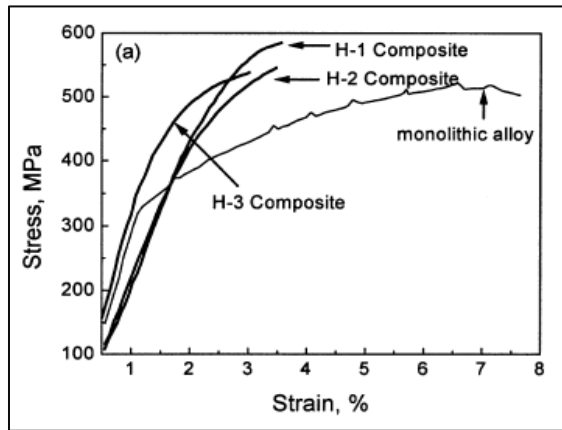
Figure 6: σ-ε diagram for aged Al 2124 (SiCw+SiCp) hybrid composites [77]

Strengthening of the composites as a result SiC incorporation may be attributed to

different mechanisms. The large difference in coefficient of thermal expansion between

Al (24×10^{-6} k^{-1}) and SiC (4×10^{-6} k^{-1}) induce large thermal residual stresses during

composites fabrication. When the residual stresses exceed the yield strength of the

matrix, dislocations are benched out. Thus, the higher dislocation density contributes

directly in strengthening the composites. Other mechanisms were also proposed such as;

Orowan strengthening, grain refinement and the load bearing effect [13, 32, 68].

Altering the reinforcement size would, definitely, change the properties of the composites as well. In general, increasing the particle size has a contrary effect of that particle content (i.e. lower tensile properties, higher ductility and toughness). Larger particle size reduces the interfacial area between the matrices and SiC particles which reduces the load transfer strengthening mechanisms [1, 78]. Moreover, large particle size, inherently, are weaker than small ones because of the higher possible existence of critical defects [1, 79]. Consequently, they are more vulnerable to fracture and decohere which maximize the stresses on the matrix and, thus, reduces the overall strength of the composites. Finally, incorporation of larger particle size generates lower dislocations density compared to the smaller sizes, hence; lower the effectiveness of dislocation density strengthening mechanism.

When one or both of the composite components (matrix and reinforcement) in the nanometer range, it is termed nano-composite [41,74]. It is expected to show better strength, toughness, stiffness, wear resistance and high temperature resistance compared to the micro-composite [74, 80, 47]. This is because nano-ceramic particles are less prone to fracture when impeded within the matrix. Moreover, due to the large number of particle present within the nanocomposite, the bearing load strengthening mechanism is more effective [81]. The main challenge in fabricating nano-composite is the difficulty of obtaining a homogenous nano-composite material with uniform distribution of nano-fillers. This is attributed to the high reactivity of nano-particles at higher temperature and the existences of strong internal attractive forces between them that promote agglomeration [41, 81].

The effect of using nano-fillers compared to micro-size ones has been investigated in the literature. Al/SiC system has been investigated for microstructural evolution during mechanical alloying using 45 micrometer and 35 nanometer SiC particle sizes [9]. It is found that nano-fillers have more significant role in grain refinement compared to micro-fillers [42]. In order to reach 100 nm composite particles, mechanical alloying of Al/SiC using 35 nm requires one-fifth the time needed to achieve the same composite particle size using 45 micrometer SiC. Similar conclusion was reached by the work of Saheb and his colleagues [82]. The particle size of Al/10 wt.% SiC was more refined than both Al/ 5 wt.% SiC and Al/ 1 wt.% SiC.

The effect of addition nano-SiC particles on the mechanical properties of the Al/SiC nanocomposites have been studied as well. Al matrix containing 1% of SiC has been found to have twice the hardness of unreinforced al matrix, and it is increasing with increasing the particle content [38]. El-Eskandarany [29] showed that increasing the volume fraction of SiC increases the hardness, density and elastic moduli of the developed nano-composites. The concluding effect of nano-SiC is in agreement with other reports investigating nano-SiC composites based on Al-Li [83] and Al–7wt%Si–0.4wt%Mg [84] matrices.

Aqeeli and co-workers have developed Al-7%Si-.3%Mg and Al-12%Si-.3%Mg / nano-SiC composites using mechanical milling and spark plasma sintering (SPS) [85, 86]. Moreover, both composites showed better performance in terms of hardness and density with increasing the sintering temperature due to the enhanced densification. Additionally, the hardness value was sensitive to the addition of nano-SiC, increasing with increasing

the nano-SiC content and reaching the optimum value at 12% SiC. Further addition of nano-SiC particles causes deterioration in hardness value because of the accumulated weak partially-sintered regions of the nano-composites.

A System Al 6061 mechanically alloyed with 100 nm SiC has been experimented to measure the toughness of the composites in terms of Charpy impact energy. They found that the lamination of composite compacts is the prime factor and is positively enhancing the toughness of the composites [87]. The result obtained has been modeled using soft computing models of artificial neural networks, gene expression programming (GEP) [88] and adaptive neuro-fuzzy interfacial systems (ANFIS) [82].

Up to the author knowledge, while there has been published work on nano and micro-SiC reinforced pure and Al alloys, no systematic work has been conducted to study the effect of augmenting nano silicon carbide particles in Al 2124 and Al 6061 alloys using mechanical milling and SPS and HIP.

CHAPTER 3

EXPERIMENTAL PROCEDURE

3.1   Powder fabrication

3.1.1 Raw material

Pre-alloyed Al matrices; Al2124 and Al6061 have been incorporated with nano-sized silicon carbide particles (SiCp) to form nanocomposites with improved properties. Al alloys and nano-SiC particles were supplied from Aluminium Powder Co. Ltd., United Kingdom and EPRUI Nanoparticles & Microspheres Co. Ltd., China, respectively. The particles size of all raw materials is found in Table 2.

Material	Particle size (µm)		
Al 2124	11.71	32.59	67.65
Al 6061	16.01	50.99	97.97
SiC	.045	-	.055

Table 2: Particle size of Al 2124, Al 6061 and Silicon carbide [97]

The exact chemical composition of Al alloys has been determined by X-ray fluorescence (XRF) using a spectrometer machine with a Rh tube at a voltage of 30 kV and a current of 1.020 mA. Table 3 shows the composition for both alloys [97].

Material	Al	Fe	Si	Cu	Mn	Mg	Zn
AA 2124	93.95	.0064	.058	3.88	.58	1.42	.034
AA 6061	97.83	.192	.69	.29	.016	.83	.012

Table 3: Chemical compositions of Al 2124 and Al 6061, respectively [97]

3.1.2 Ball milling procedure

Pre-alloyed Al alloys with (5, 10 and 15) wt. % SiC particles were ball milled to attain a homogenous mixture between the matrices and the reinforcement and bring down the material to the nano-range. In addition to the starting powder, 1.5 wt. % of Stearic acid was added in each patch as a process control agent (PCA) to avoid excessive cold welding. The milling was performed in a planetary ball mill (Fritsch Pulverisette 5) ; using stainless steel vials and balls (3.8 g/ball). Furthermore, a 10:1 ball-to-powder-ratio (BPR) was selected in all processes, greater BPR means higher chances for balls hitting the powder subjected to milling. The rotational speed of the vials is set to be 300 revolutions per minutes (rpm) and the milling process was halted for 30 minutes after one operational hour to avoid temperature build-up. To minimize oxygen contamination, the process ran under argon (Ar) atmosphere, and samples were taken after 1, 3, 5 and 10 hours for analysis and for removing any accumulation of unprocessed powder on the vials' walls.

3.1.3 Powder characterization using XRD, SEM, EDS and DSC

The milled powders after 1, 3, 5 and 10 hours of operation were subjected to analysis as mentioned earlier. The purpose of these investigations is to see the effect of milling time

and the reinforcement content on the morphology and homogeneity of the processed powder. JOEL-6510 series (Japan) Scanning Electron Microscope (SEM) and Tescan Lyra-3 (Czech Republic) Field Emission Scanning Electron Microscope (FE-SEM) were used to study the morphology of the powders. Furthermore, both machines are equipped with Oxford system for Energy-dispersive X-ray spectroscopy (EDS) and mapping that was utilized for compositional analysis. The number of frames was kept constant in all samples for the purpose of consistency. In addition, Bruker D8- X-Ray Diffractometer was employed for phase identification and crystallite size determination. Moreover, the XRD utilizes a Cu-Kα radiation with wavelength 0.154nm operating at a voltage of 40kV and a current of 40mA. The crystallite size was determined using the basic Scherer relation since Williamson-Hall relation was obsolete as well be discussed in the respective section. Furthermore, a shape factor (K) of (0.9) was used as shown in the following equation.

$$D = \frac{K\lambda}{\beta Cos(\theta)}$$

Where D is the mean crystallite size, K is the shape factor and it is usually between 0.8-1.0, β is the full-width at half maximum (FWHM), λ is wavelength of Cu-Kα radiation. DSC analysis was carried on using to see the structural evolution with aging as a function of content of nano-SiC.

3.2 Nanocomposite Consolidation

Most of the strength is attained when the developed powder is consolidated because most of the densification is occurring during sintering. Two approaches has been undertaken to

consolidate Al/SiC nanocomposite powders. Firstly, Spark plasma sintering was performed using a fully automated SPS machine (Type HP D-5, FCT Systeme, Rauenstein, Germany). Secondly, HIP sintering was accomplished using American Isostatic Press Inc; hold press HP 630, (USA). In either of the methods, the nanocomposite powders that were chosen for consolidation are those milled for five hours.

3.2.1 Spark Plasma Sintering (SPS)

In SPS, 3 grams of Al2124-x wt. % SiC and Al6061-X wt. % SiC composites were directly poured into a 20 mm graphite circular die through which the current is passed. Both the die and punches were covered with graphite sheet to ease the ejection of consolidate samples after the process completion. During sintering and before applying heat, a vacuum was created and a pressure of 35 MPa was applied between the graphite punches and maintained throughout the whole process; including cooling. After reaching the required pressure, samples were heated at a rate of 100 ^{o}C/minute to 400, 450 and 500 ^{o}C and held for 20 minutes before cooling at 100 ^{o}C/minute as well. The temperature is measured using a thermocouple inserted into the die through a drilled hole.

3.2.2 Hot isostatic pressing (HIP)

For HIPing nanocomposite powders, they were first cold compacted into a cylindrical billet of diameter 20 mm. The compaction was done at a pressure of 375 MPa and held for two minutes using an automated uniaxial press (Carver, USA). The compacted samples were stacked above each other in an alumina crucible and separated by a

graphite sheet to eliminate any possibility of contact between the samples. The vessel which contained the samples was first pressurized with high purity argon to 69 MPa and maintained during the whole process. Then, at a heating rate of 25 ^{o}C/minutes, the Sintering temperatures were also varied at 400, 450, and 500 ^{o}C for 20 minutes. Finally, the samples were cooled at the same rate as heating; 25 ^{o}C. The temperature was measured through two fixed thermocouples near to the alumina crucible.

3.2.3 Characterization of sintered samples

3.2.3.1 Density measurement

The density of the sintered nanocomposites was calculated using Archimedes principle and weights were measured using an electronic Densimeter. For the purpose of accuracy, the arithmetic average of three separate measurements was taken as the density of each sample.

3.2.3.2 Microstructural analysis

In order to study the different structural features such as distribution of nano SiC, presence of pores and defects and Al/SiC interfaces, JEOL JSM-6460LV (Japan); scanning electron microscopes (SEM) as well as optical microscope (MEIJI-Techno microscope, Japan) have been utilized. Prior to the analysis, the consolidated samples were cut into approximately two halves, and, then, one half was mounted using IPA 40 Remet, Bologna, Italy with the aid of Buehler Transoptic powder, IL, USA. After that, grinding and polishing were carried on using Handimet 2 Roll Grinder Buehler USA. Mechanical characterization

Micro-Hardness of the nanocomposites, prepared through SPS and HIP was measured using Vickers hardness machine (MMT-3 digital micro- hardness tester, Buehler, USA) using 300gf. The average value of 10 readings along the cross section was used as representative of the hardness of the samples. Moreover, nanocomposites that were consolidated at 500 ^{o}C were subjected to compression test using Instron standard 3367 Dual Column Tabletop Universal Testing System. The samples' length was 8 mm and the diameter was 4 mm i.e. L/D is 2 and the strain rate was 0.005 mm/minutes.

Alloy	PS (µ)	Reinf.	PS (µ)	Cont. (wt. %)	Mil. Time (h)	Other Condition	Characterization
Al 2124						BPR 10:1 Ar atmosphere Speed : 300 rpm PCA : 1.5 wt. % Material vials/balls: Stainless steel	XRD, SEM, EDS, Mapping and DSC
Al 6061	75	SiC	.055	5, 10, 15	0, 1, 3, 5, 10		

Table 4: Summary of the powder fabrication experimental process parameters

Alloy	Reinf.	Cont. (wt. %)	Mil. time(h)	SPS	HIP	Characterization
Al 2124	SiC	5, 10, 15	5	Temp : 400, 450, 500 oC Holding time : 20 min Pressure : 35 MPa Heating/cooling rate : 100 oC/min	Temp : 400, 450, 500 oC Holding time : 20 min Pressure : 69 MPa Heating/cooling rate : 20 oC/min	SEM, OM, density, hardness and compression tests
Al 6061						

Table 5: Consolidation experimental process parameters

CHAPTER 4

RESULTS AND DISCUSSION

4.1   Powder fabrication

4.1.1 SEM micrograph of the milled powder

Figure 7 shows the morphologies of the as-received pre-alloyed Al 2124 and Al 6061 particles, respectively. From the micrograph, the particles have nearly spherical shapes with broad size distribution.
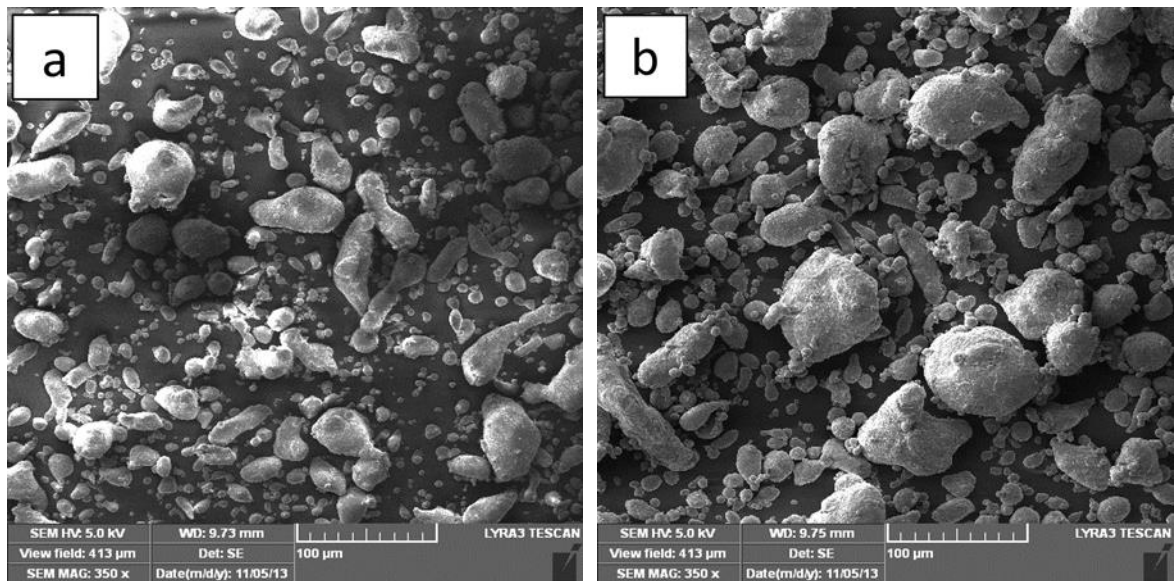
Figure 7: SEM micrographs showing the morphologies of (a) Al 2124 (b) Al 6061

As for the reinforcement, the TEM micrograph in figure 8 (a) illustrates that nano-SiC particles are almost spherical and within the specified particle size of the product. Moreover, the tendency to agglomeration of nano-SiC is shown in figure 8 (b) and is explained by the strong frictional forces that exist between particles. These forces are

greater in the nano-range and they include electrostatic, van der Waals, and surface adsorption [60].
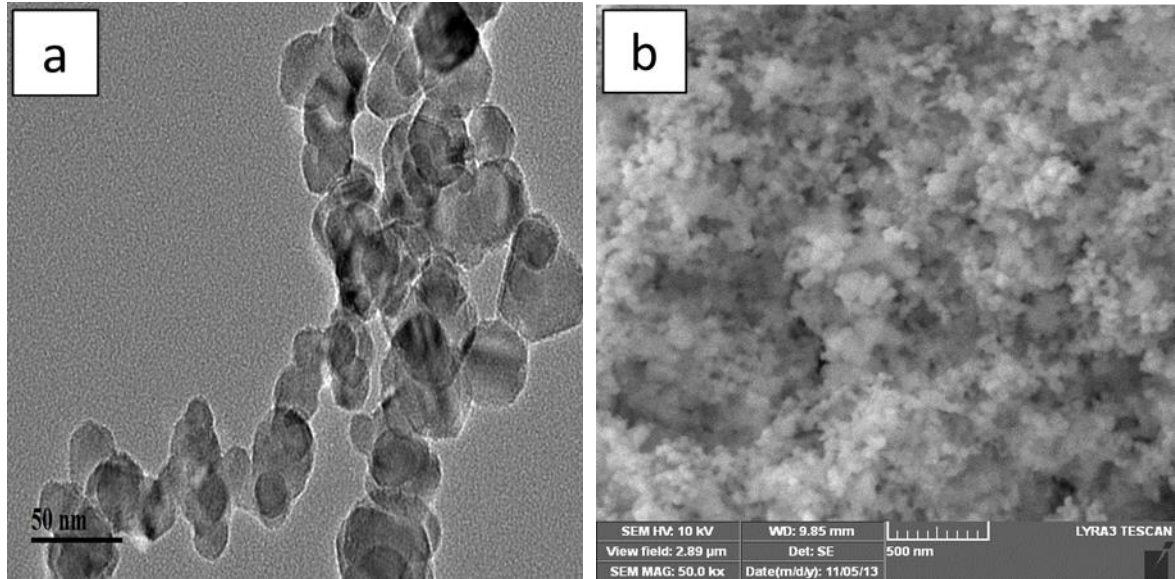
Figure 8: Nano-sized SiC morphology as shown by (a) TEM and (b) SEM

The pre-alloyed Al 2124 was milled with nano-sized Silicon Carbide used a reinforcement, (1-2) grams were taken after (0, 1, 3, 5 and 10) hours of operation for analysis. Figure 9 (a), (b) and (c) shows the starting powder before starting the milling where we can see that nano-sized SiC particles are attached to the large Al 2124 particles as evident by EDS spot analysis (d) .

31
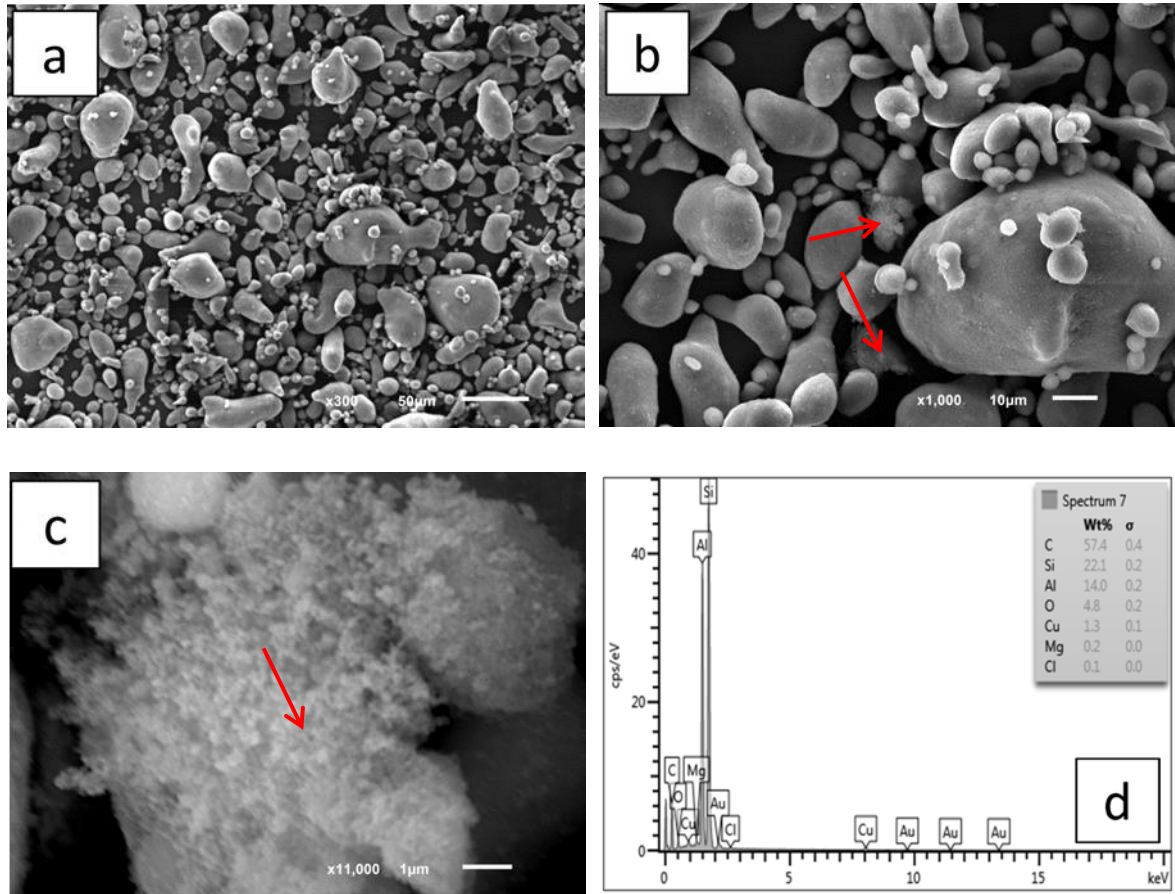
Figure 9: SEM micrograph showing Al 2124/ 5 wt.% SiC before milling (a) 300x (b) 1000x (c) 11 kx and (d) Spot analysis of the selected area.

Figure 10 shows the effect of milling time on the morphology of Al 2125/ 5 wt. % SiC composite powder. During the early stages of milling, the soft Al 2124 particles were seen to be plastically deformed and flattened due to balls-powder-ball and ball-powder-wall collisions [Figure 10 (a)]. At the same time, the brittle nano-SiC particles were expected to embed within the ductile flattened aluminum particles according to the general theory of milling [40]. Next, it is observed that the flattened Al 2124 shape was still preserved; however, with a smaller size due to the plastic deformation energy exceeding the compressive strength of composite powders [Figure 10 (b)]. After that, the ongoing collisions that cause welding/re-welding phenomena formed rounded and

equiaxed Al 2124/SiC composite particles [Figure 10 (c)]. As the milling proceeded to 10 hours, no significant reduction in the particle size, though more equiaxed particles were formed [Figure 10 (d)].
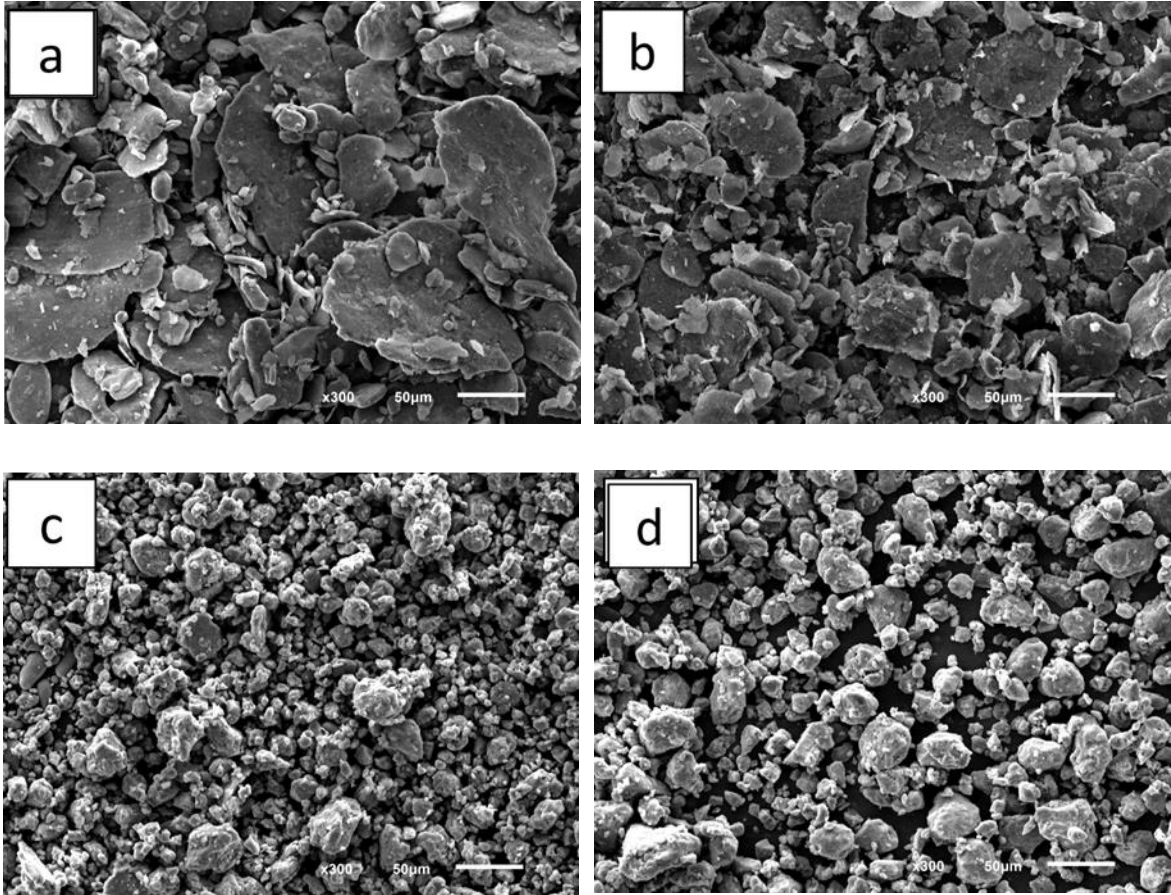
Figure 10: SEM micrographs showing Al 2124/5 wt% SiC at 300x after (a)1 h (b)3h (c) 5 h (d) 10 h

Another important observation is that with increasing the SiC content, the milling process is accelerated because the hard silicon carbide particles assist the grinding process of powder (Figure 11). A comparison has been made between Al-4.5% Cu and Al-4.5% Cu/SiC composites and found that the composite reached to a steady state of milling faster [49].
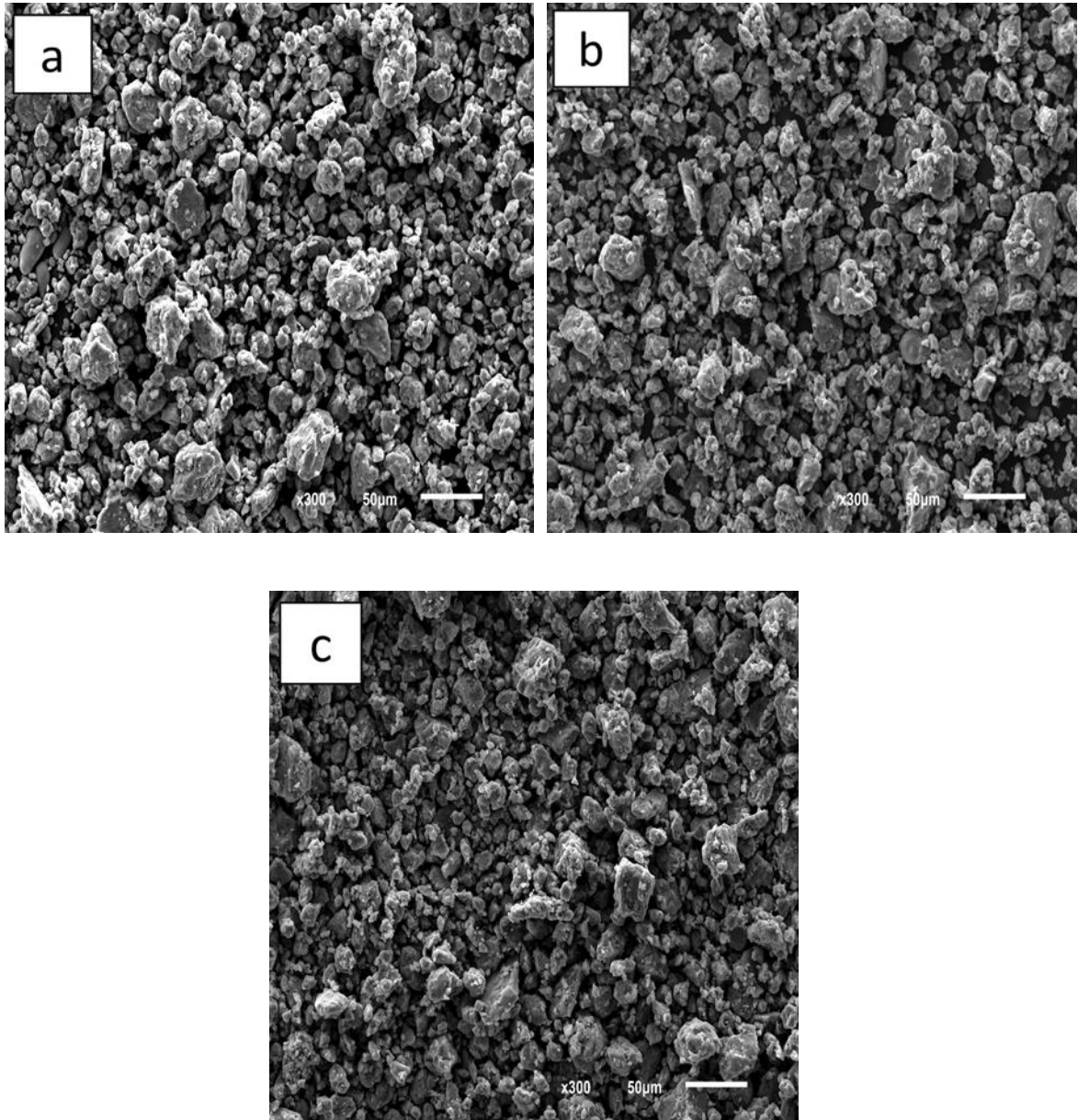
Figure 11: SEM micrographs showing Al 2124/x wt% SiC at 300x milled for 5 hours (a) 5% SiC (b) 10% SiC (c) 15% SiC

To investigate the milling time factor effect on homogenizing the two ingredient (i.e. Al 2124 and nano-SiC), EDS and mapping were carried on. Figure 12 shows the mapping for Al 2124/ 5 wt. %SiC nanocomposite with milling time; – from left to right - the original micrograph, Aluminum and Silicon traces, respectively. The concentrated areas

of silicon element in [Figure 12 (a) and (b)] for 1 and 3-hour milled powders are higher than those of 5 and 10.

As the milling progressed, the silicon traces become more distributed among the matrix which indicates that nano-sized silicon carbide particles embedded within the aluminum particles and formed relatively homogenous Al 2124/SiC composites. Moreover, no significant distinction between five-hour milled and 10-hour milled nano-composites [Figure 12 (c) and (d)]. Thus, by analyzing powder composition using mapping for Al 2124/5% SiC for 5 hours, this milling time gives an appropriate distribution of SiC with Aluminum matrix. Mostaed reached to the same conclusion but using micron-size SiC and BPR of 20:1 for Al-4.5% Cu/SiC composite [49].

The effect of nano-SiC content was, also, monitored. Figure 13 shows the EDS mapping for 5%, 10% and 15 wt.% SiC reinforced Al 2124. It can be noticed that a greater presence of nano-SiC within the area of investigation as a result of increasing the reinforcement content.

Original micrograph	Aluminum traces	Silicon traces
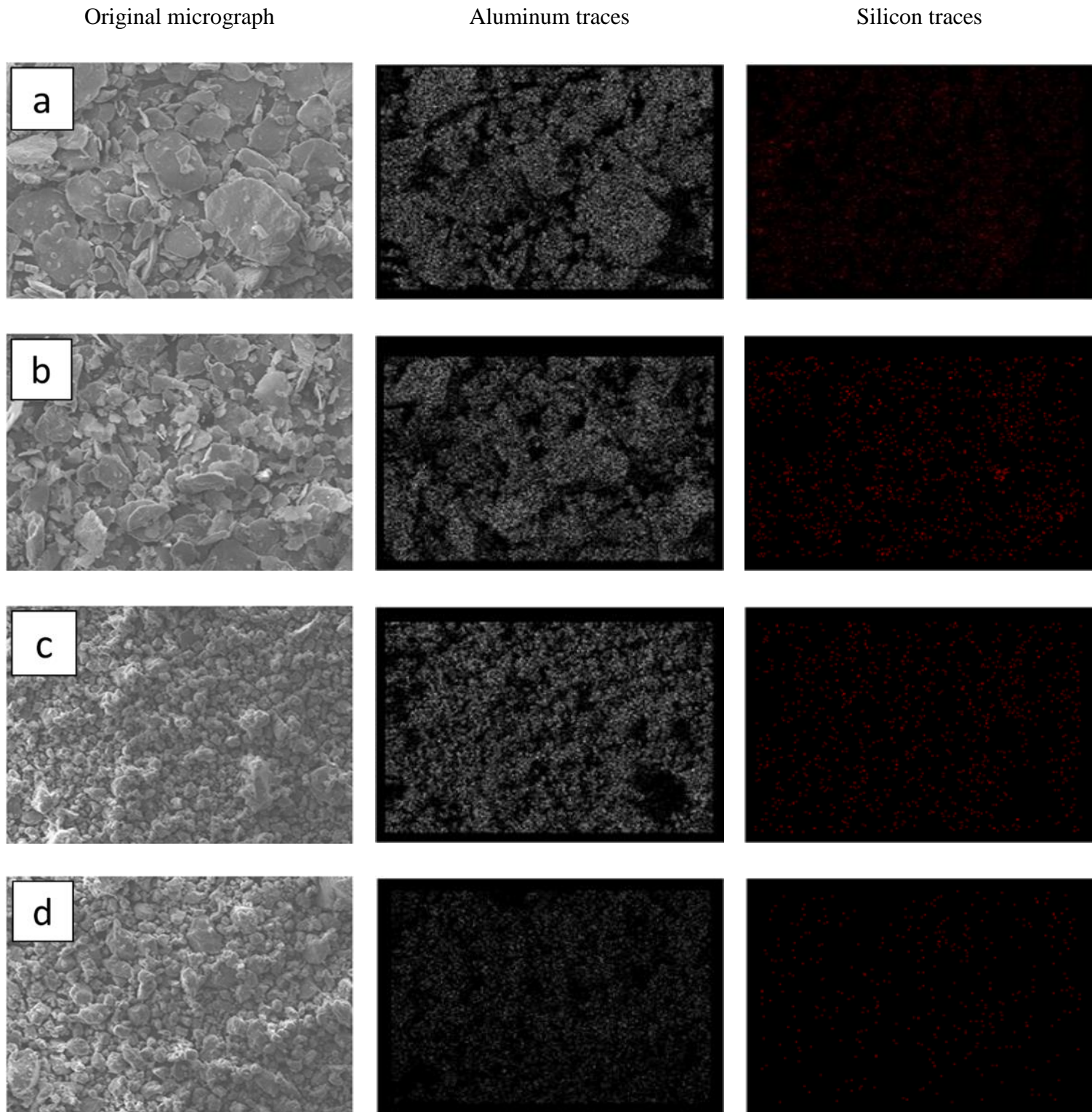
Figure 12: EDS mapping showing the distribution of 5 wt.% SiC in Al 2124 after (a) 1 h, (b) 3 h, (c) 5 h, (d) 10 h

Original micograph	Aluminum traces	Silicon traces
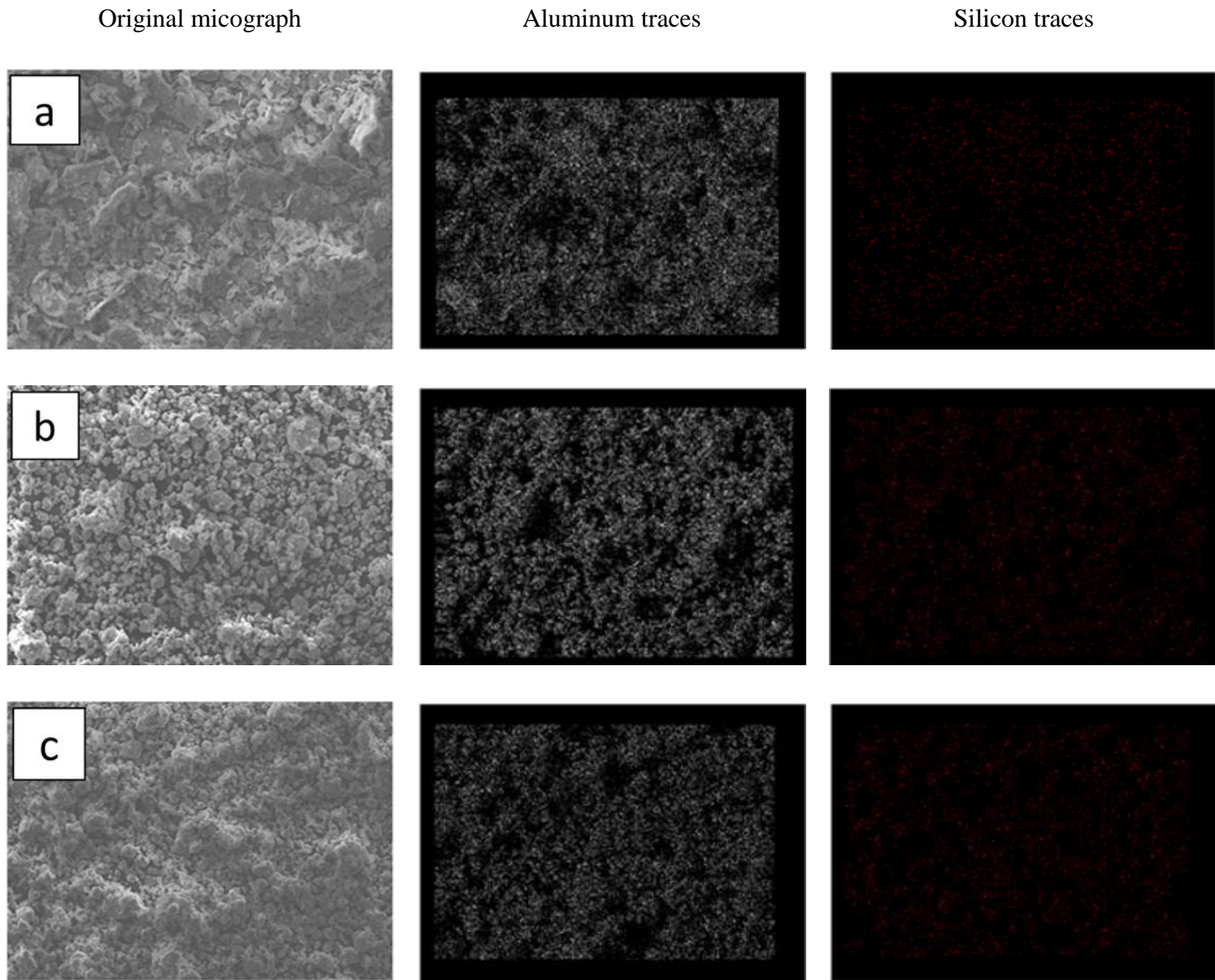
Figure 13: EDS mapping showing the distribution 5-hour milled of x. % SiC in Al 2124 (a) 5%, (b) 10%, (c) 15%

Typical behavior that was discussed earlier for Al 2124/nano-SiC composite powder was exhibited by Al 6061/nano-SiC composite powder. Higher milling time produces more equiaxed particles and potentially facilitates the good distribution of nano-SiC within the Al 6061 matrix particles as a result of consecutive collisions [Figure 14]. At higher milling time or higher concentration of nano-SiC, the particles were no longer capable of

37

flattening because embedding nano-SiC made them harder (i.e. more brittle). Therefore, they started to fracture due to the developed brittleness among powders and, hence, the energy transferred to the powder exceeded the compressive strength which resulted in more fracturing. Increasing the milling time further will only generate more equiaxed powder with similar particles sizes. This agrees with the general theory of mechanical milling process.

Similarly, mapping was done on the Al 6061/SiC powders. Increasing milling time – as expected – promote good distribution of nano-SiC in Al 6061 powders [Figure 15]. After 5 hours of milling, it can be seen that there is a relatively good homogeneity between the matrix and the reinforcement particles.
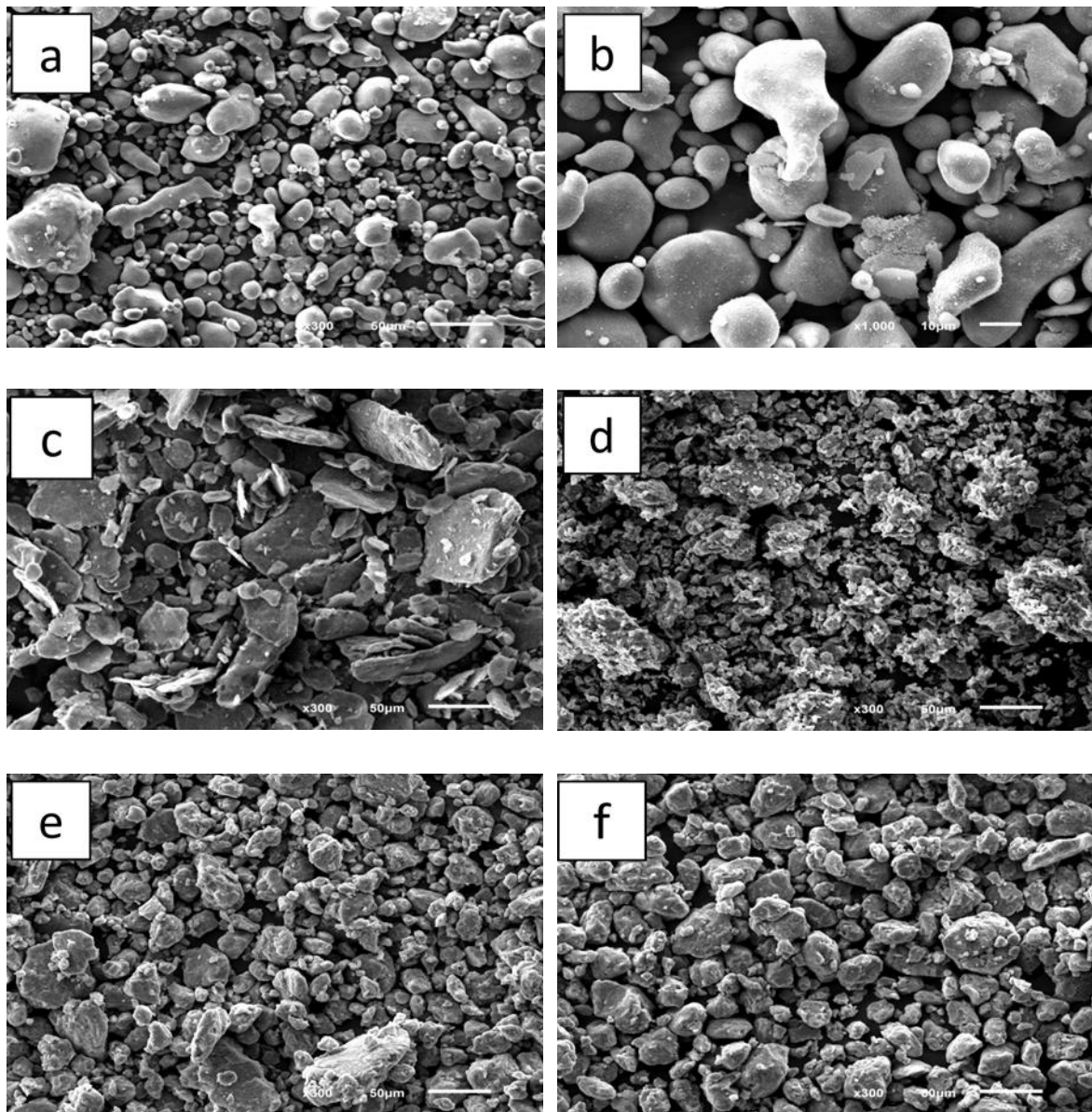
Figure 14: SEM micrograph showing Al 6061/5 wt% SiC after (a) 0 h, 300x, (b) 0 h, 1000x, (c)1 h. 300x, (d)3h, 300x, (e) 5 h, 300x, (f) 10 h, 300x

Original micograph   Aluminum traces   Silicon traces
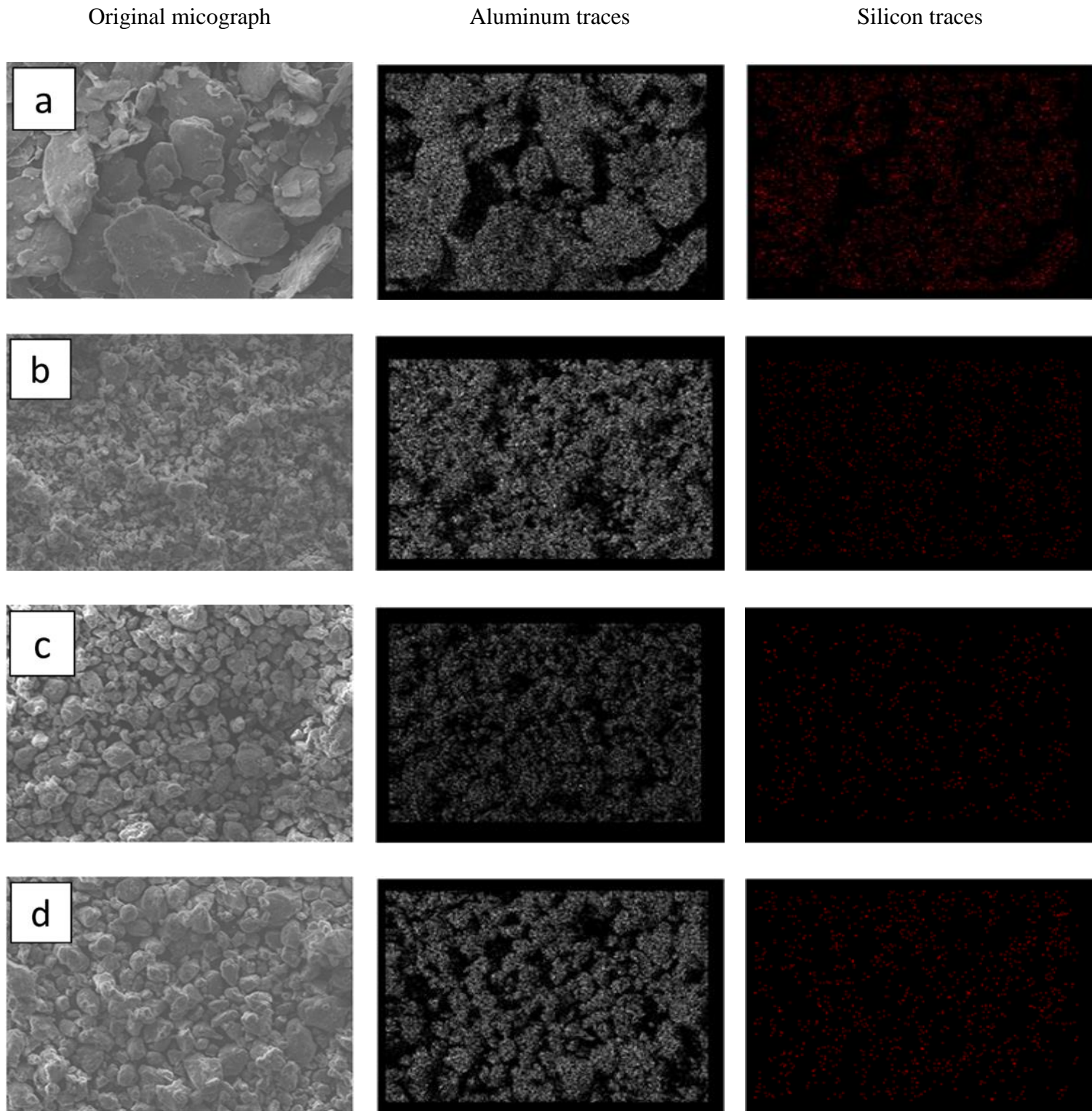
Figure 15: EDS mapping showing the distribution of 5 wt.% SiC in Al 6061 after (a) 1 h, (b) 3 h, (c) 5 h, (d) 10 h

| Original micrograph	Aluminum traces	Silicon traces
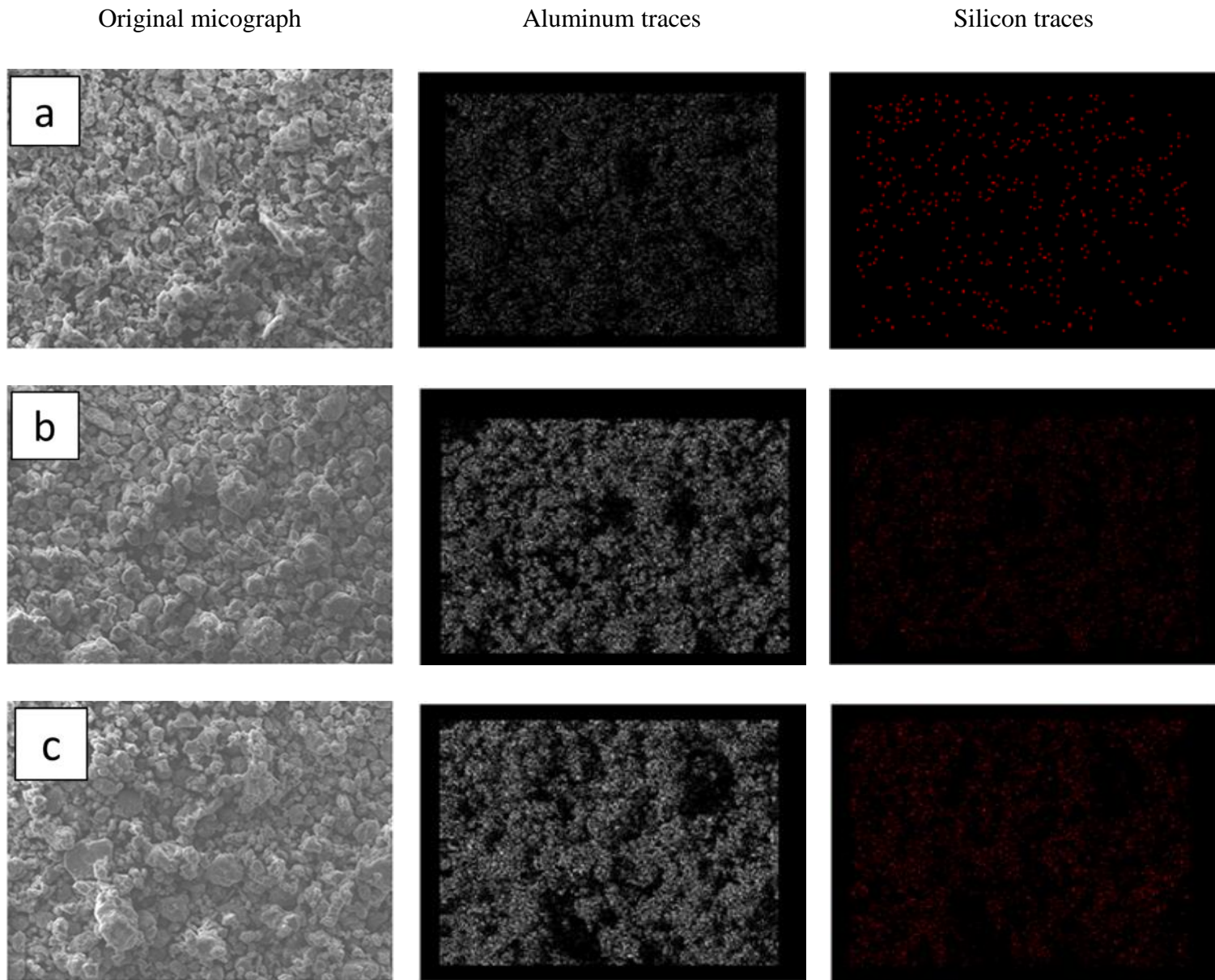
Figure 16: EDS mapping showing the distribution 5-hour milled of x. % SiC in Al 6061 (a) 5%, (b) 10%, (c) 15%

4.1.2 X-ray diffractometer of milled powder

X-ray diffractometer was utilized to identify the formed phases – if any - and to determine – roughly - crystallite size. Mechanically milled Al 2124/ 5 wt. % SiC composite powders for 1, 3, 5 and 10 hours diffraction pattern is shown in figure 17. It worth noting that no phases – other than Aluminum and SiC - were detected as result of mechanical milling and this is one of the advantages of using solid-state processing of materials. Parvin [95] studied the effect of milling on 6061/SiC composites and he showed that after 5 hour of milling a precipitate of Mg_2Si is detected by a small peak using XRD which wasn't the case in our experiments and this could be because of the processing condition.

Moreover, at low concentration of nano-SiC (i.e. 5 wt. %), only aluminum peaks were apparent. However, for higher concentration (i.e. 10 wt. % and 15 wt. %) of nano-SiC, peaks that corresponds to SiC were detected as illustrated in figure 18. This is presumably that 5 wt% SiC is under the detectability limit of XRD.
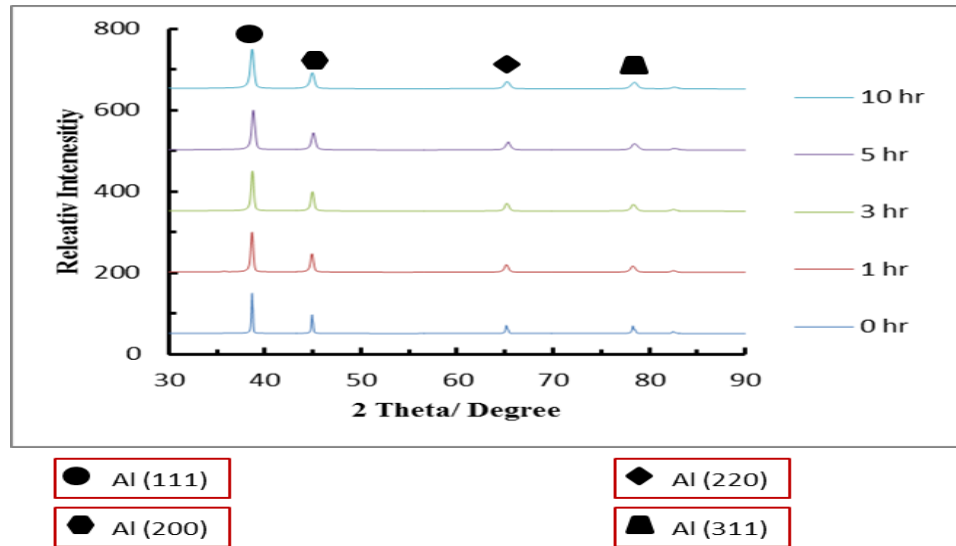
Figure 17: X-ray diffraction patterns of Al 2124/ 5 wt. % SiC at different milling time
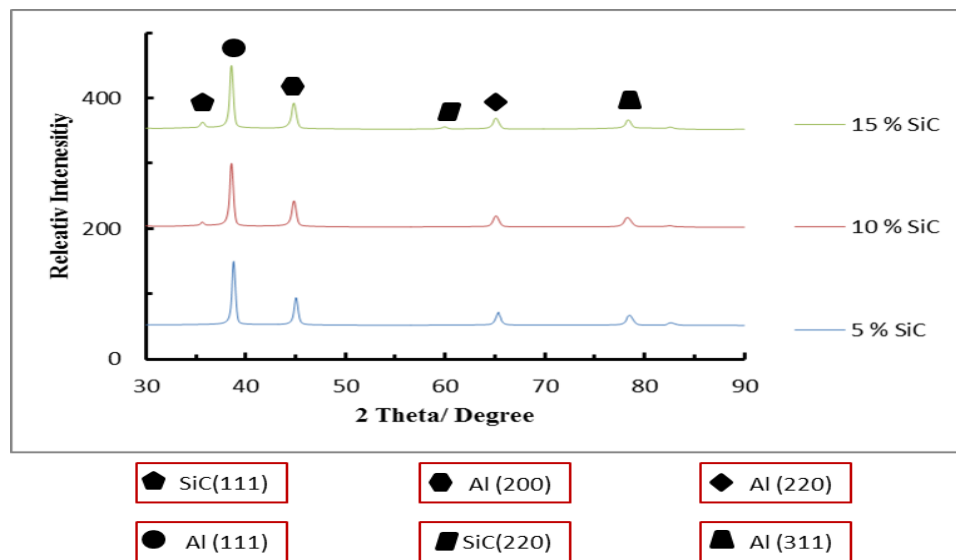
Figure 18: X-ray diffraction patterns of Al 2124/ x wt. % SiC at 5 hours of milling

Also, it can be seen that as the milling time increased, the peaks were broadened and their intensities were lowered which suggest a reduction in the crystallite size and the accumulated strains induced through the process.

In order to estimate the mean crystallite size, the famous Williamson-Hall method has been followed which separates crystallite sizes and micro-strain from the integral breadth or FWHM of peaks [99]. The Williamson-Hull plots are shown in figure 19 for Al 2124/5% SiC milled for 1, 3, 5 and 10 hours.
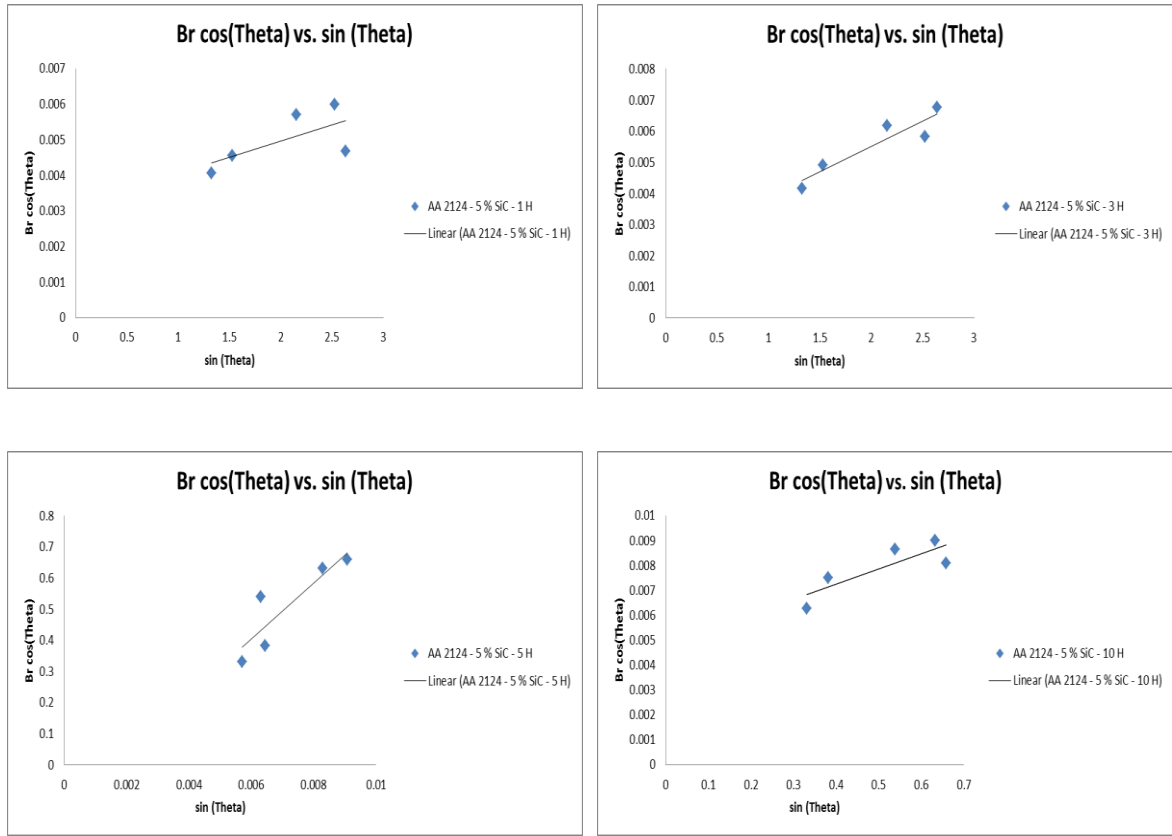
Figure 19: W-H plots for Al2124/5% SiC for different milling time

As seen from the graphs, the linear fitting doesn't represent the calculated points which give erroneous y-intercepts and, hence, un-realistic crystallite size [100]. Furthermore, the source behind this deviation is attributed to the anisotropic strain which is related to the strain broadening of XRD peaks and is ignored in W-H method. Anisotropic strain

44

can explain the scattering in the data and it can be evaluated by several advanced models and algorithms [101]. Ungar has proposed a new modification on the conventional W-H method by incorporating a contrast factor of dislocation and termed it as the modified W-H method [102]. Several other approaches such as: whole powder pattern modelling (WPPM) has been proposed to use physical models of the microstructures and then develop theoretical expression in order to mimic the experimental line profile [103, 104].

Despite these advancements in computing the mean crystallite size, the basic Scherer equation is still much used for its simplicity [104]. Figure 20 is a graph showing the effect of milling time and nano-SiC concentration on crystallite size of Al 2124 as calculated by Scherer equation. It can be seen that increasing the milling time resulted in a smaller crystallite size due to more chances for fracturing. However, we couldn't see any marginal effect of increasing the amount of SiC reinforcement.
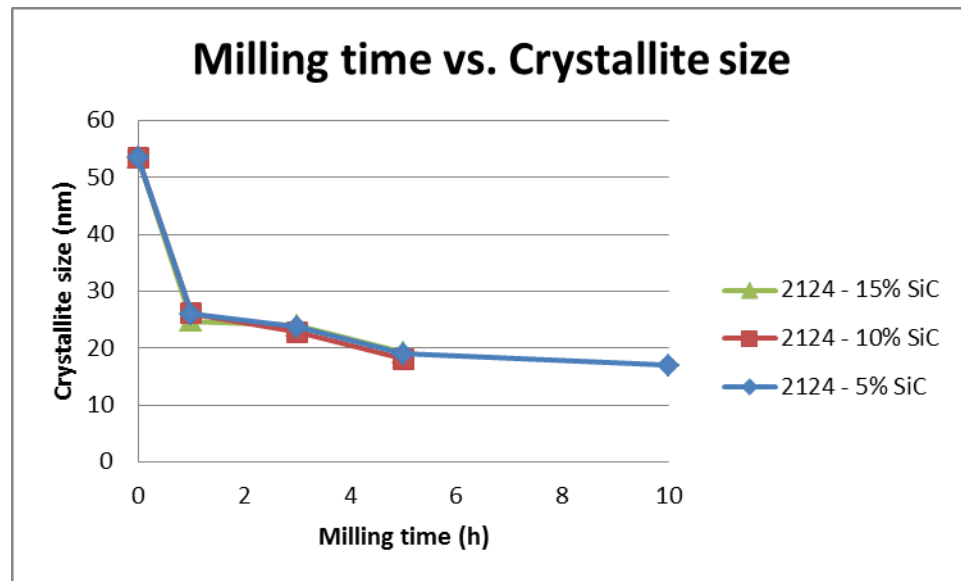
Figure 20: Scatter plot shows the reduction in crystallite size as the milling progress for Al 2124/ x wt. % SiC

The statements and conclusions that were made for Al 2124/nano-SiC composites are still true in the case of Al 6061/nano-SiC composites. XRD didn't detect any phases – other than aluminum and SiC – in all duration and stages of mechanical milling as illustrated in figure 21. Furthermore, the XRD graph showed that a decreased in the peak intensity as well as a broadening in the peaks which indicates the decrease in the crystallite size [69]. The crystallite size is brought down to nano-range after the milling process as indicated in figure 22 and it is calculated by Scherer in figure 23. By the use of HRTEM, Mostaed [49] proved the starting micro-sized Al-4.5% Cu and SiC reached to the nano level after 5 hours of milling
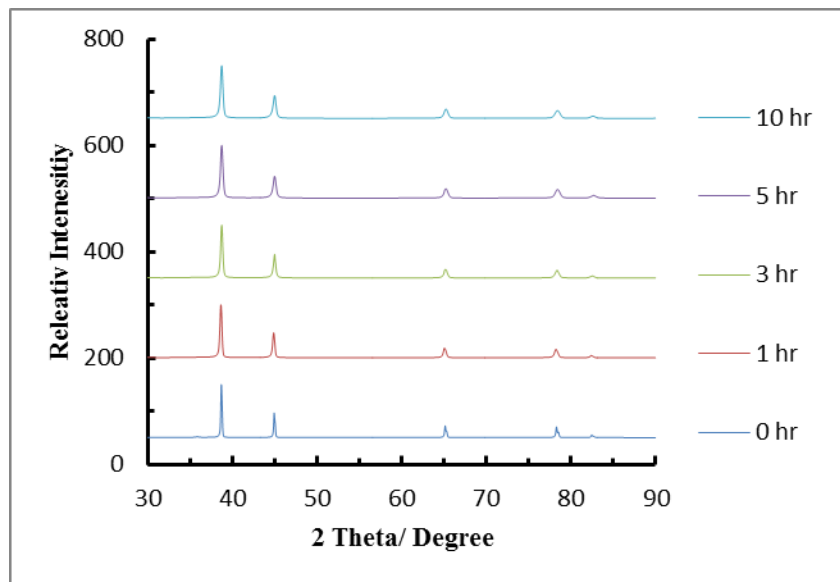
Figure 21: X-ray diffraction patterns of Al 6061/ 5 wt. % SiC at different milling time
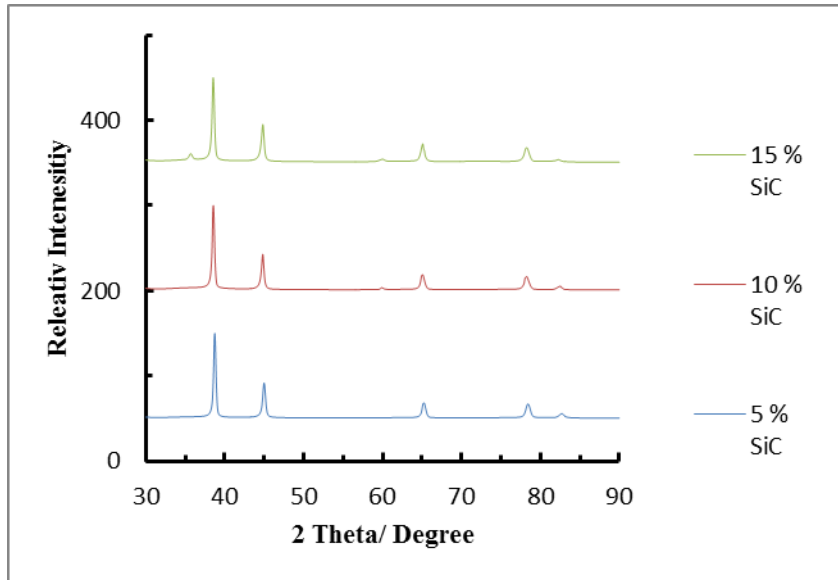
Figure 22: X-ray diffraction patterns of Al 6061/ x wt. % SiC at 5 hours of milling
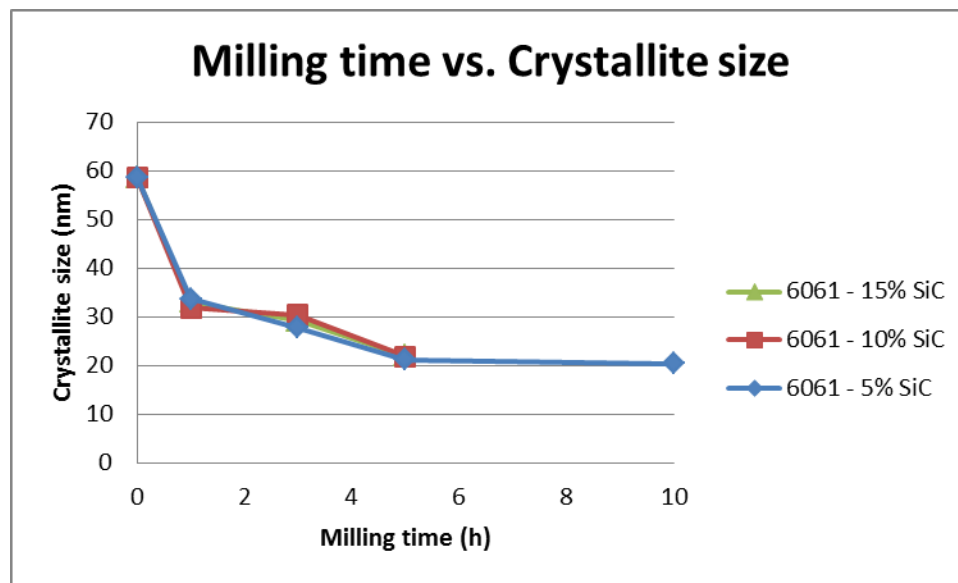
Figure 23: Crystallite size versus the milling progress for Al 6061/ 5 wt. % SiC

4.1.3 Calorimetric study on the milled powder by DSC

An artificial aging has been experimented on Al 2124/SiC and Al 6061/SiC nanocomposite to understand the role of nano-SiC on aging kinetics of both alloys. Figure 24 and 25 show the DSC thermographs of the studied MMCs at a heating rate of

10 ^{o}C/ min in order to increase the resolution of the data.
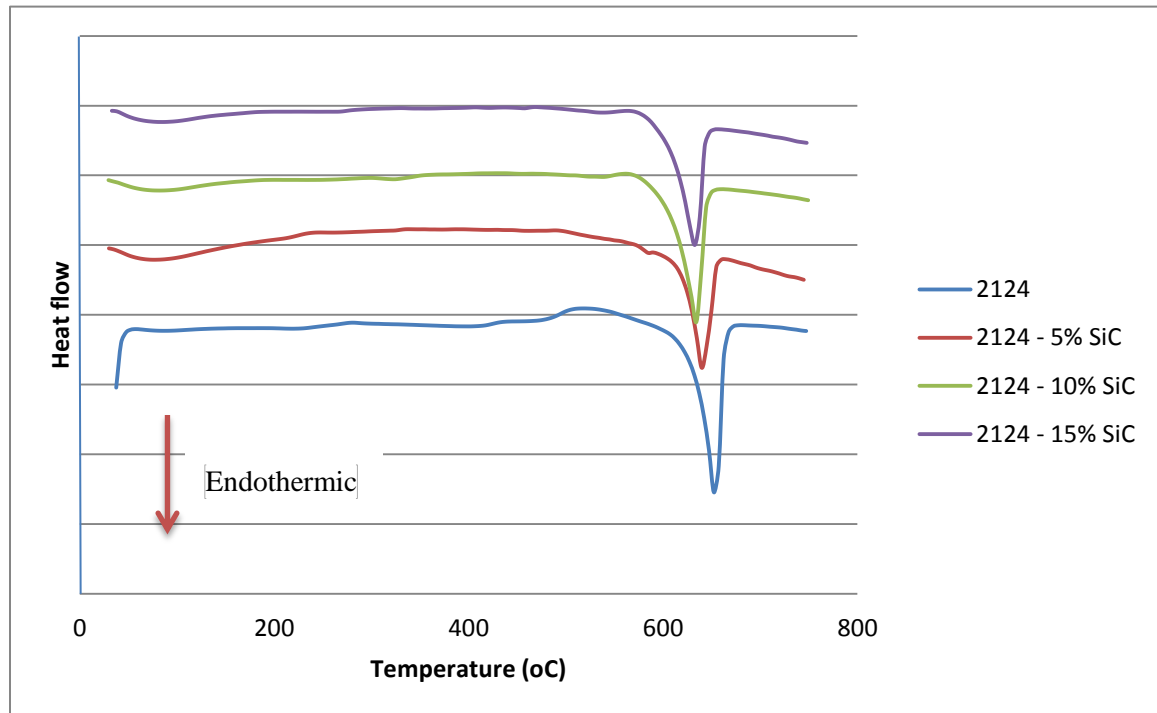
Figure 24: DSC thermographs showing aging kinetic of Al 2124/SiC nano-composite milled for 5 hours
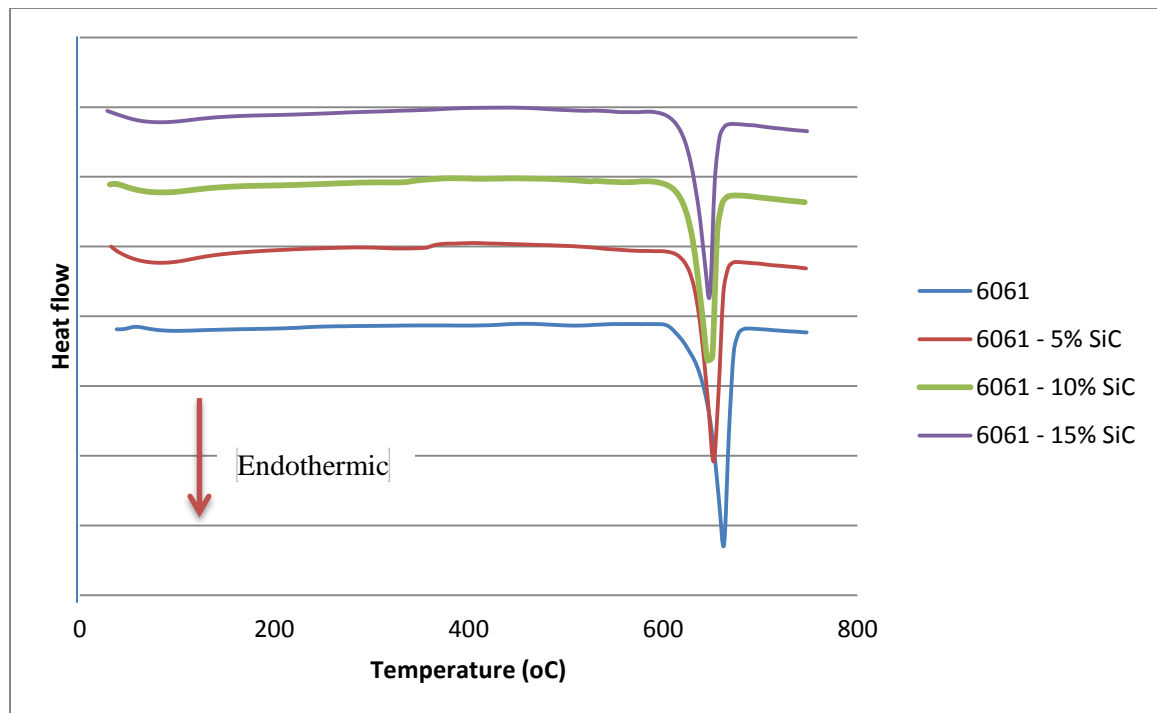
Figure 25: DSC thermograph showing aging kinetic of Al 6061/SiC nano-composite milled for 5 hours

The melting points and the approximate onset of melting for the unreinforced alloys and their composites have been detected and summarized in Table 6. Generally, the thermographs show that alloys and their composites are look-alike which indicates the minimal effect of nano-SiC on the aging kinetics compared to their alloys. Moreover, from the table, it is seen that the additions causes an accelerated aging. At first, the melting point dropped by 10-15 ^{o}C compared to the unreinforced alloys for Al 6061/5 wt.% SiC and Al 2124/5 wt.% SiC, respectively. After that and with further addition of nano-SiC, the shifting toward a lower melting temperature decreased by~5 ^{o}C and~1 ^{o}C for 5 to 10 wt. % and 10 to 15 wt. %, respectively.

Alloy	% SiC	Melting temperature (^{o}C)	Approx. Onset of melting (^{o}C)
Al 2124	0	654	630.9
	5	640.9	616.5
	10	635.6	604
	15	634.4	601.9
Al 6061	0	662	640.6
	5	652.0	632.2
	10	648.3	624.1
	15	647.3	623.7

Table 6: Peak and onset melting points of Al 2124 and Al 6061/SiC nanocomposites.

The shift of the melting temperature can be attributed to sever plastic deformations during milling and the thermal miss-match between the matrices and reinforcements. Thus, those lead to generation of point and lattice defects: vacancies, interstitials,

49

dislocations, antiphase domain boundaries, etc. [90, 91]. The high number of defects densities offer a rapid diffusion baths which result in accelerated aging [90, 92, 93].

4.2   Consolidation of composite powder

The potential applications of the developed powder rely heavily on the consolidation process; this is because most of the strength and density are attained during consolidation. Two methods have been followed, one is non-conventional Spark Plasma Sintering SPS, and the other is the conventional Hot Isostatic Pressing (HIP). This chapter is divided into two broad sections, the first is going to address Al 2124/ x wt. % SiC consolidation and characterization, then Al 6061/x wt. % will be discussed in the second section. In both consolidation methods, the nanocomposite powders that were chosen are those which were milled for five hours. Five hours of milling as shown from the previous chapter lead to a good distribution of nano-SiC within the aluminum alloys. Even after the consolidation, the sample preserved their distribution as shown in figure 26. Parvin studied the effect of milling Al 6061/SiC composites on the hardness. He used furnace sintering coupled with hot extrusion [68]. No significant increase in hardness value between those milled at 5 hour (70 HRB) and 9 hour (82 HRB). Combining the crystallite size and hardness values at 5 hour and 9 hour milling suggest that the choice of 5 hour milling for our experiments is reasonable.

Original micograph	Aluminum traces	Silicon traces
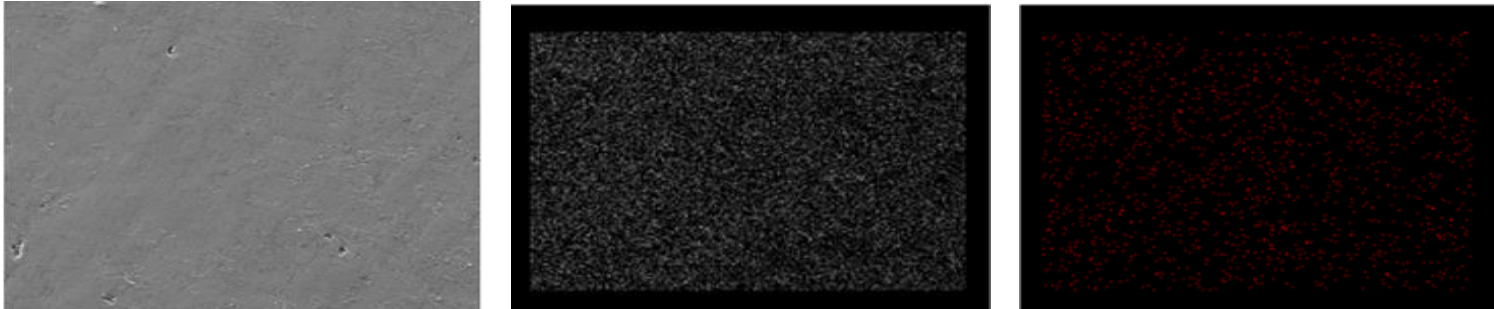
Figure 26: EDS mapping for Al 6061/5% SiC sintered by SPS at 400 °C

4.2.1 Al-based alloy 1 (Al2124) containing SiC

4.2.1.1 Spark Plasma Sintered samples

Figure 27 shows the optical micrographs magnified 200 times of Al 2124/ 5 wt. % SiC sintered at 400, 450 and 500 °C, respectively. It can be shown that porosity content is decreased as the sintering temperature increases. This is due to higher diffusivity of materials at higher temperature and sintering is considered as a thermally activated process. Moreover, figure 28 illustrates that increasing the SiC content results – generally - in higher porosity due to the overall improvement in hardness.
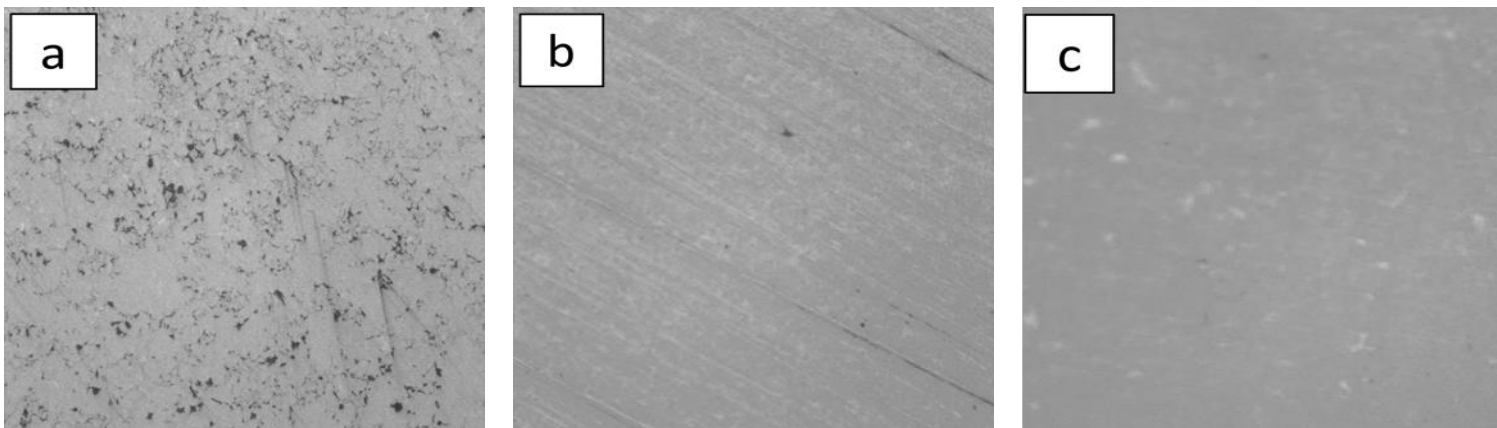
Figure 27: Optical micrograph showing SPS fabricated Al 2124/5 wt. % SiC sintered at (a) 400 (b) 450 and (c) 500 °C magnified to 200X
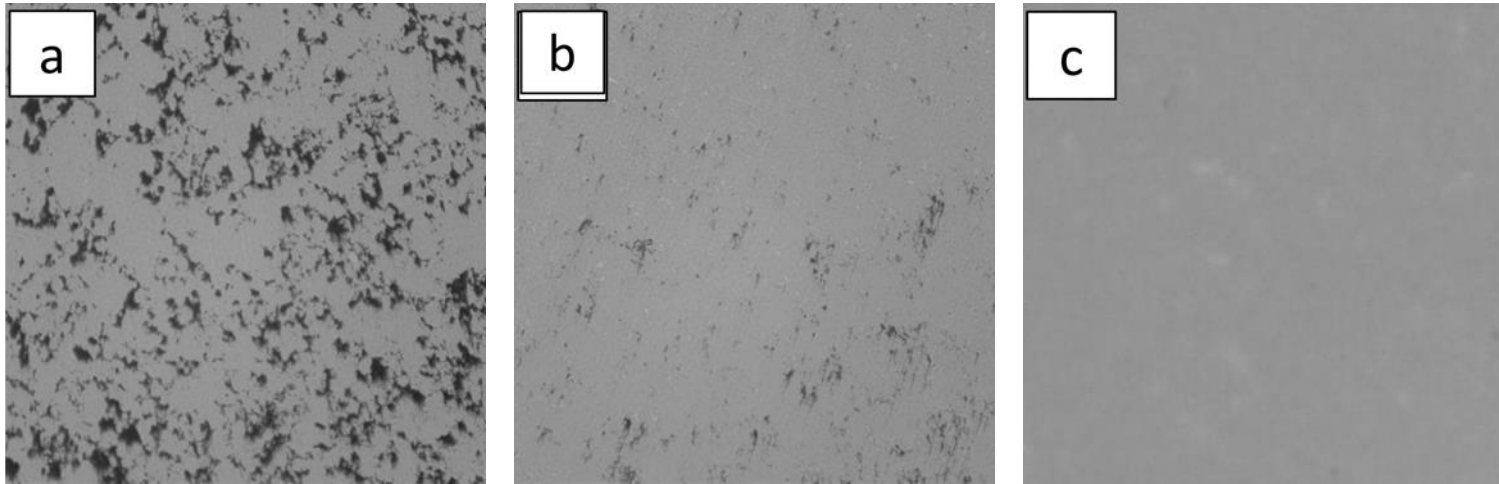
Figure 28: Optical micrograph showing SPS fabricated Al 2124/15 wt. % SiC sintered at (a) 400 (b) 450 and (c) 500 ^{o}C magnified to 200X

Figure 29 shows the SEM micrograph of Al 2124/ 5% SiC sintered at 400, 450 and 500 ^{o}C using Spark Plasma Sintering (SPS). As illustrated from the Optical Micrograph (OM) figures, increasing the sintering temperature reduced the amount of porosity. Figure 30 replicates figure 29 except changing the concentration of SiC reinforcement. At 400 and 450 ^{o}C, the porosity level can be seen high compared to samples sintered at 500 ^{o}C. Thus, SEM micrographs in both cases, also, suggest that increasing the sintering temperature promotes higher densification.
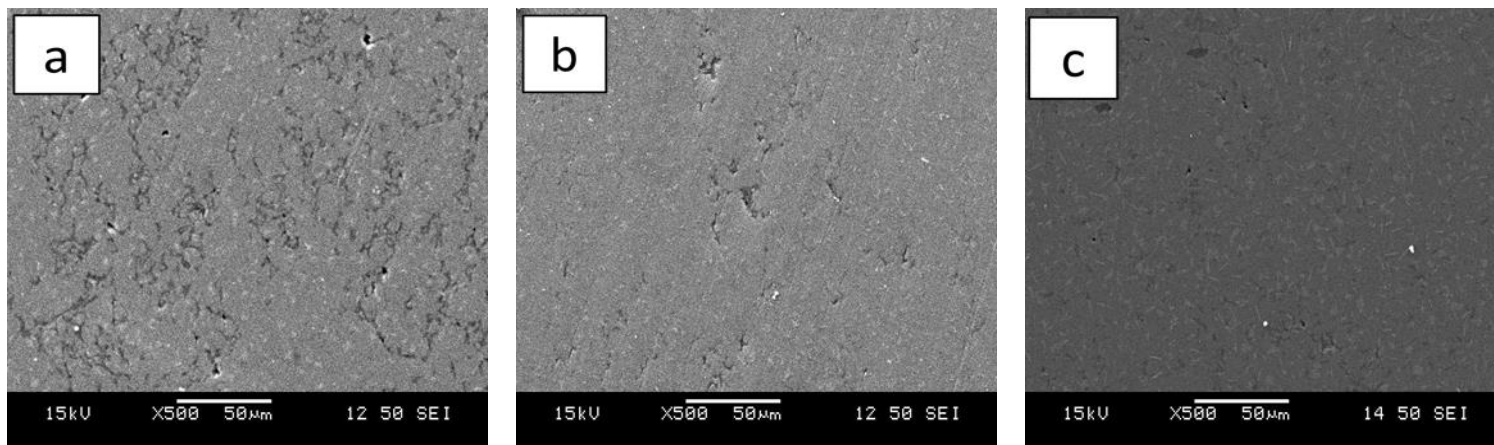
Figure 29: SEM micrograph showing SPS Al 2124/ 5 wt. % SiC sintered at (a) 400 (b) 450 (c) 500 ^{o}C
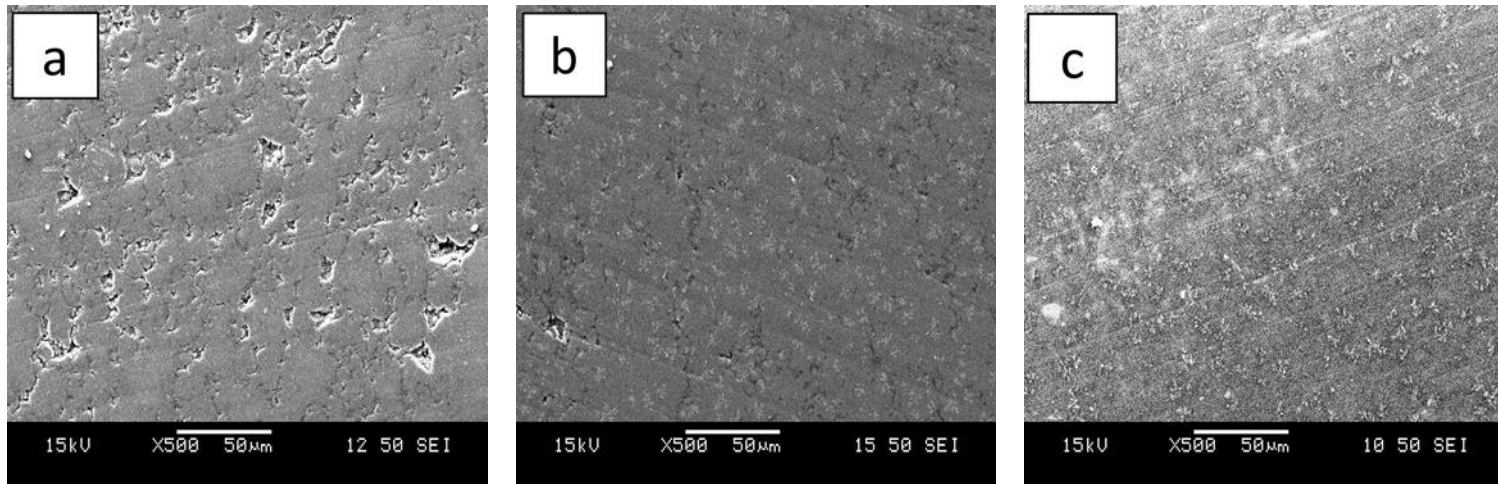
Figure 30: SEM micrograph showing SPS Al 2124/ 15 wt. % SiC sintered at (a) 400 (b) 450 (c) 500 °C

The densification and hardness are related properties; highly dense material is usually harder than those with lower density. Al 2124/x wt. % SiC composites fabricated by SPS were no exception. It has been mentioned earlier that increasing the sintering temperature results in increasing the density. This is attributed to the elimination of porosity as evident by optical and SEM micrographs [Figures 27-30].

Figure 31 shows the densification of Al 2124/ x wt. % SiC composites as a function of temperature and SiC content. From the figure, it is seen that increasing the SiC content – due to the gained hardness – gives a lower density in samples sintered 400 and 450 °C, respectively. However, at 500 °C, Al 2124 reinforced with 10% and 15% of SiC showed higher densification than Al 2124/ 5 wt. % SiC. This could be as a result of formation of liquid phase and the good wettability between the SiC and the melt [40]. Another aspect is that silicon carbide particles induce stress fields which enhance the diffusivity of the melt. Matrices with higher SiC content showed higher densification [40, 96].

Updhayay sintered his Al 6061 and Al 2014/SiC composites using furnace sintering at 635 ^{o}C. He reasoned that enhanced densification is due to liquid formation during sintering. Moreover, the formed liquid diffuses when more silicon carbide is added since it is subjected to higher stress fields induced by SiC particles [40]. Madej [96] also noticed similar behavior for WC-steel composites. He explained the results by liquid phase formation as a result of reaction between tungsten carbide and steel.
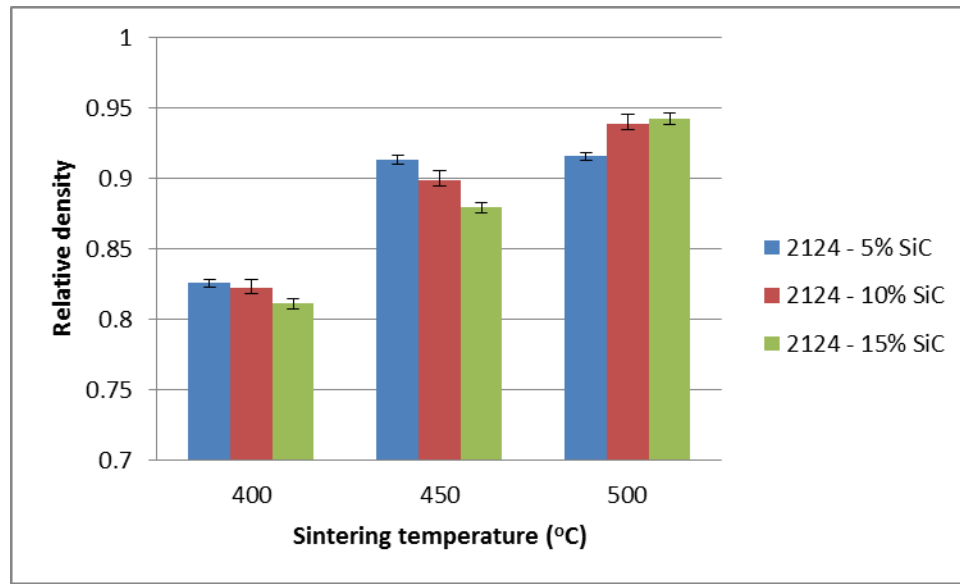
Figure 31: Bar graph showing the relative density SPS sintered Al-2124/x wt. % SiC composites sintered at 400, 450 and 500 ^{o}C

On the other hand, hardness increases with increasing the content of silicon carbide as well sintering temperature [Figure 32]. Nouari studied the effect of sintering temperature using SPS and MS on pre-alloyed 6061 and 2124, which is shown in the dotted curve [97] .It is believed that the increase in hardness is caused by the increased densification and pores annihilation. Moreover, there could be fine hard precipitates such as: Mg_2Si, $CuAl_2$, and $CuMgAl_2$ which contributes to the improved hardness [97]. Table 7 shows the values for the hardness and density of Al 2124/x wt% SiC.
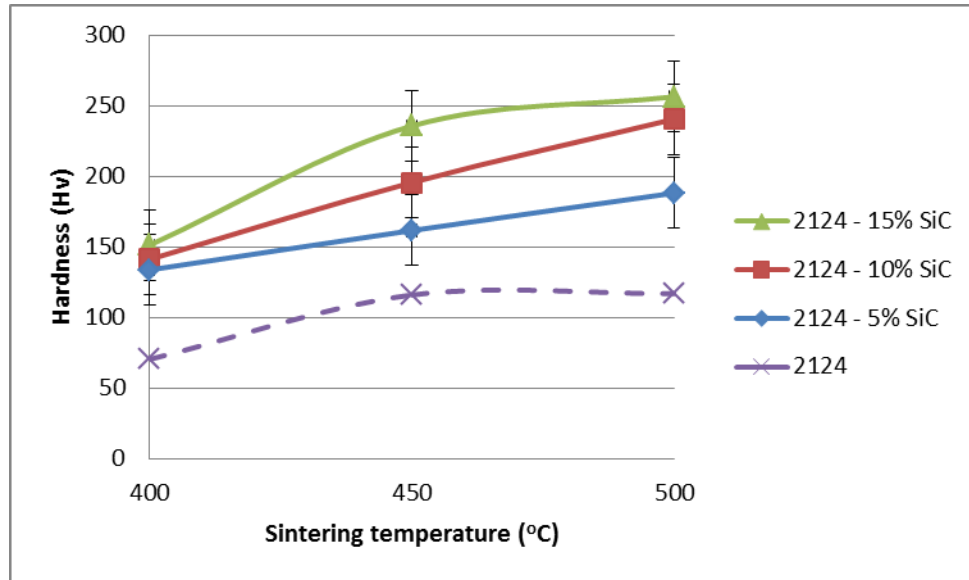
Figure 32: A line graph showing the hardness values of SPS Al 2124/x wt. % SiC as a function of SiC content and sintering temperature

		Density			Hardness		
Alloy	**% SiC**	Sintering Temperature			Sintering Temperature		
		400	450	500	400	450	500
2124	5	82.56	91.34	91.54	133.91	161.78	188.26
	10	82.20	89.84	93.89	141.37	195.72	240.58
	15	81.09	87.91	94.20	151.44	235.69	256.41

Table 7: Hardness and relative density of SPS sintered Al 2124/SiC nanocomposites

X-ray diffractions of SPS sintered samples are shown in Figure 33, and no significant phases were detected as a result of sintering.
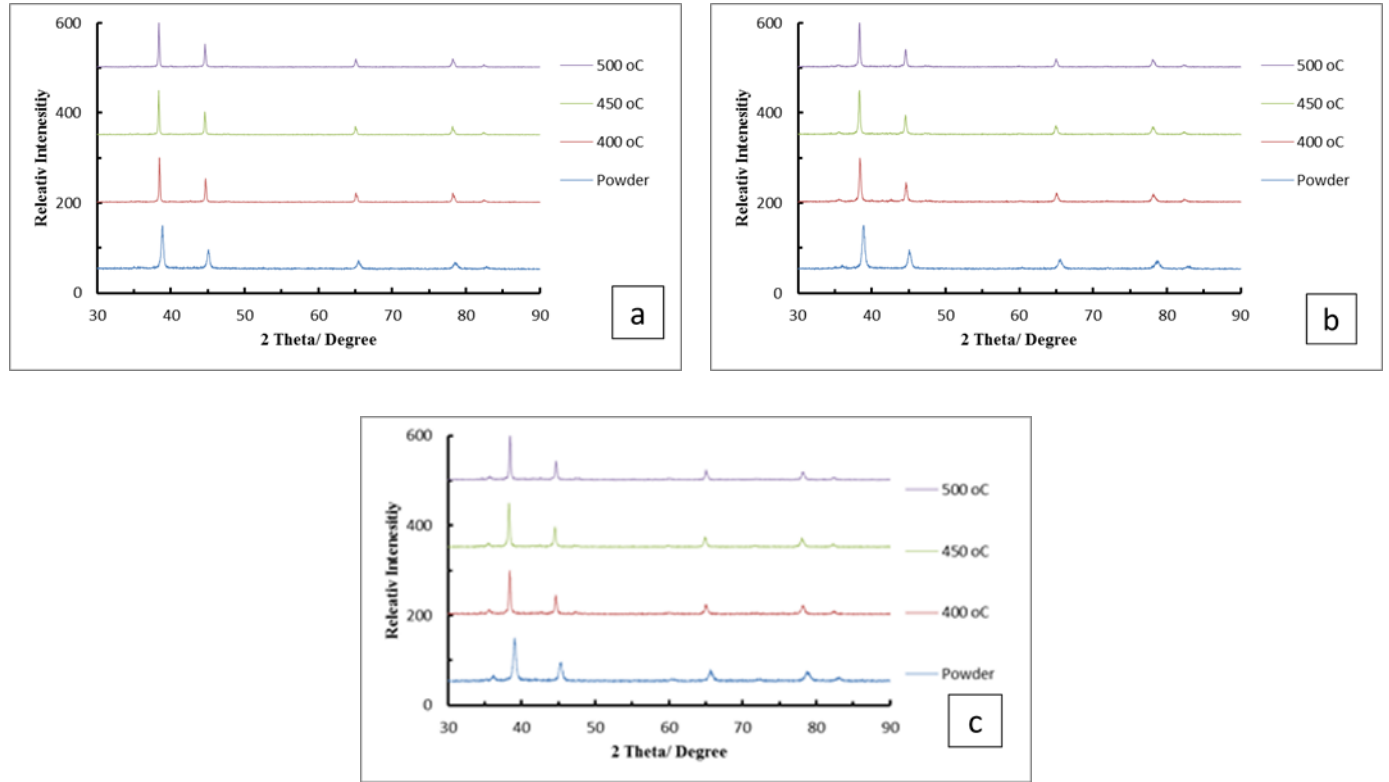
Figure 33: XRD pattern powder and SPS sintered Al 2124- (a) 5% SiC (b) 10 % SiC (c) 15% SiC

The crystallite size, again, was measured through Scherer equation and the computed values are listed in the following table. It can be seen that increasing the sintering temperature results in increasing the crystallite size. Moreover, the crystallite sizes for higher silicon carbide content were smaller compared to lower SiC content. It has been reported that adding harder phase particles restrict the growth of grains [106].

	Powder	400 $^\circ$C	450 $^\circ$C	500 $^\circ$C
2124 – 5% SiC	23.73	35.00	39.63	48.79
2124 – 10% SiC	20.77	27.77	28.67	28.97
2124 – 15% SiC	17.90	26.66	27.37	29.65

Table 8: Crystallite size of powder and SPS sintered Al 2124/SiC nanocomposites

The compressive strength of Al 2124/x% SiC has been measured using Instron equipment with L/D ratio of 2. Figure 33 shows that increasing the silicon carbide content increase the compressive strength. This is attribute to the mainly to two factors; dislocation densities generated during the mechanical milling and the load-bearing effect as a result of dispersion of hard particles [45].
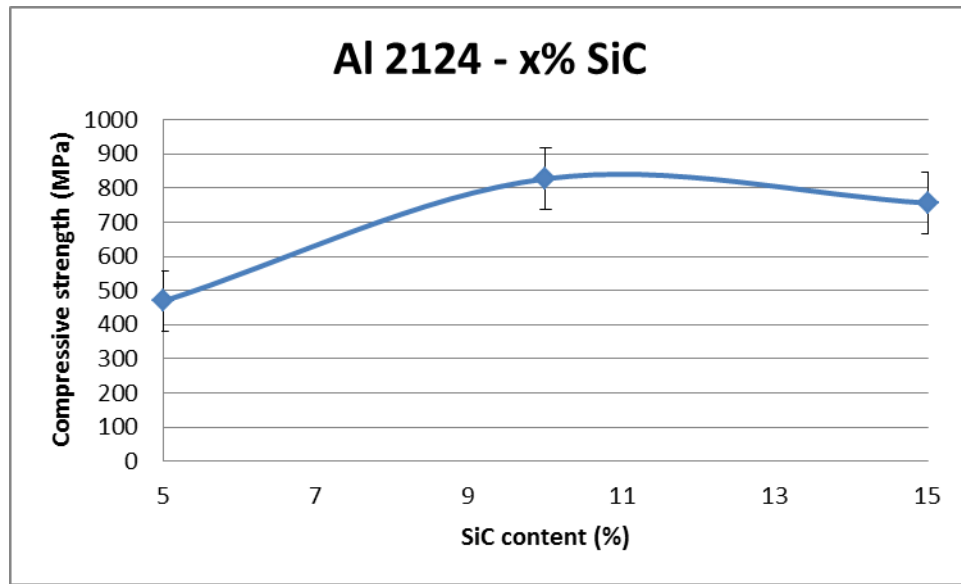
Figure 34: Scatter diagram showing the compressive strength values of Al 2124/ x % SiC nanocomposite

4.2.1.2 Hot Isostatically Pressed samples (HIPed)

Unlike SPS, HIPing requires samples of specific shapes prior introducing them to HIP process. Thus, nanocomposite powders were first cold pressed using uniaxial cold pressing machine. A compressibility test was done to the pressed samples in order to attain two criteria. The criteria were to choose the lowest compaction pressure that gives above 50% densification. The density is measured through taking the average height of ten reading per sample according to this equation.

$$Density = \frac{Mass}{Area\ X\ Height}$$

57

3 grams of each nanocomposite were pressed by an automated uniaxial press at 125, 375, 625 and 875 MPa, respectively. The figure below shows the relative density of the cold pressed samples to fully dense composites as a function of compaction pressure and nano-SiC content.
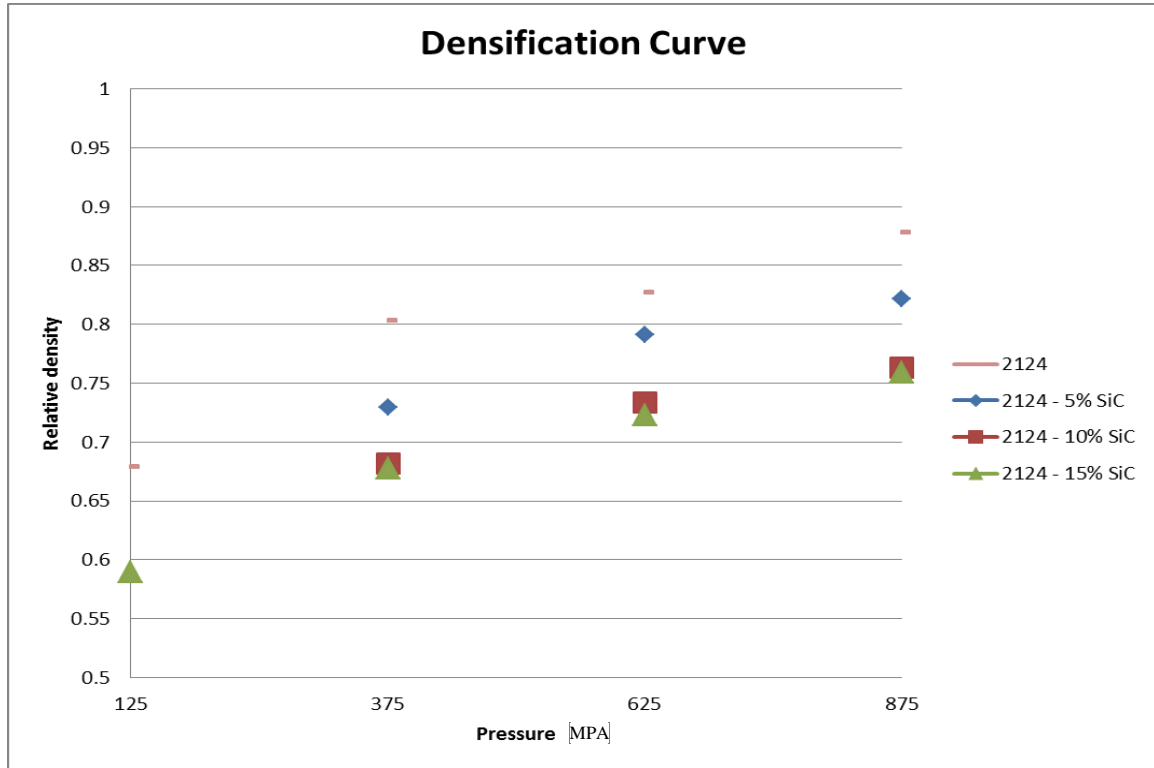
Figure 35: Density versus compaction pressure curve for Al 2124/ (0, 5, 10 and 15) % SiC composites

It can be seen that increasing the pressure produced samples with higher densification [Figure 35]. Harder and more strain hardened nanocomposites are expected with increasing the content of SiC, which resulted in lower densification. Thus, some of the nanocomposites were not compacted under 125 MPa, however, at 375 MPa, all nanocomposites were compacted with more than 50 % densification. Therefore, 375 MPa was chosen as a compaction pressure for the nanocomposite powders.

Cold pressed nanocomposites powders were subjected to sintering using hot isostatic pressing (HIP) at 400, 450 and 500 ^{o}C while keeping the pressure at 69 MPa. Figure 36 and 37 show the optical micrograph of Al 2124/5% SiC and 15% SiC, receptively. On a similar trend, relatively lower porosities were detected at increasing the sintering temperature. Comparing 5% with 15% SiC concentration in Al 2124/SiC composites, we can see that the structure at 5% is lamella with partially sintered regions (dark), whereas at 15% the structure is nearly spherical.
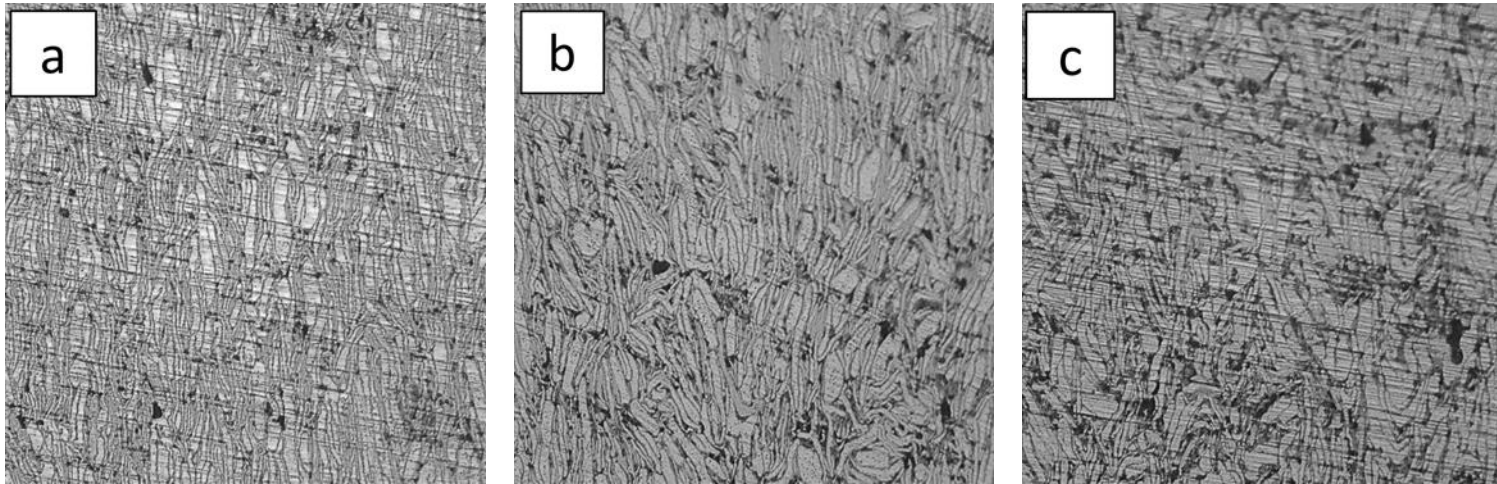
Figure 36: Optical micrograph showing hot isostatically pressed Al 2124/5 wt. % SiC sintered at (a) 400 (b) 450 and (c) 500 ^{o}C magnified to 200X
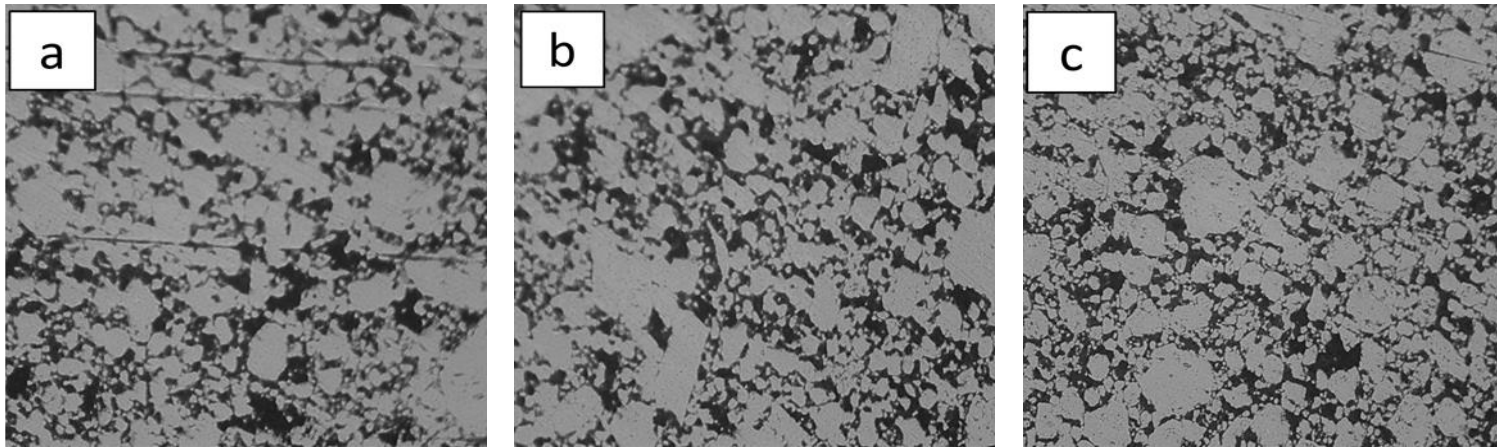
Figure 37: Optical micrograph showing hot isostatically pressed Al 2124/15 wt. % SiC sintered at (a) 400 (b) 450 and (c) 500 ^{o}C magnified to 200X

As emphasized earlier, densification is greatly driven by temperature. At 400 ^{o}C, the porosities are found with large content in 5% SiC (figure 38 a) as well as in 15% SiC (figure 39 a). Once the temperature was elevated to 450 and 500 ^{o}C, the quantity of porosity was reduced – though it might not be clear in micrograph – as evident by the densification value.
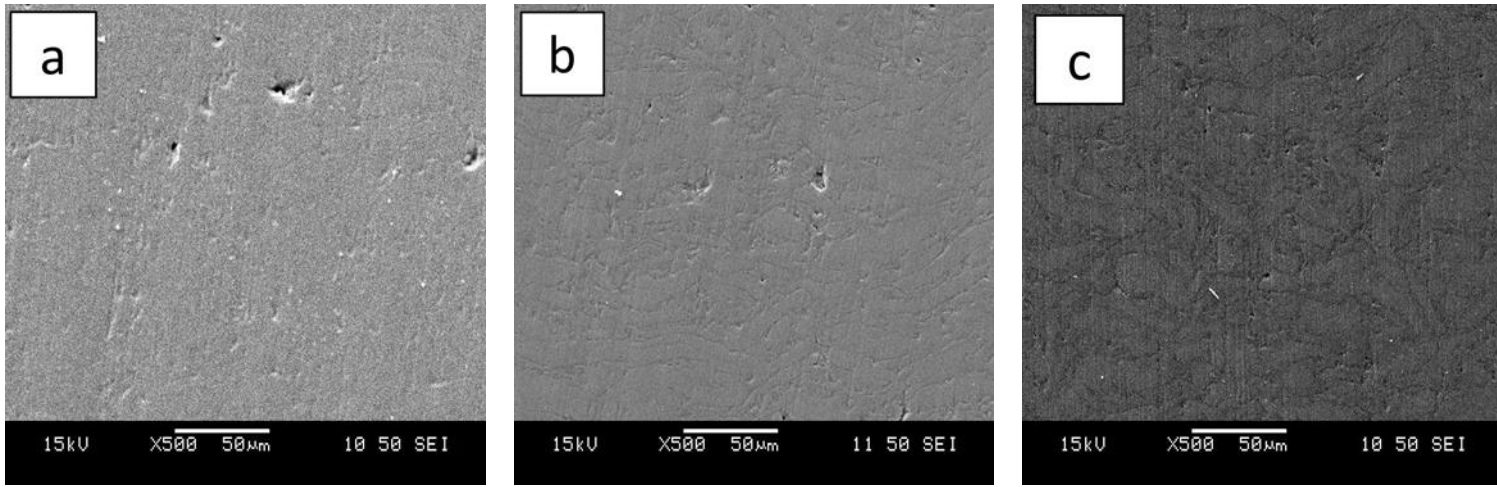
Figure 38: SEM micrograph showing hot isostatically pressed Al 2124/5 wt. % SiC sintered at (a) 400 (b) 450 and (c) 500 ^{o}C
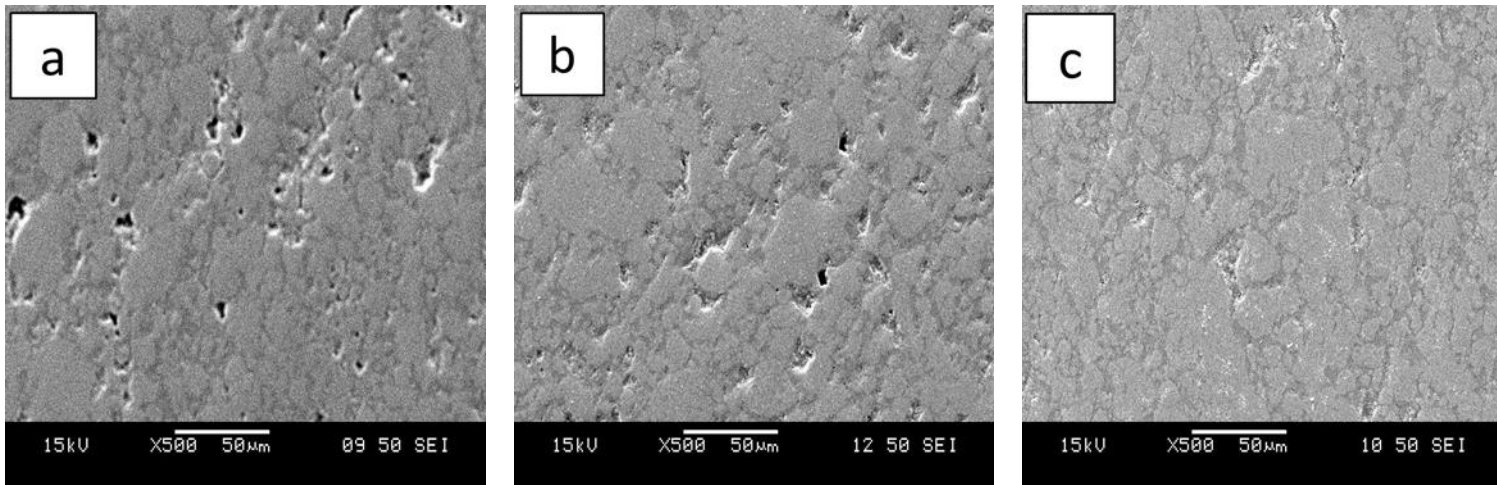
Figure 39: SEM micrograph showing hot isostatically pressed Al 2124/15 wt. % SiC sintered at (a) 400 (b) 450 and (c) 500 ^{o}C

Similar studies on the hardness and densification were performed on sintered Al 2124/x % SiC nanocomposites produced by HIP. The densification curves confirmed that higher sintering temperature gave higher densities. The presence of higher SiC content within the matrix lowers the densification due to the improved hardness and straining of the composites [Table 9 and Figure 40]. Compared to SPS, HIPed samples gave lower densities as well lower hardness [Figure 41].

Figure 40: Densification curves of HIPed Al 2124/ (5, 10 and 15) % SiC nanocomposites.
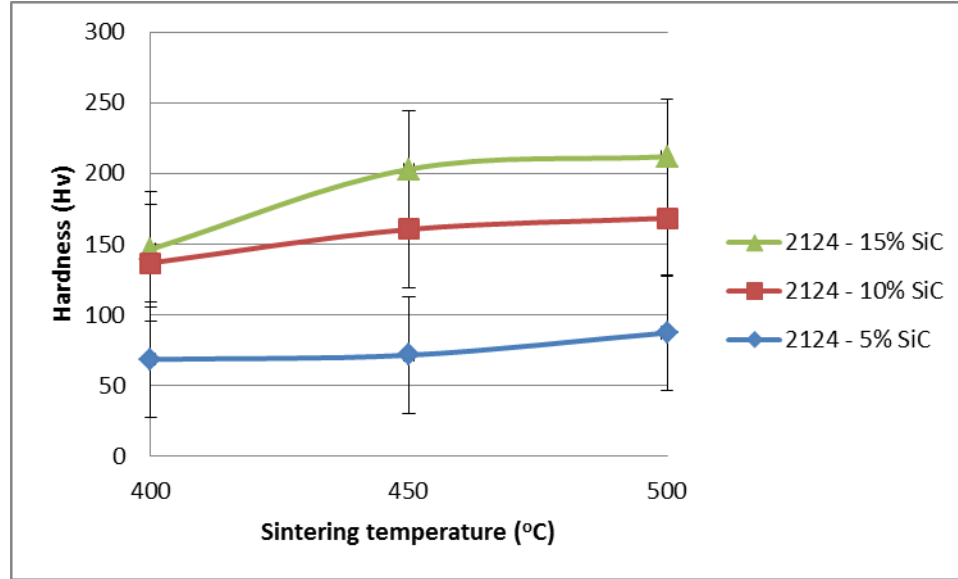
Figure 41: Vickers hardness curves of HIPed Al 2124/ (5, 10, 15) % SiC nanocomposites.

Alloy	% SiC	Densification (%)			Hardness (H_v)		
		Sintering Temperature			Sintering Temperature		
		400	450	500	400	450	500
2124	5	77.67	79.88	81.40	68.46	71.48	87.25
2124	10	77.54	79.77	81.28	136.72	160.42	168.34
2124	15	76.84	79.45	80.75	146.34	202.97	211.89

Table 9: Relative density and hardness values of HIPed Al 2124/SiC nanocomposites

4.2.2 Al alloy 2 (Al6061) containing SiC

4.2.2.1 Spark Plasma Sintered samples

Pre-alloyed Al 6061 was milled along with different percentages of SiC for five hours and charged directly into a 20-mm graphite die for SPS process. Optical micrographs had been taken for samples sintered at 400, 450, 500 ^{o}C. First, the structure can be described as lamella structures with dark areas represent partially sintered specimens for Al 6061/ 5

wt. % SiC. It has been reported that this partially sintered regions lead to a weaker material [Figure 42].Samples that were sintered at 500 ^{o}C showed little porosity compared to those at 450 and 400 ^{o}C.
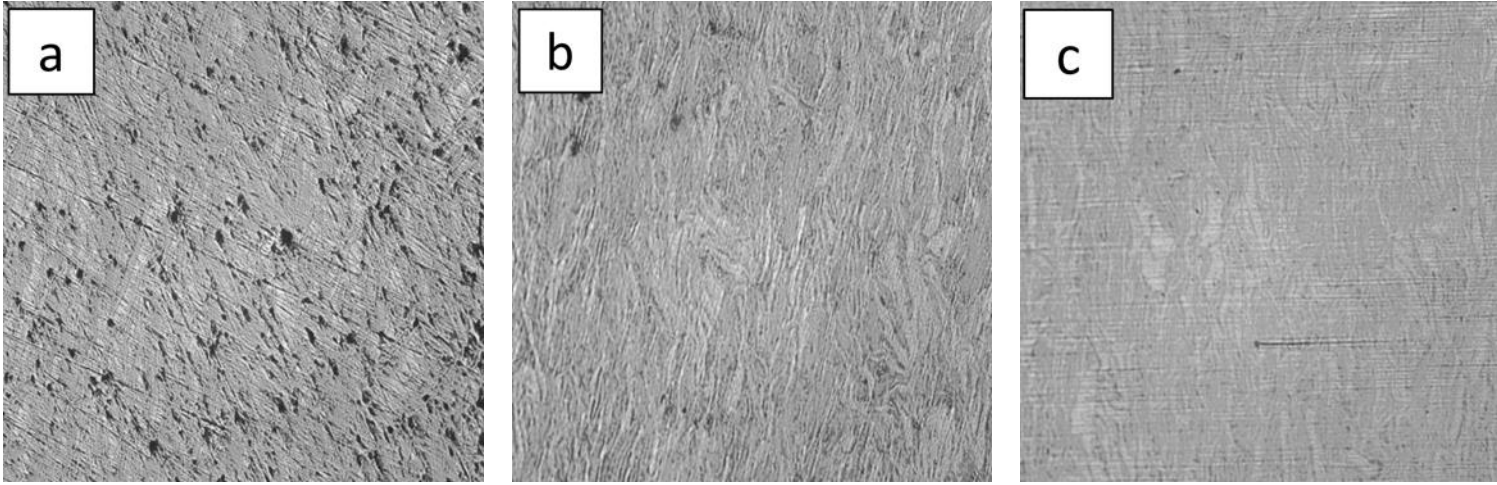
Figure 42: Optical micrograph showing SPS samples of Al 6061/ 5 wt. % SiC sintered at (a) 400 (b) 450 (c) 500 ^{o}C
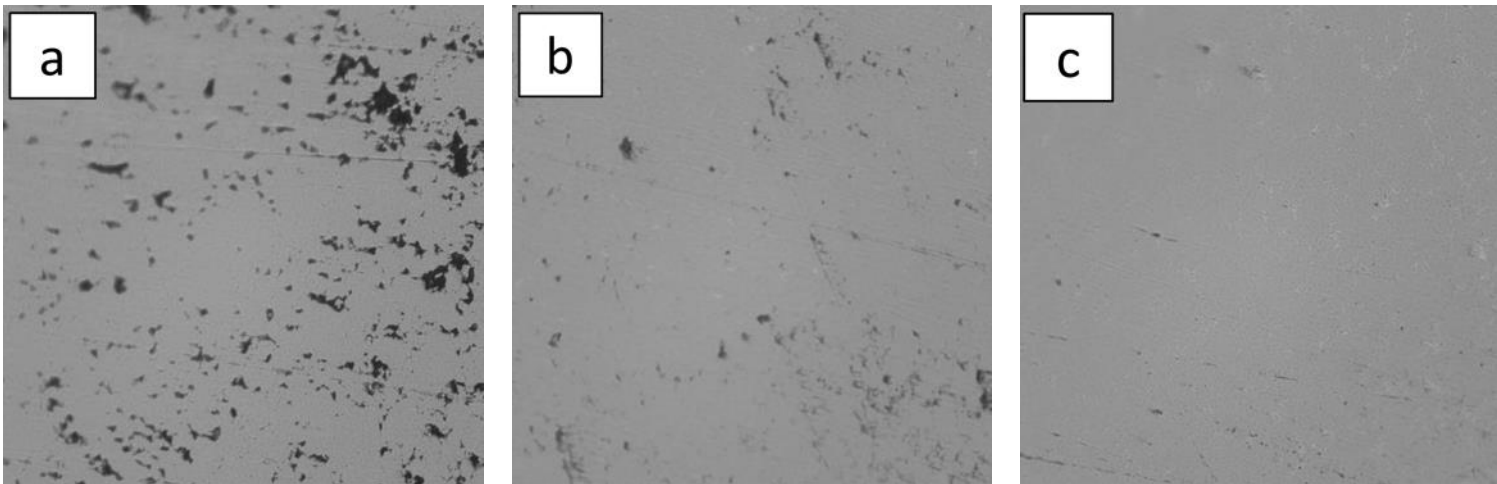
Figure 43: Optical micrograph showing SPS Al 6061/ 15 wt. % SiC sintered at (a) 400 (b) 450 (c) 500

The SEM micrographs showed in figures 44 and 45 represent Al 6061/5% SiC and Al 2124/15% SiC sintered using SPS at 400, 450, 500 ^{o}C, respectively. The sintering temperature plays an important role in determining the structure of the sintered samples.

Figure 39 illustrates that at 400 and 450 ^{o}C; the porosities are clear and can be seen. However, at 500 ^{o}C, no porosities were detected by microscopy though they didn't achieve 100% densification.
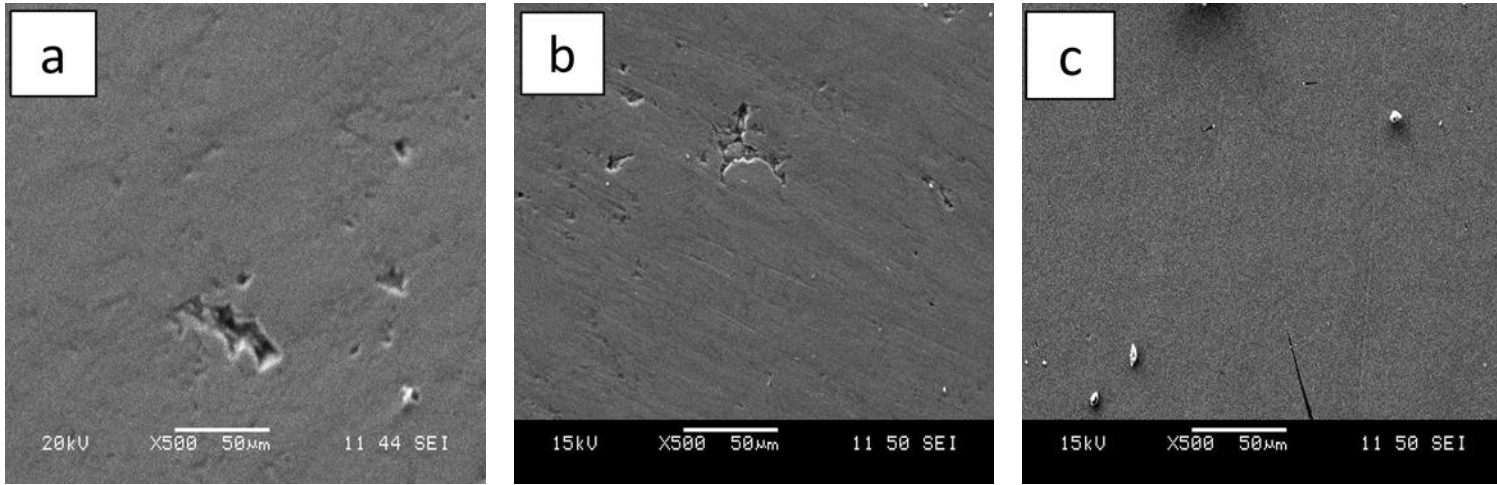
Figure 44: SEM micrograph showing SPS samples Al 6061/ 5 wt. % SiC sintered at (a) 400 (b) 450 (c) 500 ^{o}C
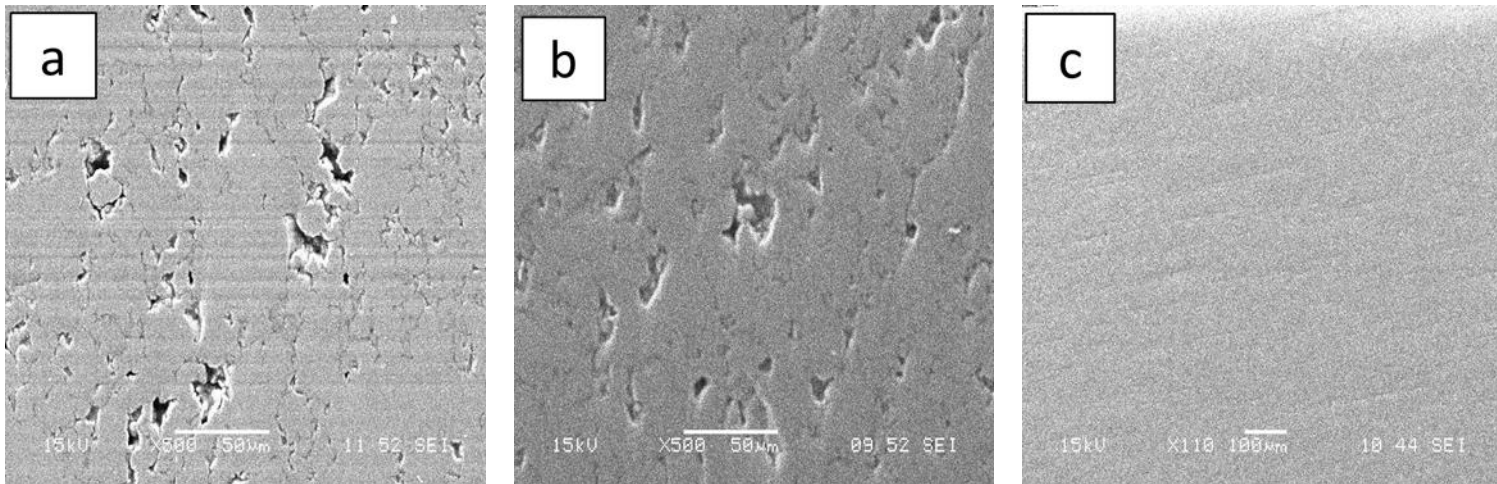
Figure 45: SEM micrograph showing SPS samples Al 6061/ 15 wt. % SiC sintered at (a) 400 (b) 450 (c) 500 ^{o}C

From the SEM and optical micrograph, porosities were rapidly annihilated with increasing sintering temperature. Densities that were measured using Archimedes are in agreement with the previous data [Figure 46]. Hardness values are increasing quickly with increasing the sintering temperature as well as increasing the silicon carbide content

[Figure 47]. This can be attributed to the increased densities as well as the fine and hard precipitates that were formed during consolidation [97]. Finally, table 10 illustrates the effect SiC content and sintering temperature on Al 6061/x% SiC consolidated using SPS.
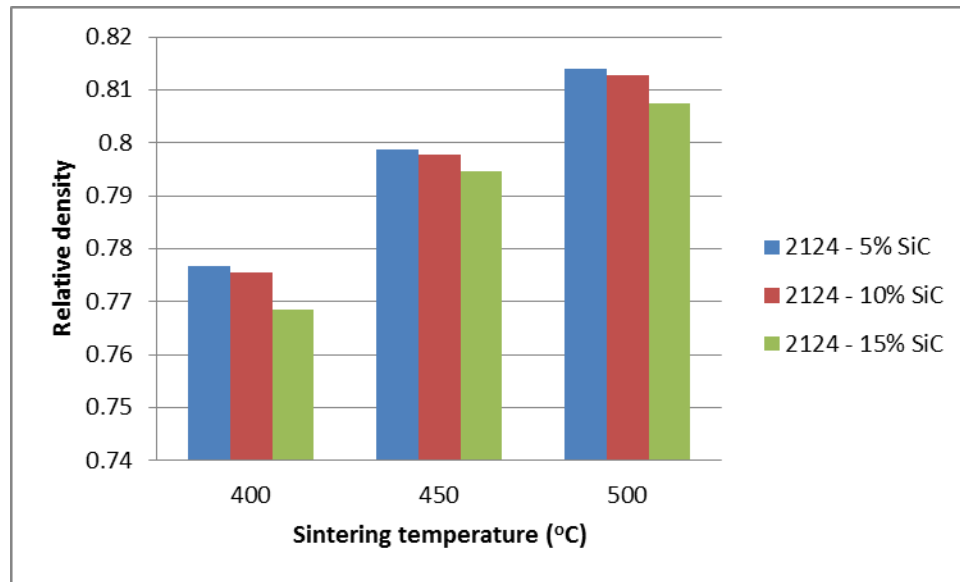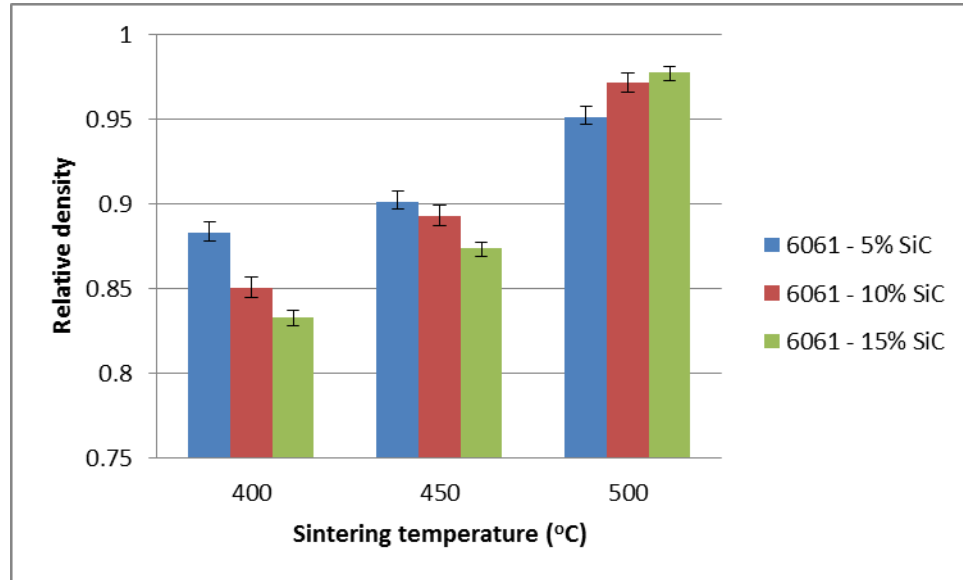

Figure 46: Densification curves of SPS Al 6061/ (5, 10 and 15) % SiC nanocomposites.
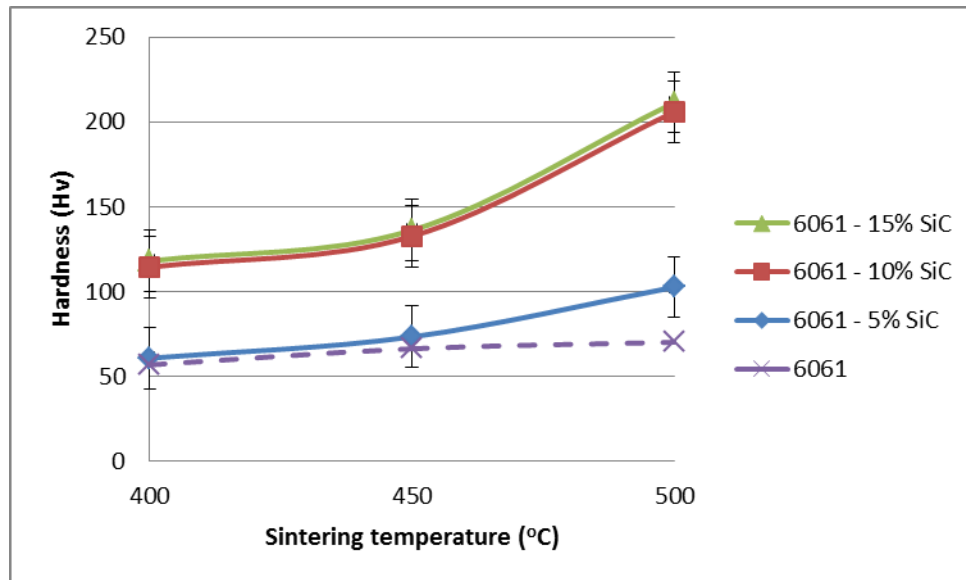
Figure 47: Vickers hardness curves of SPS Al 6061/ (5, 10, 15) % SiC nanocomposites.

Alloy	% SiC	Densification (%)			Hardness (H_v)		
		Sintering Temperature			Sintering Temperature		
		400	450	500	400	450	500
2124	5	88.26	90.10	95.09	60.71	73.29	102.63
2124	10	85.02	89.25	97.10	114.38	132.58	205.95
2124	15	83.32	87.39	97.72	118.05	136.12	211.4

Table 10: Hardness and relative density of SPS sintered Al 6061/SiC nanocomposites

It is apparent that increasing the sintering temperature increases the value of hardness due to the enhanced densification and lower porosity. Moreover, the improved hardness in both alloys could be attributed to fine hard precipitates that is below the detectability limit of XRD; such as: Mg2Si, CuAl2, and CuMgAl2. The precipitated is resulted from elements in the pre-alloyed alloys exceeding the solubility limit at the sintering temperature and, hence, they form the precipitates [97]. Moreover, the values of Al 2124/5% SiC compared to Al 2124 are greater than Al 6061/5% SiC compared to Al 6061. This is attributed to the partially sintered phase found in Al 6061/5% SiC and not found in Al 2124/5% SiC [86].
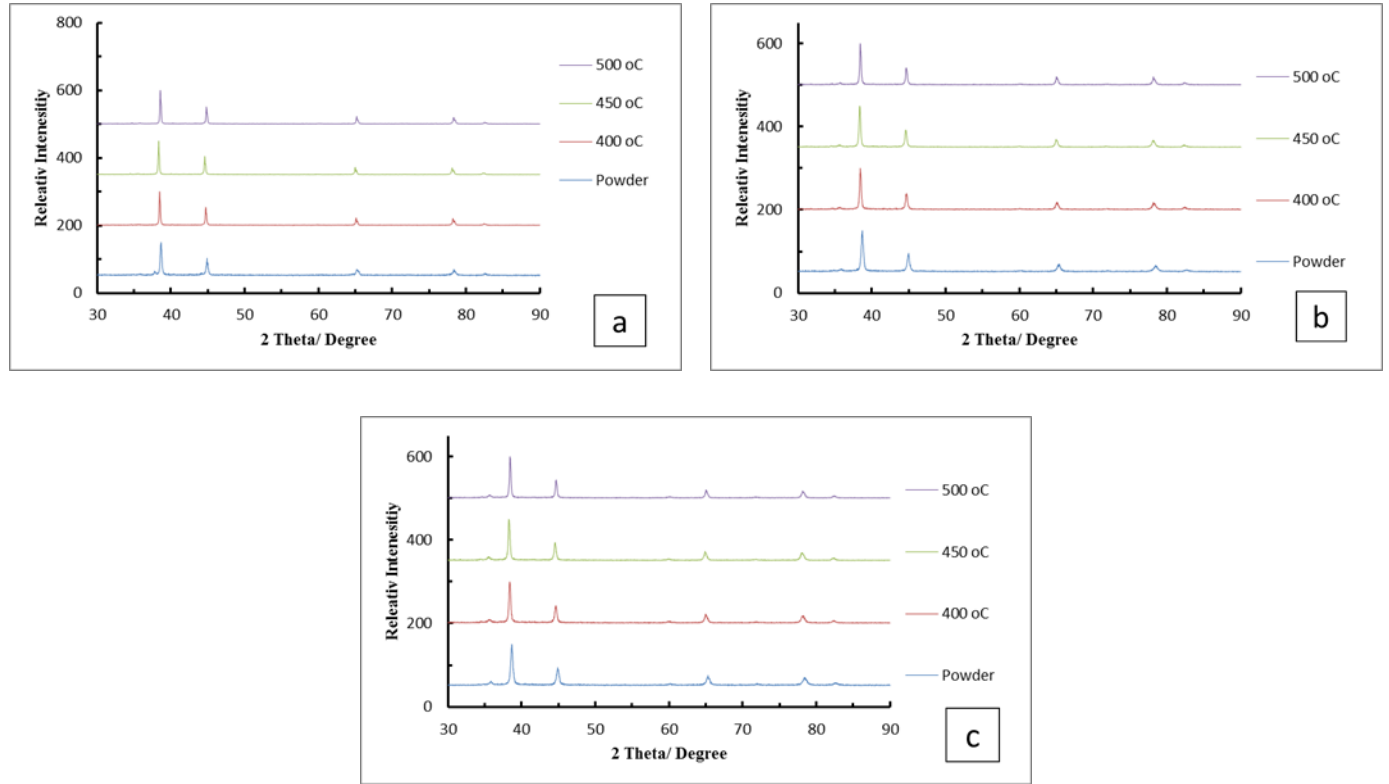
Figure 48: XRD pattern powder and SPS sintered Al 2124- (a) 5% SiC (b) 10 % SiC (c) 15% SiC

	Powder	400 $^{\circ}$C	450 $^{\circ}$C	500 $^{\circ}$C
6061 – 5% SiC	33.91	40.75	41.21	43.20
6061 – 10% SiC	23.78	26.63	29.02	32.00
6061 – 15% SiC	21.42	24.04	25.91	27.32

Table 11: Crystallite size of powder and SPS sintered Al 6061/SiC nanocomposites

Similarly, the compressive strength has been computed to the see the effect of adding nano-SiC to Al 6061. It is seen from figure 49 that increasing the SiC content result in increasing the compressive strength, and the reasons were explained previously in the case of Al 2124/ x% SiC nanocomposite. Though there is no marginal difference between

Al 6061/ 10 and 15 wt.% SiC nanocomposites and it within the stastical error, the slight decrease can be explained by the defects that are more effective in the compressive properties than hardness values. Such defects are clustering of particles and poor bonding between the matrix and reinforcement phase [105].
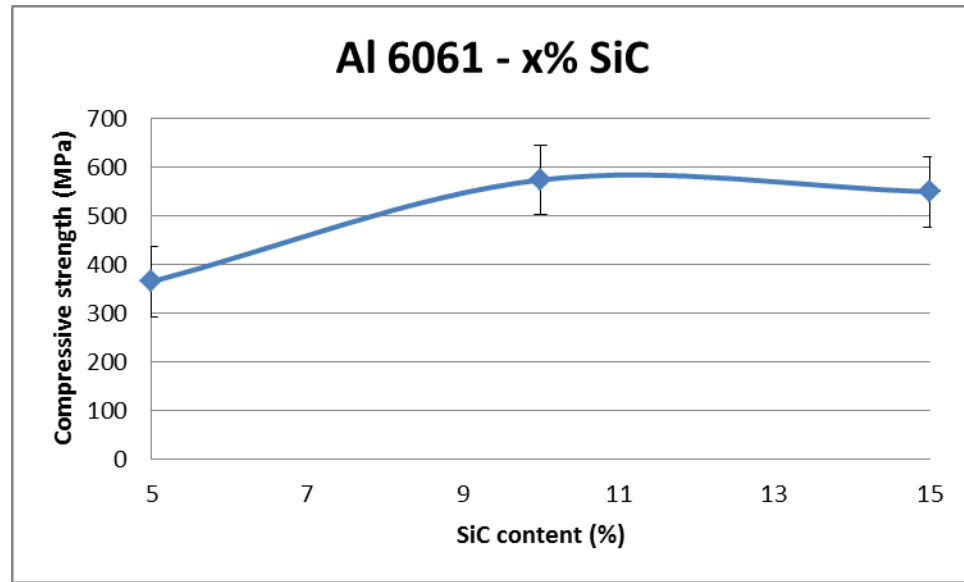
Figure 49: Scatter diagram showing the compressive strength values of Al 2124/ x % SiC nanocomposite

4.2.2.2 Hot Isostatically Pressed samples (HIP)

A compressibility curves for Al/6061/ (0, 5, 10, 15) % SiC is shown in figure 50. The purpose, again, is to find a suitable compaction pressure that insures a densification of 50% or more with the lowed possible pressure. At 125 MPa, some of the nanocomposite powder didn't compacted because the pressure wasn't enough to cause particle rearrangement. For a similar reason as in the case of Al 2124/x wt. % SiC, 375 MPa was chosen as the optimum compaction pressure.
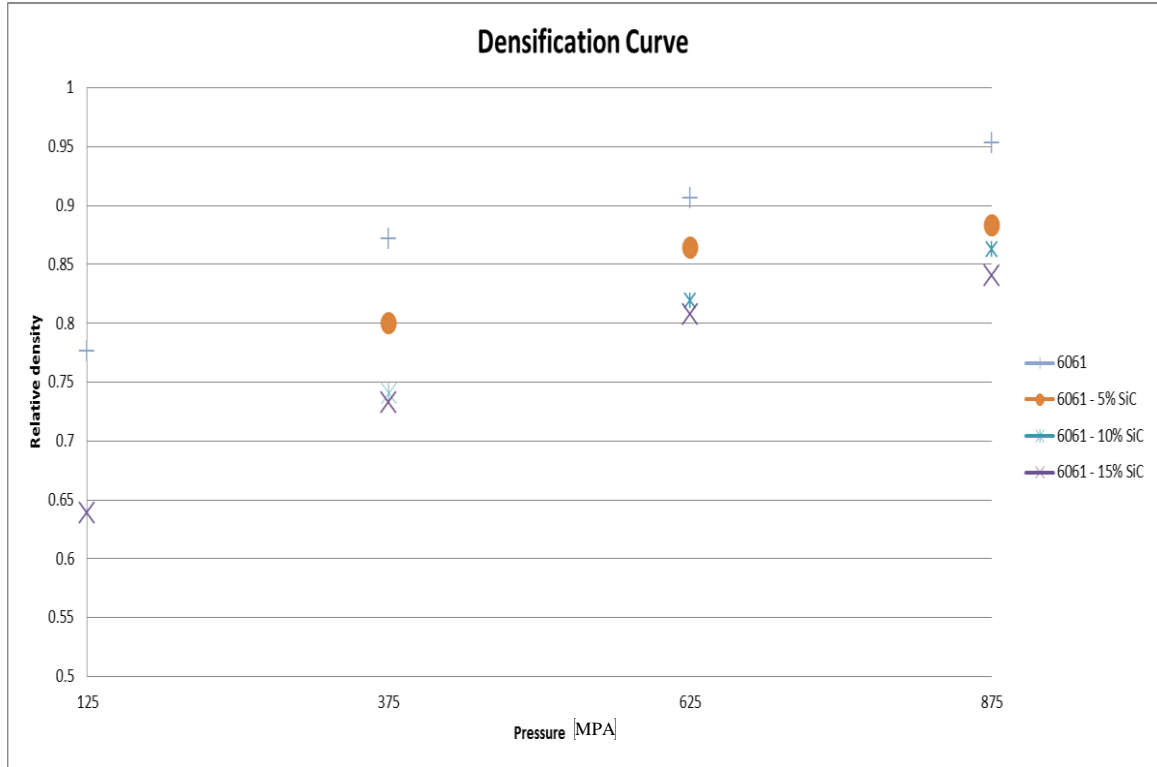
Figure 50: Compressibility curve for Al 6061/ (0, 5, 10 and 15) % SiC composites

Densification is a thermally activated process, the higher the sintering temperature means a higher diffusion possibility between particles and, hence, lowers porosities. This is shown in figure 51 and 52 for Al 6061/5% SiC and Al 6061/15% SiC sintered at 400, 450 and 500 ^{o}C, respectively. Figures from a-c show a decrease in the quantities of porosities as expected by increasing the sintering temperature and the increased densification. Increasing the silicon carbide content resulted in a change in structure from lamella to nearly a circular structure.
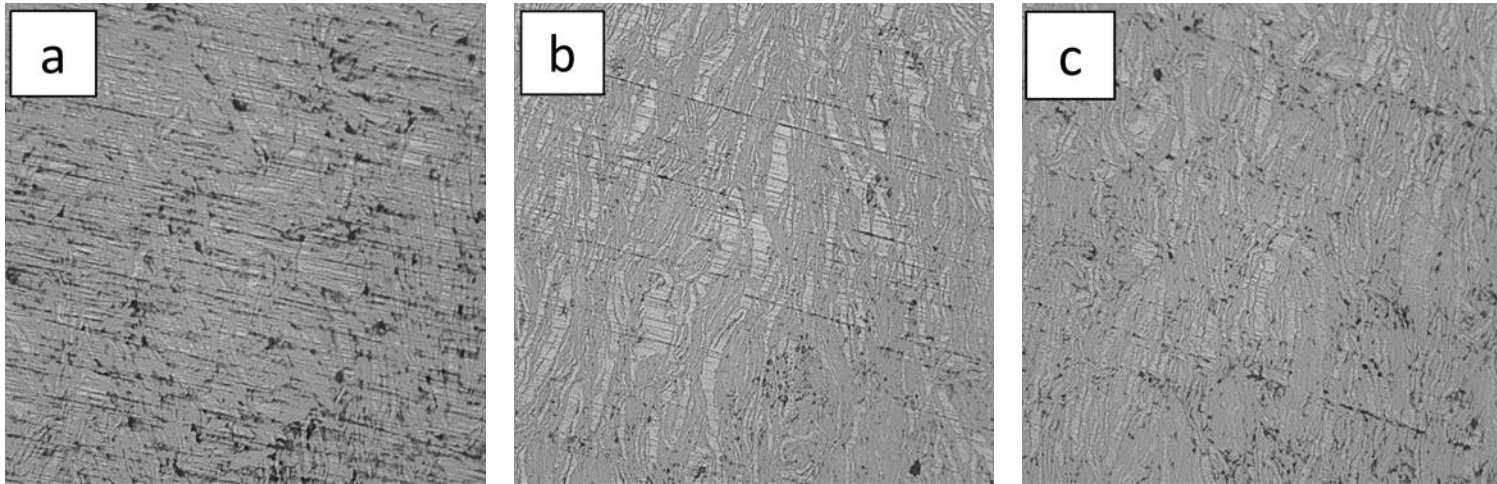
Figure 51: Optical micrograph showing hot isostatically pressed Al 6061/5 wt. % SiC sintered at (a) 400 (b) 450 and (c) 500 ^{o}C
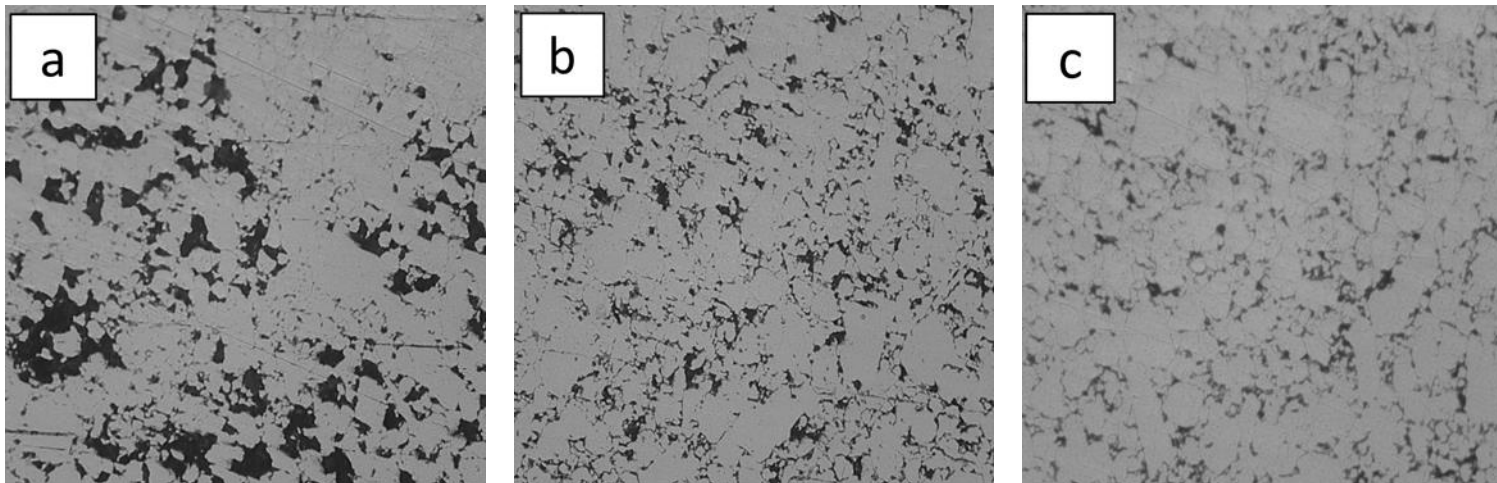
Figure 52: Optical micrograph showing hot isostatically pressed Al 6061/15 wt. % SiC sintered at (a) 400 (b) 450 and (c) 500 ^{o}C

The SEM micrographs below [Figures 53 and 54] represent the hot isostacally pressed Al 6061/5% and 15% SiC, respectively. Samples that were sintered at lower temperature (i.e. 400 ^{o}C) showed a lower densification compared to higher once (i.e. 500 ^{o}C). This indicates higher densification -as shall be seen in the next section- for higher temperature.

70
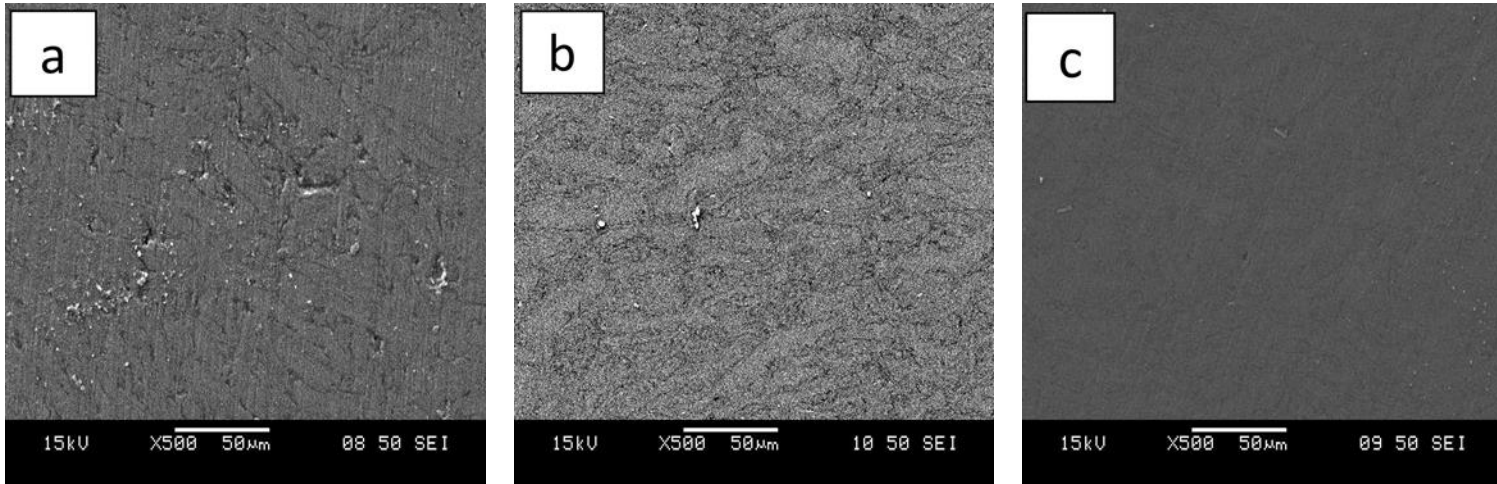
Figure 53: SEM micrograph showing hot isostatically pressed Al 6061/5 wt. % SiC sintered at (a) 400 (b) 450 and (c) 500 ^{o}C
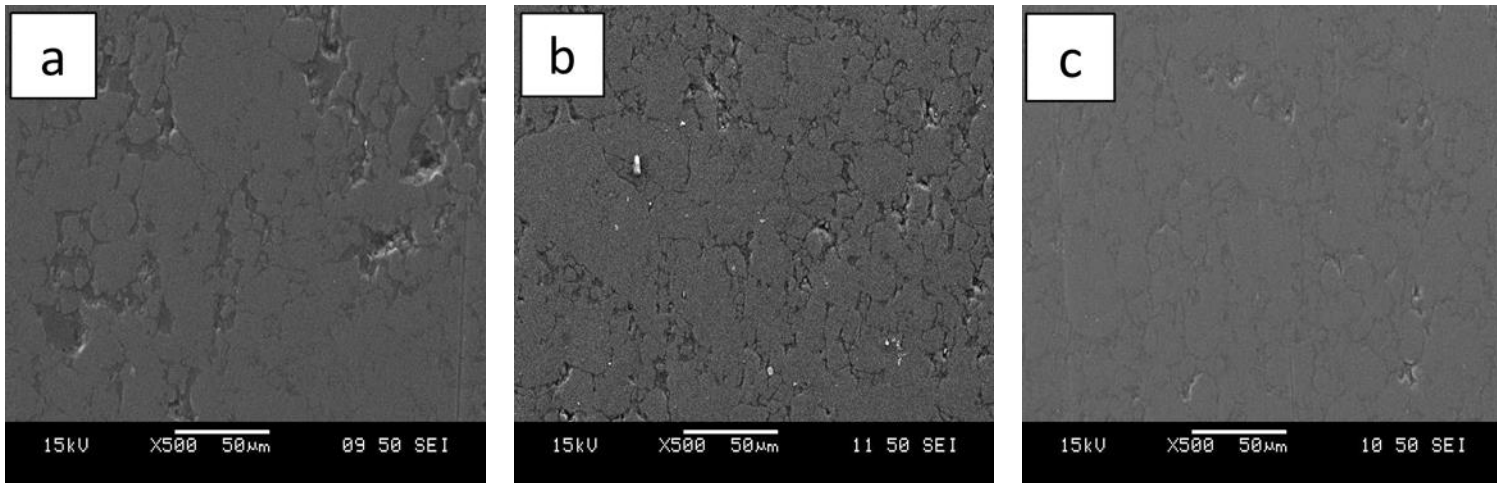
Figure 54: SEM micrograph showing hot isostatically pressed Al 6061/15 wt. % SiC sintered at (a) 400 (b) 450 and (c) 500 ^{o}C

The densification and Vickers hardness values are shown in figure 55 and 56, respectively. Al 6061/5% SiC in all sintering temperatures showed higher densification as compared to Al 6061/10% SiC and Al 6061/15% SiC [Figure 55]. This can be related to the comparatively higher hardness of Al 6061/ 15% SiC compared to the others which made the consolidation process more difficult. Hardness, on the other hand, showed a remarkable improvement at Al 6061/ 10% and 15% SiC as to compare with Al 6061/5%

71

SiC [Figure 56]. The lack of hardness in Al 6061/5% SiC can be reasoned by the partially

sintered region [Figure 44] which weakened the composite [66].
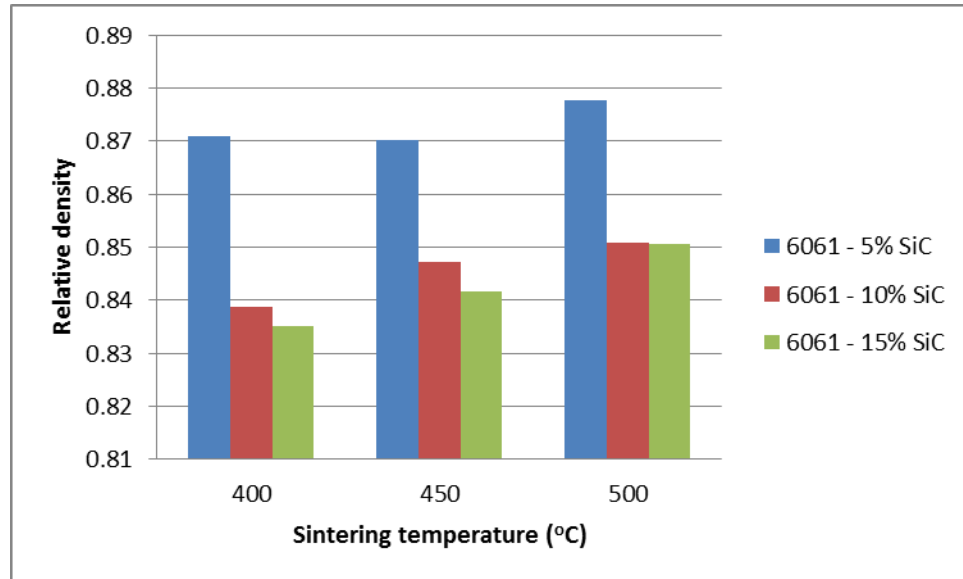
Figure 55: Densification curves of HIPed Al 6061/ (5, 10 and 15) % SiC nanocomposites.
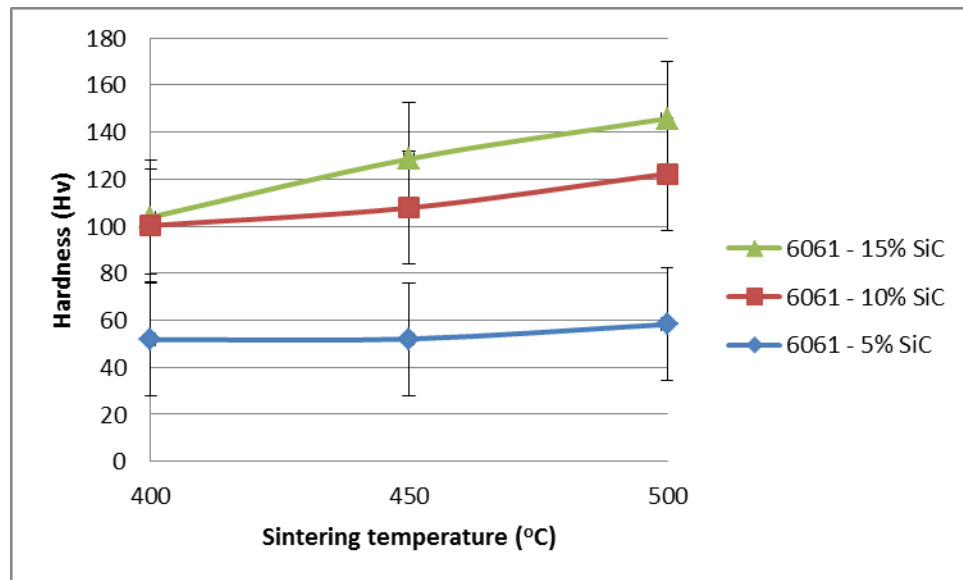
Figure 56: Vickers hardness curves of HIPed Al 6061/ (5, 10, 15) % SiC nanocomposites.

Alloy	% SiC	Densification (%)			Hardness (H_v)		
		Sintering Temperature			Sintering Temperature		
		400	450	500	400	450	500
2124	5	87.09	87.02	87.78	51.78	52.04	58.25
2124	10	83.87	84.72	85.07	100.26	107.8	122.28
2124	15	83.51	84.16	85.06	103.81	128.54	145.73

Table 12: Relative density and hardness values of HIPed Al 6061/SiC nanocomposite

In general, SPS samples showed improved densification and hardness properties. The difference in the results can be attributed to the different mechanism of heating [107]. Figures 57 and 58 illustrate the difference between SPS and HIP obtained properties.
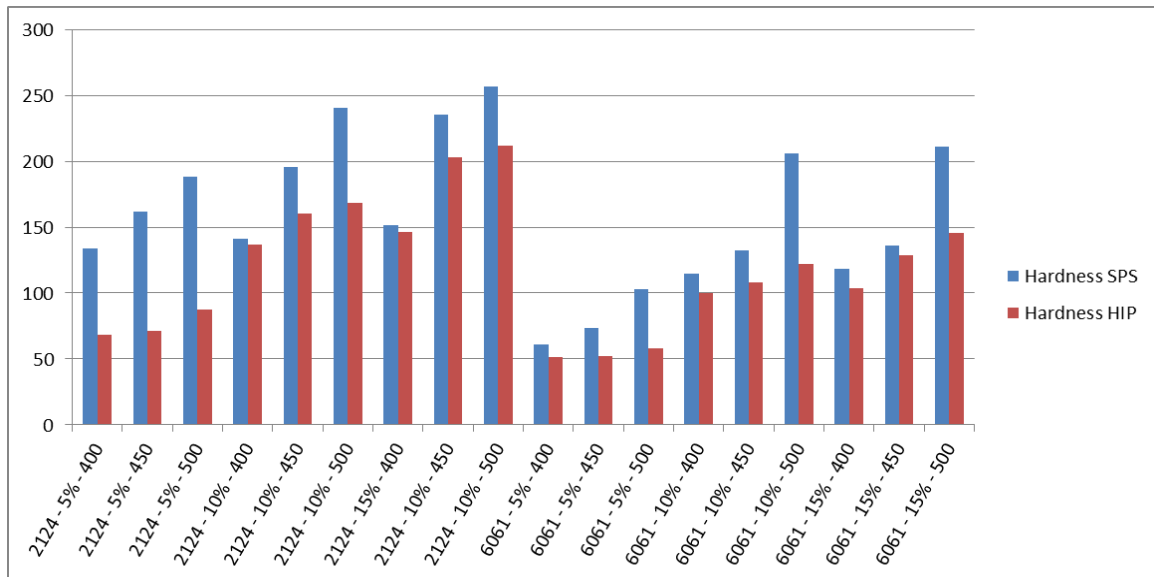
Figure 57: Shows the difference between values of hardness for samples obtained by SPS and HIP
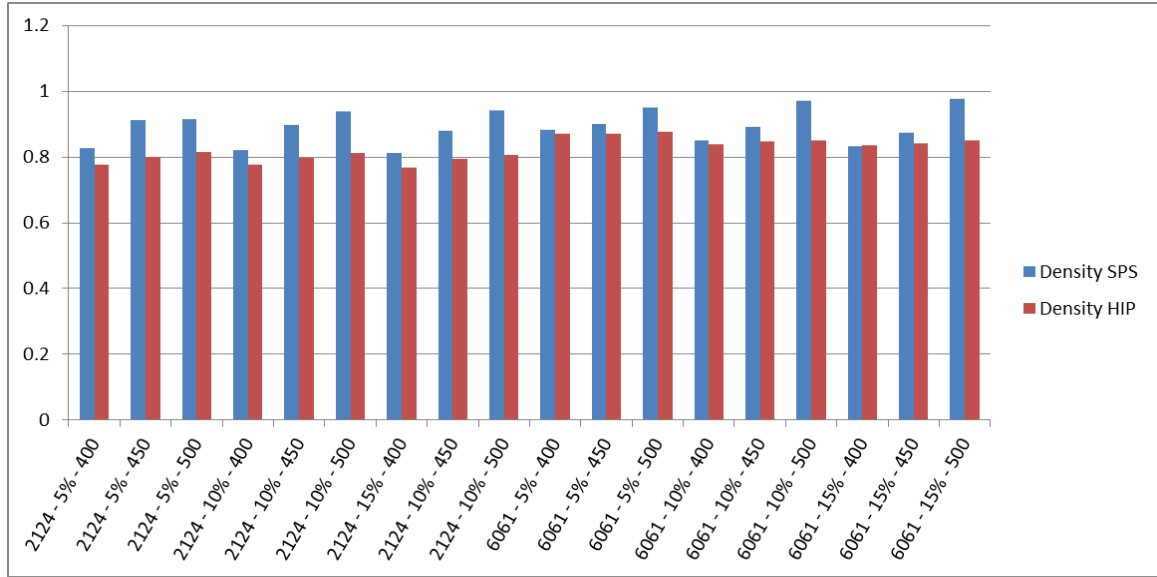
Figure 58: Shows the difference between densification for samples obtained by SPS and HIP

A comparison between the value of hardness obtained by this system versus other systems are shown in table 13.

Alloy	Reinforcement	(wt.%)	Sint. tech/ T (^{o}C)	Hv	Ref.
2124	nano-SiC	15	SPS (500)	256.41	This work
2124	CNT	1	SPS (500)	121.67	98
6061	nano-SiC	15	SPS (500)	211.4	This work
6061	CNT	1	SPS (450)	71.30	98
Pure Al	nano-SiC	10	SPS (600)	171.53	97
Al–7Si–0.3Mg	nano-SiC	12	SPS (500)	75	85
Al–12Si–0.3Mg	nano-SiC	12	SPS (500)	82	85
Al–7Si–0.3Mg	CNT	0.5	SPS (500)	68	107
Al–12Si–0.3Mg	CNT	0.5	SPS (500)	81	107

Table 13: Different composite's hardness values reproduced from published work

CHAPTER 5

CONCLUSIONS AND RECOMMENDATION

5.1 Conclusion

Pre-alloyed Al 2124 and Al 6061 matrices reinforced with nanosized SiC were synthesized to form nanocomposites using ball milling technique and sintered using non-conventional method i.e spark plasma sintering (SPS) and conventional method i.e. Hot isostatic press (HIP) at 400, 450 and 500ºC sintering temperature, 20mins holding time and applied pressure of 35MPa and 69 MPa, respectively. The effect of variables such as; milling durations, SiC content, sintering techniques and temperature on the microstructure, densification and hardness were investigated. The following specific conclusions can be drawn:

- Relatively homogenous distribution is attained when milling nanocomposite powder for five hours. No compositional fluctuation was detected by the use of mapping. The trend is almost similar for both alloys. In addition, after sintering the homogeneity was maintained.

- Differential thermal scanning of both alloys showed that increasing the silicon carbide content resulted in lowering both the melting and the onset of melting temperature as a result of short path diffusion created by plastic deformation.

- As the milling time increases, the crystallite size decreases reaching to about 20 nm. No significant difference is noticed when increasing further to 10 hours.

Similar trend, again, was observed for both alloys. Moreover, after sintering, the crystallite sizes increased with increasing the sintering temperature.

- 98% average relative density was possible to attain for Al 6061/15% SiC sintered by SPS at 500 $^{\circ}$C. Increasing sintering temperature resulted in an increase in densification for all composites. The silicon carbide content act as a barrier to attain full densification, however, at 500 $^{\circ}$C, 10 wt.% and 15 wt.% SiC reinforced Al based composited showed higher relative density compared to Al-x/ 5wt.% SiC possibly by formation of a liquid phase.

- Higher hardness is attained when increasing the silicon carbide content from 0 to 15%. An increase of 118% is detected when two samples are sintered for Al 2124 and Al 2124/15% SiC and almost twice of that for Al 6061 case.

- Evaluated Compressive strengths showed that increasing SiC content from 5 wt.% to 10 wt.% resulted in increasing the strength, and no significant difference between 10 wt.% and 15 wt.%.

- SPS has proven to be a better consolidation process than HIP. The densification and hardness measurement for SPS samples were marginally greater than those sintered by HIP. The maximum densification by SPS reached to 98% for Al 6061/ 15% SiC sintered at 500 $^{\circ}$C, while HIP only achieved 85%. Hardness values for the same sample achieved using SPS (211 Hv) versus HIP (145 Hv).

5.2 Recommendation

Based on the wide scope of such experiments from applications points of view the following recommendations are paramount in any future work using these techniques:

- More in-depth analysis needs to be done on sintered samples; this includes: compressive and tensile tests, tribological experiments and other mechanical testing. The purpose is to obtain a get a thorough understanding on the mechanical behavior of these composite.

- Software simulation would be useful to be able to easily predict the values for hardness, densification and other results based on the experimented samples.

References

1. Milan, M.T., Bowen, P. Tensile and fracture toughness properties of SiCp reinforced Al alloys: Effects of particle size, particle volume fraction, and matrix strength(2004) Journal of Materials Engineering and Performance, 13 (6), pp. 775-783

2. Milan, M.T., Bowen, P. Tensile and fracture toughness properties of SiCp reinforced Al alloys: Effects of particle size, particle volume fraction, and matrix strength(2004) Journal of Materials Engineering and Performance, 13 (6), pp. 775-783

3. Chawla, N., Andres, C., Jones, J.W., Allison, J.E. Effect of SiC volume fraction and particle size on the fatigue resistance of a 2080 Al/SiCp composite (1998) Metallurgical and Materials Transactions A: Physical Metallurgy and Materials Science, 29 (11), pp. 2843-2854

4. Kamrani, S., Simchi, A., Riedel, R., Seyed Reihani, S.M. Effect of reinforcement volume fraction on mechanical alloying of Al-SiC nanocomposite powders(2007) Powder Metallurgy, 50 (3), pp. 276-282

5. Zhao, N., Nash, P. Effect of degassing of SiC reinforced 6061 aluminium alloy composites on properties (2001) Powder Metallurgy, 44 (4), pp. 333-338

6. Purohit, R., Sagar, R.Fabrication and testing of Al-SiCp composite poppet valve guides (2010) International Journal of Advanced Manufacturing Technology, 51 (5-8), pp. 685-698

7. Gnjidic, Z., Grbovic, J., Mitkov, M., Bozic, D. Influence of SiC particles on compressive strength of sintered aluminium alloy(2003) Powder Metallurgy, 46 (1), pp. 21-24

8. Nam, T.H., Requena, G., Degischer, P. Thermal expansion behaviour of aluminum matrix composites with densely packed SiC particles(2008) Composites Part A: Applied Science and Manufacturing, 39 (5), pp. 856-865

9. Popov, V.A., Cherdyntsev, V.V. Formation of a nanodispersed metal-matrix structure during a combined high-energy mechanical alloying of powders of aluminum-based SiC-containing alloys(2009) Physics of Metals and Metallography, 107 (1), pp. 45-52

10. Jian Ku Shang, Weikang Yu, R.O. Ritchie, Role of silicon carbide particles in fatigue crack growth in SiC-particulate-reinforced aluminum alloy composites, Materials Science and Engineering: A, Volume 102, Issue 2, July 1988, Pages 181-192

11. Gül Tosun, Mehtap Muratoglu, The drilling of an Al/SiCp metal-matrix composites. Part I: microstructure, Composites Science and Technology, Volume 64, Issue 2, February 2004, Pages 299-308

12. Introduction to aluminum alloys and tempers, Kaufman, J. Gilbert, 2000

13. Bekir Sadık Ünlü, Investigation of tribological and mechanical properties Al2O3–SiC reinforced Al composites manufactured by casting or P/M method, Materials & Design, Volume 29, Issue 10, December 2008, Pages 2002-2008

14. Ali Mazahery, Mohsen Ostad Shabani, Nano-sized silicon carbide reinforced commercial casting aluminum alloy matrix: Experimental and novel modeling evaluation, Powder Technology, Volume 217, February 2012, Pages 558-565

15. Leszczyńska-Madej, B. The effect of sintering temperature on microstructure and properties of Al - SiC composites(2013) Archives of Metallurgy and Materials, 58 (1), pp. 43-48

16. Hassan, A.M., Alrashdan, A., Hayajneh, M.T., Mayyas, A.T. Wear behavior of Al-Mg-Cu-based composites containing SiC particles(2009) Tribology International, 42 (8), pp. 1230-1238

17. Zhang, Z., Zhang, L., Mai, Y.-W. The running-in wear of a steel/SiCp-Al composite system(1996) Wear, 194 (1-2), pp. 38-43

18. M. Sherif El-Eskandarany, 4 - Fabrication of Nanocomposite Materials, Mechanical Alloying, William Andrew Publishing, Norwich, NY, 2001, Pages 45-61, Mechanical Alloying

19. Chen, Z.Z., Tokaji, K. Effects of particle size on fatigue crack initiation and small crack growth in SiC particulate-reinforced aluminium alloy composites (2004) Materials Letters, 58 (17-18), pp. 2314-2321

20. C.S. Shin, J.C. Huang, Effect of temper, specimen orientation and test temperature on the tensile and fatigue properties of SiC particles reinforced PM 6061 Al alloy, International Journal of Fatigue, Volume 32, Issue 10, October 2010, Pages 1573-1581

21. Sutton, R.A., Huo, S.H., Schaffer, G.B. Effect of particle size ratio and particle clustering on sintering and stiffness of aluminium matrix composite(2006) Powder Metallurgy, 49 (4), pp. 323-327

22. Singh, I.B., Mandal, D.P., Singh, M., Das, S. Influence of SiC particles addition on the corrosion behavior of 2014 Al-Cu alloy in 3.5% NaCl solution(2009) Corrosion Science, 51 (2), pp. 234-241

23. Hafizpour, H.R., Simchi, A. Investigation on compressibility of Al-SiC composite powders (2008) Powder Metallurgy, 51 (3), pp. 217-223

24. M.R. Dashtbayazi, A. Shokuhfar, Statistical modeling of the mechanical alloying process for producing of Al/SiC nanocomposite powders, Computational Materials Science, Volume 40, Issue 4, October 2007, Pages 466-479

25. Hesabi, Z.R., Kamrani, S., Simchi, A., Reihani, S.M.S.Effect of nanoscaled reinforcement particles on the structural evolution of aluminium powder during mechanical milling(2009) Powder Metallurgy, 52 (2), pp. 151-157

26. Zhang, J.-T., Liu, L.-S., Zhai, P.-C., Fu, Z.-Y., Zhang, Q.-J. Effect of fabrication process on the microstructure and dynamic compressive properties of SiCp/Al composites fabricated by spark plasma sintering (2008) Materials Letters, 62 (3), pp. 443-446

27. M. Montoya-Dávila, M.I. Pech-Canul, M.A. Pech-Canul, Effect of SiCp multimodal distribution on pitting behavior of Al/SiCp composites prepared by reactive infiltration, Powder Technology, Volume 195, Issue 3, 10 November 2009, Pages 196-202

28. J. Rams, A. Ureña, M. Campo, Dual layer silica coatings of SiC particle reinforcements in aluminium matrix composites, Surface and Coatings Technology, Volume 200, Issues 12–13, 31 March 2006, Pages 4017-4026

29. Y. Sahin, M. Acılar, Production and properties of SiCp-reinforced aluminium alloy composites, Composites Part A: Applied Science and Manufacturing, Volume 34, Issue 8, August 2003, Pages 709-718

30. M Sherif El-Eskandarany, Mechanical solid state mixing for synthesizing of SiCp/Al nanocomposites, Journal of Alloys and Compounds, Volume 279, Issue 2, 2 October 1998, Pages 263-271

31. Mohammad Moazami-Goudarzi, Farshad Akhlaghi, Effect of nanosized SiC particles addition to CP Al and Al–Mg powders on their compaction behavior, Powder Technology, Volume 245, September 2013, Pages 126-133

32. F. Bonollo, R. Guerriero, E. Sentimenti, I. Tangerini, W.L. Yang, The effect of quenching on the mechanical properties of powder metallurgically produced Al□SiC (particles) metal matrix composites, Materials Science and Engineering: A, Volume 144, Issues 1–2, 1 October 1991, Pages 303-309

33. Rao, C.S., Upadhyaya, G.S. 2014 and 6061 aluminium alloy-based powder metallurgy composites containing silicon carbide particles/fibres(1995) Materials and Design, 16 (6), pp. 359-366

34. Ehsan Mostaed, Hassan Saghafian, Ali Mostaed, Ali Shokuhfar, Hamid Reza Rezaie, Investigation on preparation of Al–4.5%Cu/SiCp nanocomposite powder via mechanical milling, Powder Technology, Volume 221, May 2012, Pages 278-283

35. P. Ravindran, K. Manisekar, P. Rathika, P. Narayanasamy, Tribological properties of powder metallurgy – Processed aluminium self lubricating hybrid composites with SiC additions, Materials & Design, Volume 45, March 2013, Pages 561-570

36. Narayanasamy, R., Ramesh, T., Pandey, K.S. Workability studies on cold upsetting of Al-Al2O3 composite material(2006) Materials and Design, 27 (7), pp. 566-575

37. (n.d.). Powder metallurgy—intrinsically sustainable. Princeton: Metal Powder Industries Federation

38. Morteza Eslamian, Joel Rak, Nasser Ashgriz, Preparation of aluminum/silicon carbide metal matrix composites using centrifugal atomization, Powder Technology, Volume 184, Issue 1, 6 May 2008, Pages 11-20

39. L. Kollo, C.R. Bradbury, R. Veinthal, C. Jäggi, E. Carreño-Morelli, M. Leparoux, Nano-silicon carbide reinforced aluminium produced by high-energy milling and hot consolidation, Materials Science and Engineering: A, Volume 528, Issue 21, 15 August 2011, Pages 6606-6615

40. Nazari, A., Abdinejad, V. R. Artificial neural networks for prediction Charpy impact energy of Al6061/SiCp-laminated nanocomposites (2012) Neural Computing and Applications

41. Suryanarayana, C. Mechanical alloying and milling(2001) Progress in Materials Science, 46 (1-2), pp. 1-184

42. Ghasemi Yazdabadi, H., Ekrami, A., Kim, H.S., Simchi, A. An investigation on the fatigue fracture of P/M Al-SiC nanocomposites(2013) Metallurgical and Materials Transactions A: Physical Metallurgy and Materials Science, 44 (6), pp. 2662-2671

43. Y. Saberi, S.M. Zebarjad, G.H. Akbari, On the role of nano-size SiC on lattice strain and grain size of Al/SiC nanocomposite, Journal of Alloys and Compounds, Volume 484, Issues 1–2, 18 September 2009, Pages 637-640

44. MAURICE, D.R., COURTNEY, T.H. The Physics of Mechanical Alloying" A First Report (1990) METALLURGICAL TRANSACTIONS A, 21A, pp. 289-303

45. Jiang, X., Trunov, M.A., Schoenitz, M., Dave, R.N., Dreizin, E.L

46. PENG, Z.,SURYANARAYANA C., FROES,F.H. Mechanical Alloying of Nb-AI Powders (1996) Metallurgical And Materials Transactions A,27A, pp. 41-48

47. Suryanarayana, C., Al-Aqeeli, N. Mechanically alloyed nanocomposites(2012) Progress in Materials Science

48. Gu, W.-L.Bulk Al/SiC nanocomposite prepared by ball milling and hot pressing method(2006) Transactions of Nonferrous Metals Society of China (English Edition), 16 (SUPPL.), pp. s398-s401

49. Benjamin, J.S. Dispersion strengthened superalloys by mechanical alloying (1970) Metallurgical Transactions, 1 (10), pp. 2943-2951

50. Benjamin, J.S., Volin, T.E. MECHANISM OF MECHANICAL ALLOYING.(1974) Metall Trans, 5 (8), pp. 1929-1934

51. Zhang, D.L. Processing of advanced materials using high-energy mechanical milling (2004) Progress in Materials Science, 49 (3-4), pp. 537-560

52. Koch, C.C., Cavin, O.B., McKamey, C.G., Scarbrough, J.O. Preparation of]] amorphous" Ni60Nb4 0 by mechanical alloying (1983) Applied Physics Letters, 43 (11), pp. 1017-1019

53. Schaffer, G.B., McCormick, P.G. Reduction of metal oxides by mechanical alloying (1989) Applied Physics Letters, 55 (1), pp. 45-46

54. Koch, C.C., Whittenberger, J.D. Mechanical milling/alloying of intermetallics(1996) Intermetallics, 4 (5), pp. 339-355

55. Simchi, A., Godlinski, D. Densification and microstructural evolution during laser sintering of A356/SiC composite powders (2011) Journal of Materials Science, 46 (5), pp. 1446-1454

56. Yoshimura, M., Ohji, T., Sando, M., Choa, Y., Sekino, T., Niihara, K., Synthesis of nanograined ZrO2 -based composites by chemical processing and pulse electric current sintering (1998) Materials Letters, 38 , pp. 18–21

57. Zhou, C., Yi, J., Luo, S., Sintering High Tungsten Content W-Ni-Fe Heavy Alloys by Microwave Radiation (2013) Metallurgical and Materials Transactions A

58. Julin Wan, Ren-Guan Duan, Amiya K. Mukherjee, Spark plasma sintering of silicon nitride/silicon carbide nanocomposites with reduced additive amounts, Scripta Materialia, Volume 53, Issue 6, September 2005, Pages 663-667

59. Ma, C.L., Kasama, A., Tan, Y., Tanaka, H., Tanaka, R., Mishima, Y., Kanada, S. Synthesis of Nb/Nb5Si3 in-situ composites by mechanical milling and reactive spark plasma sintering (2000) Materials Transactions, JIM, 41 (6), pp. 719-726

60. Duan, R.-G., Zhan, G.-D., Kuntz, J.D., Kear, B.H., Mukherjee, A.K. Spark plasma sintering (SPS) consolidated ceramic composites from plasma-sprayed metastable Al2TiO5 powder and nano-Al2O3, TiO2, and MgO powders (2004) Materials Science and Engineering A, 373 (1-2), pp. 180-186

61. Viswanathan, V., Laha, T., Balani, K., Agarwal, A., Seal, S. Challenges and advances in nanocomposite processing techniques(2006) Materials Science and Engineering R: Reports, 54 (5-6), pp. 121-285

62. Kim, H.-C., Shon, I.-J., Garay, J.E., Munir, Z.A. Consolidation and properties of binderless sub-micron tungsten carbide by field-activated sintering (2004) International Journal of Refractory Metals and Hard Materials, 22 (6), pp. 257-264

63. Zhan, G.-D., Mukherjee, A.K. Carbon nanotube reinforced alumina-based ceramics with novel mechanical, electrical, and thermal properties (2004) International Journal of Applied Ceramic Technology, 1 (3), pp. 161-171

64. Garay, J.E., Glade, S.C., Asoka-Kumar, P., Anselmi-Tamburini, U., Munir, Z.A. Characterization of densified fully stabilized nanometric zirconia by positron annihilation spectroscopy (2006) Journal of Applied Physics, 99 (2), art. no. 024313

65. Kumar, R., Cheang, P., Khor, K.A. Spark plasma sintering and in vitro study of ultra-fine HA and ZrO 2-HA powders (2003) Journal of Materials Processing Technology, 140 (1-3 SPEC.), pp. 420-425

66. Al-Aqeeli, N., Abdullahi, K., Hakeem, A.S., Suryanarayana, C., Laoui, T., Nouari, S. Synthesis, characterisation and mechanical properties of SiC reinforced Al based nanocomposites processed by MA and SPS (2013) Powder Metallurgy, 56 (2), pp. 149-157

67. K.D. Woo, D.L. Zhang, Fabrication of Al–7wt%Si–0.4wt%Mg/SiC nanocomposite powders and bulk nanocomposites by high energy ball milling and powder metallurgy, Current Applied Physics, Volume 4, Issues 2–4, April 2004, Pages 175-178

68. Naiqin Zhao, Philip Nash, Xianjin Yang, The effect of mechanical alloying on SiC distribution and the properties of 6061 aluminum composite, Journal of Materials Processing Technology, Volume 170, Issue 3, 30 December 2005, Pages 586-592

69. N. Parvin, R. Assadifard, P. Safarzadeh, S. Sheibani, P. Marashi, Preparation and mechanical properties of SiC-reinforced Al6061 composite by mechanical alloying, Materials Science and Engineering: A, Volume 492, Issues 1–2, 25 September 2008, Pages 134-140

70. Lauri Kollo, Marc Leparoux, Christopher R. Bradbury, Christian Jäggi, Efraín Carreño-Morelli, Mikel Rodríguez-Arbaizar, Investigation of planetary milling for nano-silicon carbide reinforced aluminium metal matrix composites, Journal of Alloys and Compounds, Volume 489, Issue 2, 21 January 2010, Pages 394-400

71. L. Lu, M.O. Lai, C.W. Ng, Enhanced mechanical properties of an Al based metal matrix composite prepared using mechanical alloying, Materials Science and Engineering: A, Volume 252, Issue 2, 15 September 1998, Pages 203-211

72. MeiJun Yang, DongMing Zhang, XiaoFeng Gu, LianMeng Zhang, Effects of SiC particle size on CTEs of SiCp/Al composites by pulsed electric current sintering, Materials Chemistry and Physics, Volume 99, Issue 1, 10 September 2006, Pages 170-173

73. Byung-Chul Ko, Yeon-Chul Yoo, The effect of aging treatment on the microstructure and mechanical properties of AA2124 hybrid composites reinforced with both SiC whiskers and SiC particles, Composites Science and Technology, Volume 59, Issue 5, April 1999, Pages 775-779

74. M. İzciler, M. Muratoglu, Wear behaviour of SiC reinforced 2124 Al alloy composite in RWAT system, Journal of Materials Processing Technology, Volume 132, Issues 1–3, 10 January 2003, Pages 67-72

75. Rodríguez-Arbaizar, M., Hamdan, H., Leparoux, M., Kollo2, L., Kwon, H., Carreño-Morelli1, E. Net-Shape Al6061/SiC Nanocomposites by Powder Injection Moulding (2010) PM2010 World Congress, San Diego State University

76. T.-W. Kim, Determination of densification behavior of Al–SiC metal matrix composites during consolidation processes, Materials Science and Engineering: A, Volumes 483–484, 15 June 2008, Pages 648-651

77. Ram B. Bhagat, Michael B. House, Elevated-temperature mechanical properties of silicon-carbide-whisker-reinforced aluminum matrix composites, Materials Science and Engineering: A, Volume 144, Issues 1–2, 1 October 1991, Pages 319-326

78. Byung-Chul Ko, Yeon-Chul Yoo, The effect of aging treatment on the microstructure and mechanical properties of AA2124 hybrid composites reinforced with both SiC whiskers and SiC particles, Composites Science and Technology, Volume 59, Issue 5, April 1999, Pages 775-779

79. H.K Jung, Y.M Cheong, H.J Ryu, S.H Hong, Analysis of anisotropy in elastic constants of SiCp/2124 Al metal matrix composites, Scripta Materialia, Volume 41, Issue 12, 19 November 1999, Pages 1261-1267

80. G. O'Donnell, L. Looney, Production of aluminium matrix composite components using conventional PM technology, Materials Science and Engineering: A, Volume 303, Issues 1–2, 15 May 2001, Pages 292-301

81. Tang, F., Hagiwara, M., Schoenung, J.M. Microstructure and tensile properties of bulk nanostructured Al-5083/ SiCp composites prepared by cryomilling (2005) Materials Science and Engineering A, 407 (1-2), pp. 306-314

82. Tang, F., Liao, C.-P., Ahn, B., Nutt, S.R., Schoenung, J.M. Thermal stability in nanostructured Al-5083/SiCp composites fabricated by cryomilling (2007) Powder Metallurgy, 50 (4), pp. 307-312

83. K. Hanada, K.A. Khor, M.J. Tan, Y. Murakoshi, H. Negishi, T. Sano, Aluminium-lithium/SiCp composites produced by mechanically milled powders, Journal of Materials Processing Technology, Volume 67, Issues 1–3, May 1997, Pages 8-12

84. Ismail Ozdemir, Sascha Ahrens, Silke Mücklich, Bernhard Wielage, Nanocrystalline Al–Al2O3p and SiCp composites produced by high-energy ball milling, Journal of Materials Processing Technology, Volume 205, Issues 1–3, 26 August 2008, Pages 111-118

85. Al-Aqeeli, N., Abdullahi, K., Hakeem, A.S., Suryanarayana, C., Laoui, T., Nouari, S. Synthesis, characterisation and mechanical properties of SiC reinforced Al based nanocomposites processed by MA and SPS (2013) Powder Metallurgy, 56 (2), pp. 149-157

86. Abdullahi, K ,Al-Aqeeli, N. Mechanical Alloying and Spark Plasma Sintering of Nano-SiC Reinforced Al–12Si–0.3Mg Alloy (2014) Arab J Sci Eng,, pp. 3161–3168

87. Nazari, A., Abdinejad, V. R. Artificial neural networks for prediction Charpy impact energy of Al6061/SiCp-laminated nanocomposites (2012) Neural Computing and Applications

88. Hesam Pouraliakbar, Ali Nazari, Pouriya Fataei, Akbar Karimi Livary, Mohammad Jandaghi, Predicting Charpy impact energy of Al6061/SiCp laminated nanocomposites in crack divider and crack arrester forms, Ceramics International, Volume 39, Issue 6, August 2013, Pages 6099-6106

89. Ali Nazari, Vahidreza Abdinejad, Modeling Charpy impact behavior of Al6061/SiCp laminated nanocomposites by genetic programming, Ceramics International, Volume 39, Issue 2, March 2013, Pages 1991-2002

90. GENG Lin, ZHANG Xue-nan, WANG Gui-son, ZHENG Zhen-zhu. Effect of aging treatment on mechanical properties of (SiCw+SiCp)/2024A1 hybrid nanocomposites, Transactions of Nonferrous Metals Society of China, 2006, Pages 387-391

91. K.D. Woo, D.L. Zhang, Fabrication of Al–7wt%Si–0.4wt%Mg/SiC nanocomposite powders and bulk nanocomposites by high energy ball milling and powder metallurgy, Current Applied Physics, Volume 4, Issues 2–4, April 2004, Pages 175-178

92. Härtel, M., Wagner, S., Frint, P., Wagner, M.F.-X. Effects of particle reinforcement and ECAP on the precipitation kinetics of an Al-Cu alloy (2014) IOP Conference Series: Materials Science and Engineering, 63 (1)

93. P. Appendino, C. Badini, F. Marino, A. Tomasi, 6061 aluminium alloy-SiC particulate composite: a comparison between aging behavior in T4 and T6 treatments, Materials Science and Engineering: A, Volume 135, 30 March 1991, Pages 275-279

94. Naiqin Zhao, Philip Nash, Xianjin Yang, The effect of mechanical alloying on SiC distribution and the properties of 6061 aluminum composite, Journal of Materials Processing Technology, Volume 170, Issue 3, 30 December 2005, Pages 586-592

95. N. Parvin, R. Assadifard, P. Safarzadeh, S. Sheibani, P. Marashi, Preparation and mechanical properties of SiC-reinforced Al6061 composite by mechanical alloying, Materials Science and Engineering: A, Volume 492, Issues 1–2, 25 September 2008, Pages 134-140

96. Marcin, M. Tungsten Carbide as an Addition to High Speed Steel Based Composites (2012) InTech, pp. 57-80.

97. Saheb, N. Spark plasma and microwave sintering of Al6061 and Al2124 alloys (2013) International Journal of Minerals, Metallurgy and Materials, 20 (2), pp. 152-159

98. Saheb, N. Sintering behavior of CNT reinforced Al6061 and Al2124 nanocomposites (2014) Advances in Materials Science and Engineering, 2014

99. G.K Williamson, W.H Hall, X-ray line broadening from filed aluminium and wolfram, Acta Metallurgica, Volume 1, Issue 1, January 1953, Pages 22-31

100. Kumari, Satchi; Singh, Dilip K.; Giri, P. K., Strain Anisotropy in Freestanding Germanium Nanoparticles Synthesized by Ball Milling, Journal of Nanoscience and Nanotechnology, Volume 9, Number 9, September 2009, pp. 5231-5236(6)

101. Dislocation model of strain anisotropy (2008) Powder Diffraction, 23 (2), pp. 125-132

102. Strain broadening caused by dislocations (1998) Materials Science Forum, 278-281 (PART 1), pp. 151-156

103. Whole Powder Pattern Modelling of cubic metal powders deformed by high energy milling (2007) Zeitschrift fur Kristallographie, 222 (3-4), pp. 129-135

104. Scardi, P., Ortolani, M., Leoni, M. WPPM: Microstructural analysis beyond the Rietveld method (2010) Materials Science Forum, 651, pp. 155-171

105. Fogagnolo, J.B., Robert, M.H., Torralba, J.M. Mechanically alloyed AlN particle-reinforced Al-6061 matrix composites: Powder processing, consolidation and mechanical strength and hardness of the as-extruded materials (2006) Materials Science and Engineering A, 426 (1-2), pp. 85-94

106. Lin, Z., Li, Y., Mohamed, F.A. Creep and substructure in 5 vol.% SiC-2124 Al composite (2002) Materials Science and Engineering A, 332 (1-2), pp. 330-342

107. N. Al-Aqeeli. 2013. Processing of CNTs reinforced al-based nanocomposites using different consolidation techniques. J. Nanomaterials 2013, Article 125 (January 2013)

Vitae

Name   :Atif Saeed Al-Zahrani

Nationality   :Saudi

Date of Birth   :5/14/1988

Email   :wazzabas@windowslive.com

Address   :Kfupm 31621, Dhahran, Saudi Arabia

Academic Background   :BS Mechanical Engineering, 2010